NRL Memorandum Report 3929

LEVEL III

Simultaneous Neutron Spectrum and Transistor-Damage Measurements in Diverse Neutron Fields: Validity of $D_{Si}(E_n)$

V. V. VERBINSKI AND C. CASSAPAKIS

Science Applications, Inc.
La Jolla, CA 92038

R. L. PEASE

BDM Corporation
Albuquerque, NM 87106

and

H. L. SCOTT

Sandia Corporation
Albuquerque, NM 87115

March 16, 1979

This research was sponsored by the Defense Nuclear Agency under Subtask Z99QAXTD072, work unit code 68, and work unit title Hardness Assurance Program.

NAVAL RESEARCH LABORATORY
Washington, D.C.

UNCLASSIFIED

SECURITY CLASSIFICATION OF THIS PAGE (When Data Entered)

REPORT DOCUMENTATION PAGE		READ INSTRUCTIONS BEFORE COMPLETING FORM
1. REPORT NUMBER NRL Memorandum Report 3929	2. GOVT ACCESSION NO.	3. RECIPIENT'S CATALOG NUMBER
4. TITLE (and Subtitle) SIMULTANEOUS NEUTRON SPECTRUM AND TRANSISTOR-DAMAGE MEASUREMENTS IN DIVERSE NEUTRON FIELDS: VALIDITY OF $D_{Si}(E_n)$		5. TYPE OF REPORT & PERIOD COVERED Final Technical Report 24 January 1977 - 12 September 1978 6. PERFORMING ORG. REPORT NUMBER
7. AUTHOR(s) V.V. Verbinski*, C. Cassapakis*, R.L. Pease†, and H.L. Scott‡		8. CONTRACT OR GRANT NUMBER(s) NRL-N00173-77-C-0044
9. PERFORMING ORGANIZATION NAME AND ADDRESS Science Applications Inc. 1200 Prospect Street La Jolla, CA 92038		10. PROGRAM ELEMENT, PROJECT, TASK AREA & WORK UNIT NUMBERS 62704 H
11. CONTROLLING OFFICE NAME AND ADDRESS Naval Research Laboratory Washington, DC 20375 Technical Monitor: Dr. Neal Wilsey		12. REPORT DATE March 16, 1979 13. NUMBER OF PAGES 138
14. MONITORING AGENCY NAME & ADDRESS(if different from Controlling Office)		15. SECURITY CLASS. (of this report) UNCLASSIFIED 15a. DECLASSIFICATION/DOWNGRADING SCHEDULE

16. DISTRIBUTION STATEMENT (of this Report)

Approved for public release; distribution unlimited.

17. DISTRIBUTION STATEMENT (of the abstract entered in Block 20, if different from Report)

18. SUPPLEMENTARY NOTES

This research was sponsored by the Defense Nuclear Agency under Subtask Z99QAXTD072, work unit 68, and work unit title Hardness Assurance Program.

*Science Applications Inc., 1200 Prospect Street, La Jolla, CA 92038

†BDM Corporation, 2600 Yale Blvd., Albuquerque, NM 87106 (Continues)

19. KEY WORDS (Continue on reverse side if necessary and identify by block number)

Hardness assurance
Neutron spectra
Neutron damage factors
Neutron transistor damage

phi(E)

20. ABSTRACT (Continue on reverse side if necessary and identify by block number)

This report contains a summary of intercalibration measurements carried out on four different reactors under various irradiation conditions. These reactors were the Northrop TRIGA, SANDIA SPR II and ACPR, and the Aberdeen APRF reactor. The intercalibration was carried out by (a) measuring neutron spectra for a variety of basic and modified ("filtered") reactor neutron fields with a standard threshold-foil-activation neutron spectrometry method, (b) folding in each spectrum $\phi(E)$ with the silicon damage function D(E) to obtain ϕ_{eq}, the number of near-1 MeV neutrons required to produce (Continues)

phi sub eq

DD FORM 1 JAN 73 1473 EDITION OF 1 NOV 65 IS OBSOLETE S/N 0102-014-6601

UNCLASSIFIED

SECURITY CLASSIFICATION OF THIS PAGE (When Data Entered)

18. Supplementary Notes (Continued)

‡Sandia Corporation, Albuquerque, NM 87115

20. Abstract (Continued)

the same damage, (c) irradiating a batch of 2N2222A transistors simultaneously with the neutron dosimetry stack and measuring the total damage $D = K\phi$, and (d) dividing $D = K\phi$ by ϕ_{eq} to obtain values of the damage coefficient K for the diverse neutron fields measured.

The values of K were constant (±5% for 1 standard deviation) for all the spectra investigated, indicating that ϕ_{eq} adequately characterizes the permanent radiation damage effectiveness from one basic (and/or modified) reactor spectrum to another for a practical type of transistor.

These results suggest that ϕ_{eq} can quantitatively relate reactor-spectrum and threat-spectrum radiation damage, since a variety of spectral shapes were utilized. For the FBR leakage spectrum modified by iron and polyethylene, the spectral shapes above the 0.2 MeV "threshold" for radiation damage in silicon were significantly different from all the others.

This work is a continuation of a Defense Nuclear Agency (DNA) sponsored effort, initiated in 1974, in which several different spectra (WSMR FBR glory hole and leakage, and TRIGA leakage) were measured and variation studies carried out to determine the sensitivity of ϕ_{eq} to the many possible sources of error. To make this report as complete as possible for the user, these previous results have been included as Appendix A.

The culmination of this work was a set of ASTM draft standards (Appendix B) which were followed in detail, except for an important improvement recently developed by one of the authors of this report (VVV). This involves a simple and highly accurate method of measuring the error in gamma-ray detector efficiency that arises for some cases where cascade-gamma-ray emissions occur (see presentation of this work in the text). Once measured, the error is corrected for in a very simple way.

One of the outputs of the intercalibration effort is a value of ϕ_{eq}/S for each reactor facility, so that ϕ_{eq} can be determined for each irradiation by the sulfur-foil activation S (i.e. the ^{32}P disintegration rate) when the sulfur-foil counter is properly calibrated, as described in this report.

TABLE OF CONTENTS

LIST OF FIGURES

LIST OF TABLES

ACKNOWLEDGEMENTS

The authors wish to express their deep appreciation to Dr. E. A. Wolicki and Dr. N. Wilsey of NRL for their continued support and helpful suggestions, to J. Odom of SANDIA for the ACPR core neutron spectrum calculation, to W. Scott, W. Hagan and L. Simmons for help in performing the ANISN calculations on FBR leakage neutrons transported through polyethylene and iron filters, to J. Humphrey of NBS and Louise Miles of NSWC, White Oak, Maryland, for help with the TLD readings, and to G. Hash of NWSC, Crane, Indiana, for his generous contribution in measuring the radiation damage of the 2N2222A transistors.

ABSTRACT

This report contains a summary of intercalibration measurements carried out on four different reactors under various irradiation conditions. These reactors were the Northrop TRIGA, SANDIA SPR II and ACPR, and the Aberdeen APRF reactor. The intercalibration was carried out by (a) measuring neutron spectra for a variety of basic and modified ("filtered") reactor neutron fields with a standard threshold-foil-activation neutron spectrometry method, (b) folding in each spectrum $\phi(E)$ with the silicon damage function $D(E)$ to obtain ϕ_{eq}, the number of near-1 MeV neutrons required to produce the same damage, (c) irradiating a batch of 2N2222A transistors simultaneously with the neutron dosimetry stack and measuring the total damage $D = K\phi$, and (d) dividing $D = K\phi$ by ϕ_{eq} to obtain values of the damage coefficient K for the diverse neutron fields measured.

The values of K were constant (±5% for 1 standard deviation) for all the spectra investigated, indicating that ϕ_{eq} adequately characterizes the permanent radiation damage effectiveness from one basic (and/or modified) reactor spectrum to another for a practical type of transistor.

These results suggest that ϕ_{eq} can quantitatively relate reactor-spectrum and threat-spectrum radiation damage, since a variety of spectral shapes was utilized. For the FBR leakage spectrum modified by iron and polyethylene, the spectral shapes above the 0.2 MeV "threshold" for radiation damage in silicon were significantly different from all the others.

This work is a continuation of a Defense Nuclear Agency (DNA) sponsored effort, initiated in 1974, in which several different spectra (WSMR FBR glory hole and leakage, and TRIGA leakage) were measured and variational studies

carried out to determine the sensitivity of ϕ_{eq} to the many possible sources of error. To make this report as complete as possible for the user these previous results have been included as Appendix A.

The culmination of this work was a set of ASTM draft standards (Appendix B) which were followed in detail, except for an important improvement recently developed by one of the authors of this report (VVV). This involves a simple and highly accurate method of measuring the error in gamma-ray detector efficiency that arises for some cases where cascade-gamma-ray emissions occur (see presentation of this work in the text). Once measured, the error is corrected for in a very simple way.

One of the outputs of the intercalibration effort is a value of ϕ_{eq}/S for each reactor facility, so that ϕ_{eq} can be determined for each irradiation by the sulfur-foil activation S (i.e. the ^{32}P disintegration rate) when the sulfur-foil counter is properly calibrated, as described in this report.

1. INTRODUCTION

This work is a continuation of an effort initiated in 1975, when a series of reactor spectral measurements and calculations were carried out on the White Sands Missile Range (WSMR) fast burst reactor (FBR) and the General Atomic (GA) TRIGA reactor. The neutron spectral measurements were made with threshold activation foils, and a sensitivity study was carried out on the effect of foil-counting errors, foil activation cross section errors, choice of trial spectrum, and choice of reactor unfolding code. These results appear as Appendix A of this report. The standard neutron threshold foil spectrometry method appears as Appendix B, as submitted in the form of a set of draft ASTM Standard Methods.

A neutron field can be uniquely specified by a table of spectral intensity versus neutron energy. An accurate spectral determination is prohibitively expensive and in general can be carried out only once. In addition, it involves the carrying of a large number set.

Historically, the neutron field has been monitored from irradiation to irradiation by means of sulfur foil activation. These foils, having an activation threshold of 3 MeV, only sense the upper "tail" of the spectrum. The spectral flux can be accurately inferred only if the spectral shape and the sulfur activation cross section $\sigma(E)$ are known accurately. Further quantification had been applied by utilizing the Pu/S ratio, since ^{239}Pu has an effective threshold at 0.001-0.01 MeV when adequately shielded inside a ^{10}B shell. The S-foil activation and the Pu/S ratio, although further quantifying the neutron field, fall far short of doing so to the extent that work carried out with, say, a TRIGA reactor can be directly compared to

Note: Manuscript submitted December 12, 1978.

FBR irradiations.

In the present work, neutron spectra $\phi(E)$ were measured for a variety of TRIGA and FBR facilities both for the free field case and for these fields modified by "filters". These spectra were characterized and quantified in terms of radiation damage effectiveness for silicon devices by a single parameter ϕ_{eq}. Here, ϕ_{eq} is the equivalent near-1-MeV fluence for producing the same radiation damage:

$$\phi_{eq} = \int_{.01}^{18\ MeV} \phi(E)\ D(E)dE \Big/ \bar{D}(0.85\text{-}1.15\ MeV) \qquad (1)$$

Here, D(E) is the calculated energy dependent neutron cross section for producing permanent atomic displacements in bulk silicon.

Both ϕ_{eq} and ϕ_{eq}/S are presented below so that ϕ_{eq} can be determined from the sulfur activation S, following proper (absolute) calibration of the sulfur-foil beta counter (see below).

In order to determine the validity of ϕ_{eq}, some measurements of radiation damage $D = K\phi$ were also made on batches of 2N2222A transistors. These were simultaneously exposed with the neutron threshold foil spectrometry stack, so that both ϕ_{eq} and $D = K\phi$ could be determined for the same exposure. From the ratios $D = K\phi$ to ϕ_{eq}, the damage coefficients K were determined. The extent to which the measured K are constant over a wide variety of neutron spectra determines the extent to which ϕ_{eq} characterizes the radiation damage from any of the radiation fields measured in this task.

The free-field FBR spectrum was modified with two different filters (10 cm of polyethylene and 5 cm of iron) in order to check ϕ_{eq} over a more diverse set of radiation fields. This yielded a total of 5 different types of spectra (TRIGA, FBR glory hole, FBR leakage, and two modified leakage spectra).

2. RADIATION FACILITIES INTERCALIBRATED

A list of the different neutron spectra measured previously and in this program is presented in Table 1. This list covers all the major reactor facilities extensively used for radiation damage studies in the United States at this time.

Table 1. Reactor Spectra Measured.

The spectra in parentheses are those measured earlier, without simultaneous irradiation of 2N2222A transistors.

FACILITY	SPECTRUM
FBR, WSMR	(Glory Hole)
FBR, WSMR	(Free Field, 50 cm)
TRIGA, G.A.	(J-Tube, Leakage)
TRIGA, NORTHROP	Exposure Room, ½" Boral
TRIGA, NORTHROP	Exposure Room, ½" Boral + 2" Pb
ACPR, SANDIA	ACPR Core
FBR, SANDIA	Glory Hole
FBR, SANDIA	Leakage, Free Field
FBR, SANDIA	Leakage, Free Field, Burst
FBR, SANDIA	Leakage, 10 cm Polyethylene
FBR, SANDIA	Leakage, 5 cm Iron
APRF, ABERDEEN	Glory Hole
APRF, ABERDEEN	Leakage, Free Field
APRF, ABERDEEN	Leakage, Free Field, Burst
APRF, ABERDEEN	Leakage, HA Table*, Free Field

*Hardness Assurance Table (∿½" Thick Aluminum Top)

3. FOIL, TRANSISTOR, and TLD IRRADIATIONS: PRESENT PROGRAM

3.1 FOIL IRRADIATIONS

The foils were stacked in order of increasing threshold energy, E_{th}, so as to minimize self-shielding effects. The lowest threshold foil was nearest the neutron source. Three separate stacks were used as follows: (1) Au, ^{235}U, ^{237}Np; (2) In, ^{238}U, ^{232}Th; and (3) Fe, Ni, Mg, Al, and Zr. Note that the first two stacks terminate on ^{237}Np and ^{232}Th, respectively, since these are the thickest foils (See Table I, Appendix A); the last five foils, on the other hand, are all relatively thin.

Short descriptions of the irradiation runs are given in Table 2 together with the corresponding calculated 1-MeV(Si) equivalent neutron fluences, some related spectrum characteristics, and the transistor damage coefficients obtained for transistors irradiated at the same time as the foils. (Discussions of the results contained in Table 2 are given in sections 6, 7, and 8.)

All foil stacks were placed in ^{10}B spheres (1.65 g/cm^2) except in the FBR glory holes. There was no room in the glory hole for the ^{10}B sphere, and the sphere was not needed there because the reactor fuel provided even better low-energy-neutron shielding. In the FBR leakage-spectrum, Runs 11 and 12, foils were placed both inside and outside the ^{10}B sphere to help determine the effect of the ^{10}B shielding (scattering) on foils with high E_{th} values. ^{10}B-Scattering corrections were the order of 10-15%, and were applied to all data where the transistors were exposed outside the ^{10}B shell while the foils were located inside the shell.

The use of the ^{10}B shell is important for providing an effective threshold for ^{235}U and Au foils, and also for drastically reducing the effects of impurities in the foils that lead to the same activation nucleus through the much more efficient route of thermal-neutron activation. Examples of foil-impurity pairs are $^{27}Al(n,\alpha)$, $^{23}Na(n,\gamma)$; $^{56}Fe(n,p)$, $^{56}Mn(n,\gamma)$; $^{238}U(n,f)$, $^{235}U(n,f)$. The second foil in each

Table 2. Radiation Damage Coefficients

Run #	Description	ϕ_{eq}	$\frac{\phi_{eq}}{\phi}$ *	ϕ_{eq}/S	K_1 10uA	K_2 100uA	K_3 1mA	K_4 10mA
1A	ACPR Core-B^{10}	9.95+12	1.06	5.86+31	4.83-6	2.79-6	1.64-6	0.87-6
1B	ACPR Core	11.44+12	1.06	5.86+31	4.84-6	2.77-6	1.59-6	0.84-6
2	SPR II Glory Hole	2.61+13	1.16	5.80+31	4.83-6	2.93-6	1.70-6	0.90-6
3	SPR II Leak. Burst	3.17+13	1.35	6.89+31	4.57-6	2.74-6	1.63-6	0.85-6
4	SPR II Leakage	4.21+13	1.42	6.97+31	4.20-6	2.68-6	1.61-6	0.84-6
5	SPR II - Ch_2	1.82+13	1.38	5.08+31	4.80-6	2.82-6	1.65-6	0.88-6
6A	SPR-II - Fe	6.26+13	0.99	1.20+32	4.50-6	2.72-6	1.74-6	0.89-6
6B	SPR II - CH_2	1.41+13	1.38	5.08+31	4.89-6	2.83-6	1.65-6	0.89-6
7A	TRIGA-Boral-B^{10}	2.45+13	1.18	5.04+31	4.24-6	2.57-6	1.48-6	0.78-6
7B	TRIGA-Boral	2.45+13	1.18	5.04+31	4.73-6	2.85-6	1.67-6	0.87-6
8A	TRIGA-Pb-B^{10}	2.37+13	1.10	5.59+31	4.64-6	2.73-6	1.58-6	0.82-6
8B	TRIGA-Pb	2.37+13	1.10	5.59+31	4.68-6	2.76-6	1.60-6	0.85-6
9	APRF-Leakage	1.00+14	1.19	6.53+31	3.91-6	2.40-6	1.64-6	0.83-6
10	APRF-Glory Hole	7.79+13	1.19	6.59+31	4.36-6	2.63-6	1.73-6	0.88-6
11	APRF on H.A. Table	9.64+13	1.42	7.02+31	3.96-6	2.50-6	1.72-6	0.85-6
12	APRF Leakage, Burst	3.49+13	1.41	7.08+31	4.50-6	2.70-6	1.57-6	0.81-6
	Mean				4.55-6	2.73-6	1.65-6	.863-6
	σ				.32-6	.14-6	.062-6	.042-6
					(7%)	(5%)	(4%)	(5%)

* $\frac{\phi_{eq}}{\phi} \equiv \phi_{eq}/\phi(.01\text{-}18\ MeV)$

case is activated via thermal neutrons, which have a disproportionately large reaction cross section. (See Appendix A for method of making accurate impurity corrections when thermal neutrons are shielded out.)

3.2 TRANSISTOR AND TLD IRRADIATIONS

Batches of 7 to 10 transistors were tightly wrapped in aluminum foil and placed ∿1 cm outside of the ^{10}B ball containing the neutron threshold-activation foils. The aluminum foil and the other transistor cans very likely shorted out the transistor leads in all cases. Great care was taken to keep the transistors and the neutron spectrometry foils at the same distance from the reactor for free-field measurements.

For the case of abundant moderated neutrons, such as for the ACPR and the Northrup TRIGA reactors, transistors were placed both inside and outside the ^{10}B sphere to determine the radiation damage due to low energy neutrons. In all cases, the measured transistor damage inside the ^{10}B shell was less than that outside by about the same factor (10-15%) as high-energy threshold foils differed inside and out. From this observation, it is concluded that in no case was any net damage observed for low energy neutrons (i.e., neutrons below the ∿10 keV neutron "threshold" for the ^{10}B shield).

A batch of 4-5 TLD's was placed next to the transistors during each irradiation to measure total dose. The TLD's were the thin CaF_2:Mn type, embedded in teflon. They were wrapped in aluminum foil of a total thickness of approximately 0.025 cm so as to shield out most of the extraneous-electron dosage.

Some of the unirradiated TLD's of the same batch were exposed to a calibrated pure ^{60}Co gamma-ray field at NBS

by J. Humphreys and read with the same equipment as the reactor-irradiated TLD's by Louise Miles of the Naval Surface Weapons Center (Silver Springs, Maryland).

The TLD data were used to provide "total dose" corrections to the neutron damage, as discussed in Section 8 below.

4. COUNTING

Counting the γ-rays activities induced by the foil irradiation was accomplished for the most part according to the ASTM standards method outlined in Appendix B. Ge(Li) Detectors were used exclusively, both in the irradiation site for the short-lived activities and at the SAI-La Jolla Laboratory for the long-lived ones. Calibration of (and intercalibration between) individual detectors was accomplished using an NBS-prepared mixed γ-ray source covering the energy range of interest (100 to ∿ 2,000 keV).

A number of different foil-to-detector distances were utilized in the measurement, depending on the exhibited total activity of each individual foil and the energy of the photopeak of interest, so as to minimize excessive dead-time and background effects. The detector efficiency for each geometry was determined using the same NBS standard 11-line source for all detectors and detector geometries. A significant addition to the ASTM Standard Method (Appendix B) during this work, was the study of the effect of γ-ray cascades on detector efficiency; significantly in the case of the 537 keV- and 1596 keV lines observed in all fission foils used in this work. This was accomplished by determining the count-rate of the relevant photopeak at different distances D from the "face" of the detector and plotting $1/\sqrt{N}$ versus D where N is the count rate. This yields a correction of the count rate due to cascades when the foil being counted is located close to the effective detector center; it also locates the approximate effective detector center for a given energy gamma ray. Figures 1 and 2 show the results of this study for the NBS standard source and the 537 keV and 1596 keV

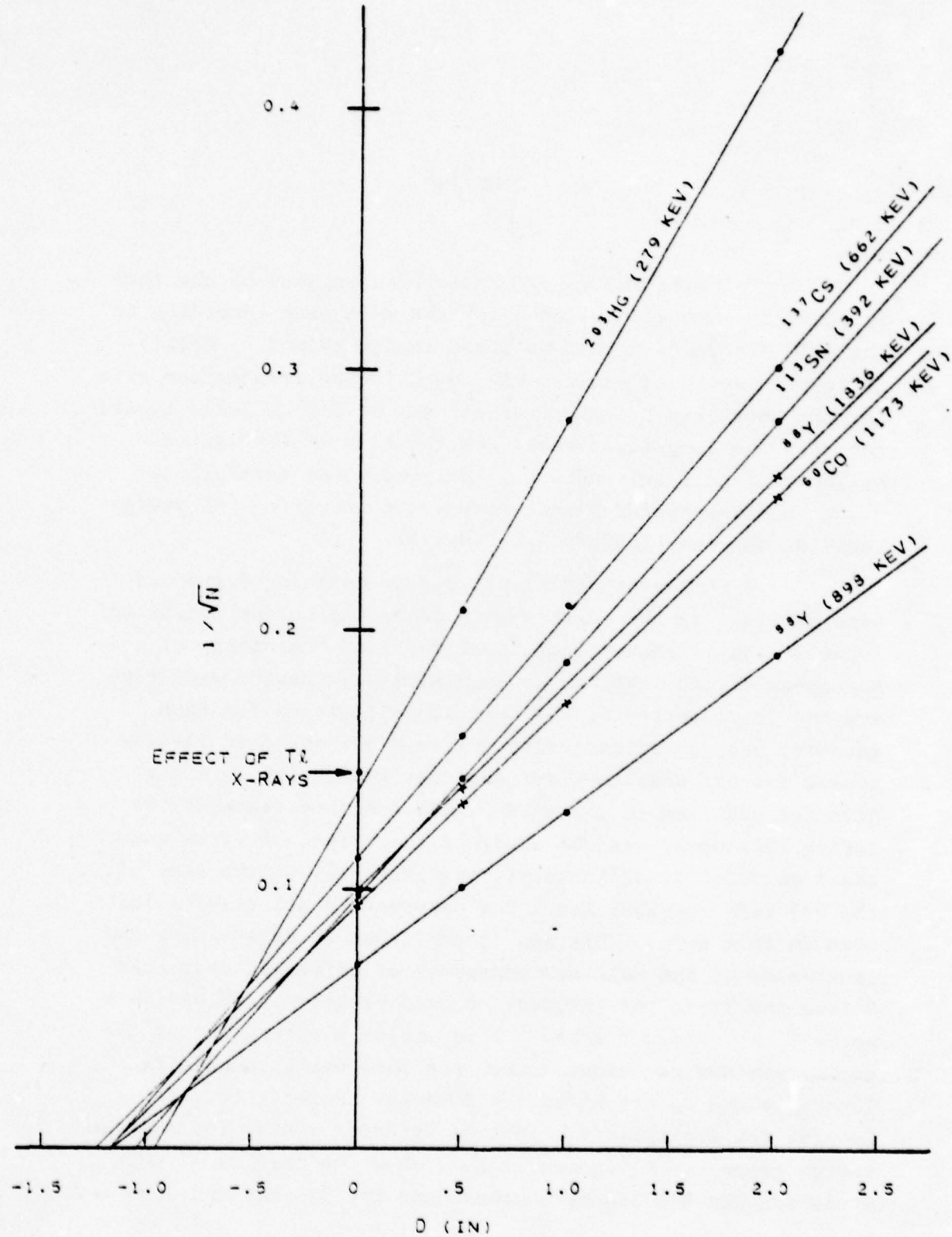

Figure 1. Cascade-Gamma Effect on Determining Detector Efficiency: Calibration Sources.

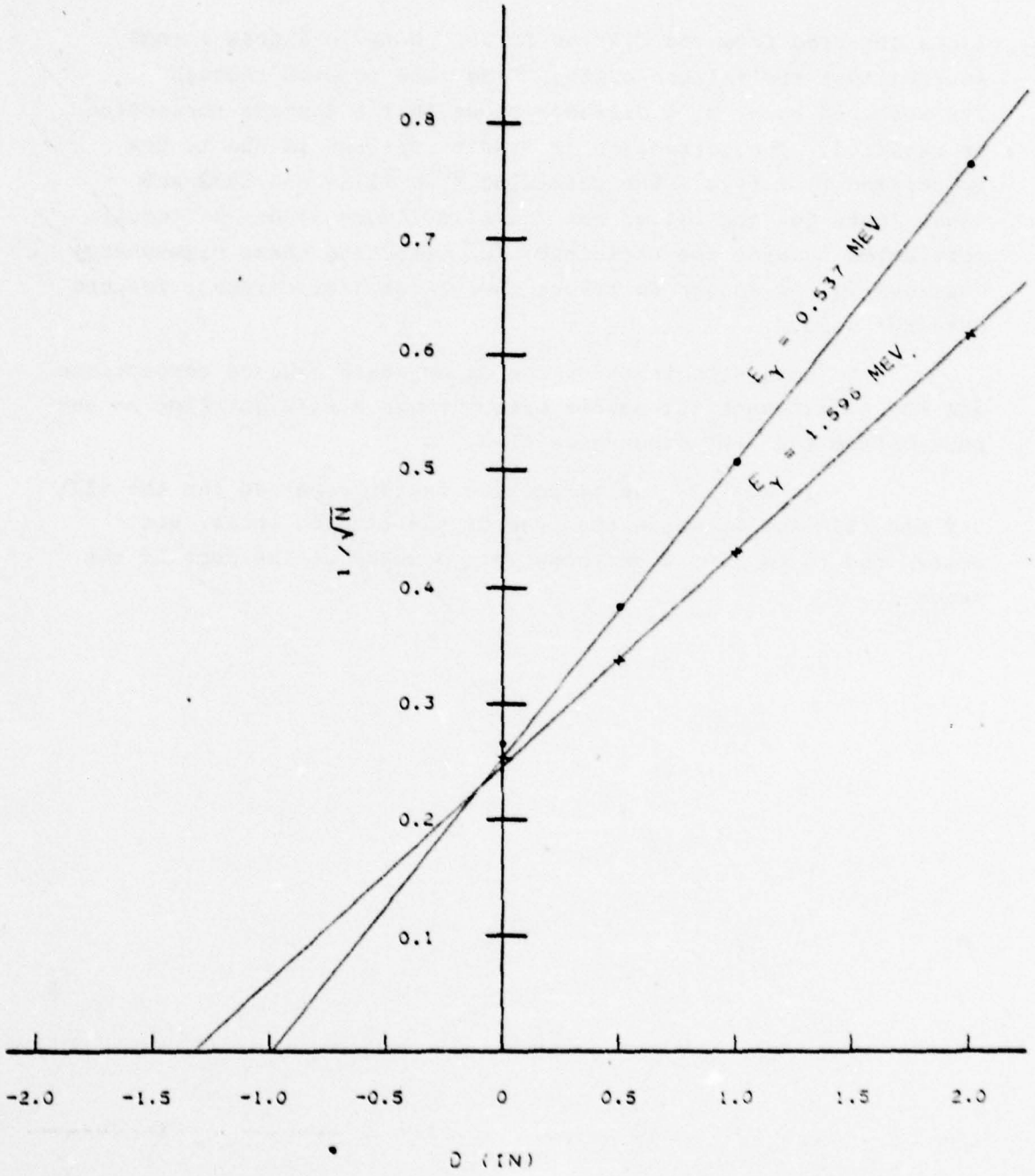

Figure 2. Cascade-Gamma Effect on Determining Detector Efficiency: ^{140}Ba and ^{140}La Lines

lines observed from the fission foils. Note in Figure 1 (NBS source) that the failure of the ^{203}Hg line to pass through the measured point at O distance shows that a cascade correction is required. The correction is significant and is due to the associated Tl x rays. The cascading ^{60}Co 1173- and 1332-keV lines (data for the latter not shown in Figure 1) do not require correction because the efficiency for detecting these high-energy cascades is low enough to render the effect insignificant for the detector used.

Note also that for the cases where cascade corrections are not significant all points pass through a straight line as expected from the $1/D^2$ dependence of N.

In Fig. 2, the correction factor required for the 537-keV and 1596-keV lines in the case of the fission foils, was determined to be 1.08 when these were counted at the face of the detector.

5. DATA ANALYSIS

The resulting gamma-ray peak areas were further corrected for decay, irradiation and counting time effects. By further taking into account fission yield, branching ratios, detector efficiency at each relevant energy and foil mass, the number of activations (fissions) per atom was determined for input into the SAND II code. The relevant formulas can be found in Appendix B.

It may be mentioned that where possible (as for instance in the case of fission foils) more than one γ-ray line was analyzed to provide a consistency check on the results.

6. UNFOLDING

Because of the limited data carried by the threshold foils, especially below 1 MeV, the unfolding code (SAND II in this case) can only be used as a mild-perturbation type unfolding code. A good trial spectrum is required; e.g., one obtained from a simple transport calculation utilizing the correct neutron source and the approximate material composition and geometry involved. For the work carried out here, the trial spectra $\{\phi_{tr}(E)\}$ were as follows:

(1) ACPR-Core calculation for ACPR and TRIGA reactors (DOT)

(2) Glory hole calculation for FBR glory-hole runs (1DF)

(3) Leakage calculation for FBR free-field runs (1DF)

(4) Polyethylene-perturbed SPRII spectrum (ANISN)

(5) Iron-perturbed SPRII spectrum (ANISN)

The code carries out the necessary number of iterations in perturbing $\phi_{tr}(E)$ until the solution $\phi(E)$ is obtained that agrees with the input foil activations.

The results of the 0^{th} iteration were used to detect spurious foil activation values. These were rejected whenever they were identified, and the SAND II unfolding code was rerun without them.

The damage function D(E) was added to our version of the SAND II code with an energy mesh matching the 620-group structure of SAND II over the energy range 10^{-10}-17.9 MeV, and the quantities

$$\phi_{eq} = \frac{\int_{0.01}^{18\ MeV} \phi(E)\ D(E)dE}{\bar{D}(.85\text{-}1.15\ MeV)} \qquad (1)$$

$$\phi(.01\text{-}18\ MeV) = \int_{0.01}^{18\ MeV} \phi(E)dE \qquad (2)$$

ϕ_{eq}/ϕ, and ϕ_{eq}/S were numerically calculated.

Note that the sulfur foil activations S are here defined as the activation rate per atom of ^{32}S initial target material transmuted via the $^{32}S(n,p)^{32}P$ reaction to ^{32}P radioactive nuclei

$$S \equiv N\lambda / N(^{32}S) \qquad (3)$$

where $N\lambda$ is the product of the number of ^{32}P nuclei produced and the ^{32}P decay constant, and $N(^{32}S)$ is the number of ^{32}S nuclei in the sulfur pellet.

Actual facility sulfur monitor counts were not used since, in one case, the counter calibration went through three different values over a time span of only a few months (Itsu Arimura, private communication, 1978). Rather, S was obtained iteratively, by choosing a value of sulfur activation that agreed with the final SAND II solution for $\phi(E)$. After performing this exercise several times, it was established that the sulfur activation could be obtained to within $\pm 2\%$ by utilizing the ratio

$$2.92 * N\lambda\ (^{58}Ni(n,p)^{58}Co) = N\lambda\ (^{32}S(n,p)^{32}P) \qquad (4)$$

This holds for all the spectral shapes investigated here because both activations have threshold energies E_{th} that are not far apart ($\sim$ 2.9 MeV in both cases).

7. NEUTRON SPECTRA

Figure 3 shows the SANDIA ACPR core spectrum, as measured by SAI and SANDIA (SAI's foils, SANDIA detectors for short-lived foils and SAI's detector for long-lived foils), and Figure 4 shows the same spectrum measured by SANDIA with their detectors and foils. All detectors were calibrated against an NBS 11-line mixed source standard. Both spectra were unfolded with SAND II, using the same trial spectrum. This trial spectrum was calculated for the ACPR with a DOT-code calculation by J. Odom of SANDIA.

The "spectral shape factor" ϕ_{eq}/ϕ is 1.06 for the data of Figure 3 and 1.03 for Figure 4. These independent runs show good reproducibility in terms of silicon radiation damage effectiveness of the neutron field.

Figure 5 shows the results of an attempt at unfolding the APRF spectrum WITHOUT the a priori knowledge of a physically meaningful trial spectrum. The IUNFOLD code of SANDIA was used to obtain the spectral shape with only the foil activation data. Above 1 MeV, where many foils have thresholds and where the spectrum is dropping rapidly, the unfolding appears to be fair even though the unfolded spectrum drops off a bit faster than the SAND II data with adequate a priori data. But below 1 MeV, where only one threshold exists between 0.01 MeV and 0.50 MeV, the unconstrained solution is physically meaningless (i.e. not possible for the source spectrum, the geometry, and the materials involved). Other attempts will be made to use IUNFOLD with a good trial spectrum, and much more reasonable results are clearly expected with the constrained solution.

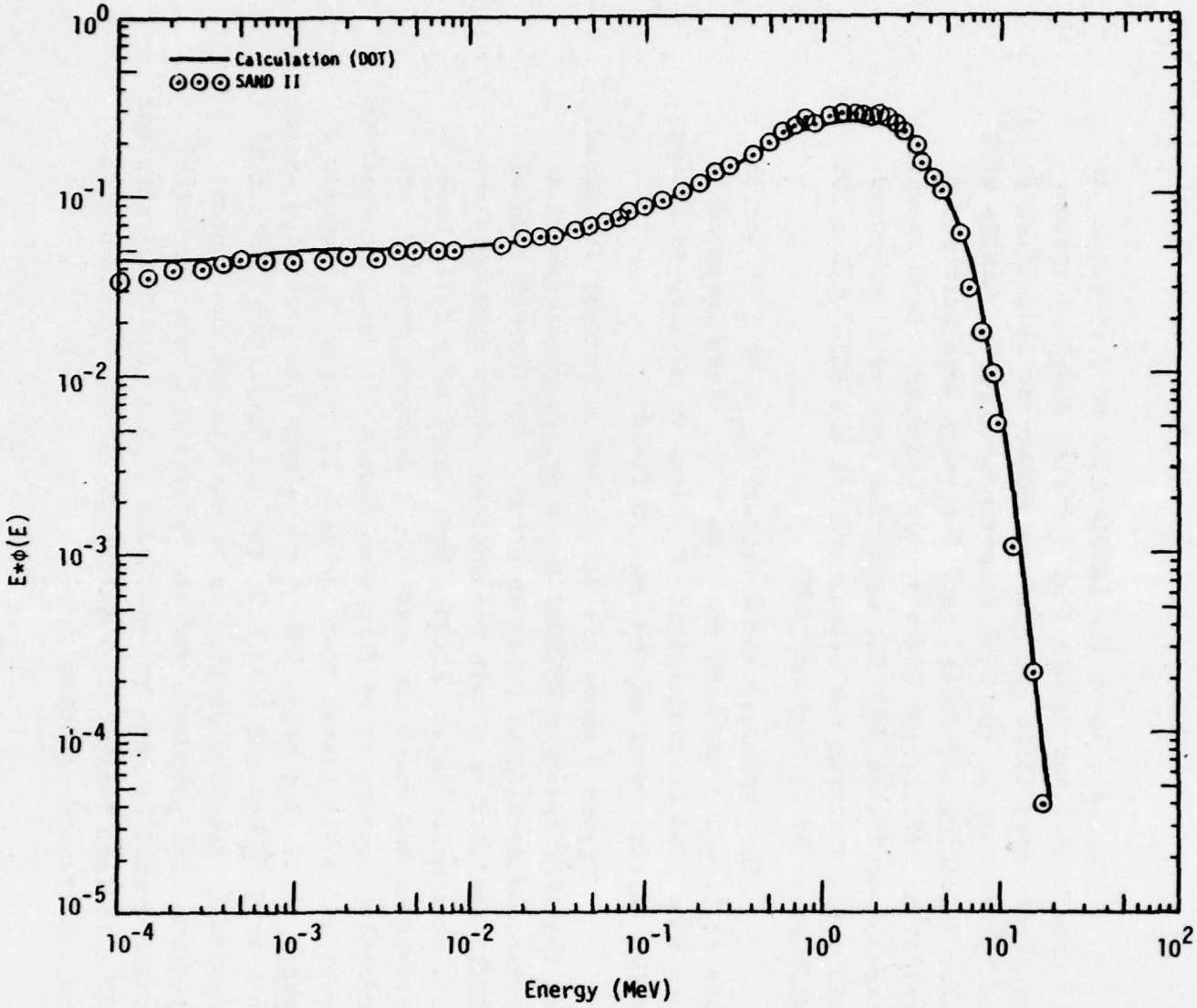

Figure 3. SANDIA ACPR Core. SAND II solution and trial spectrum (DOT calculation). Unfolded at SAI with SAI foils and detector, but with SANDIA detectors for short-lived activations.

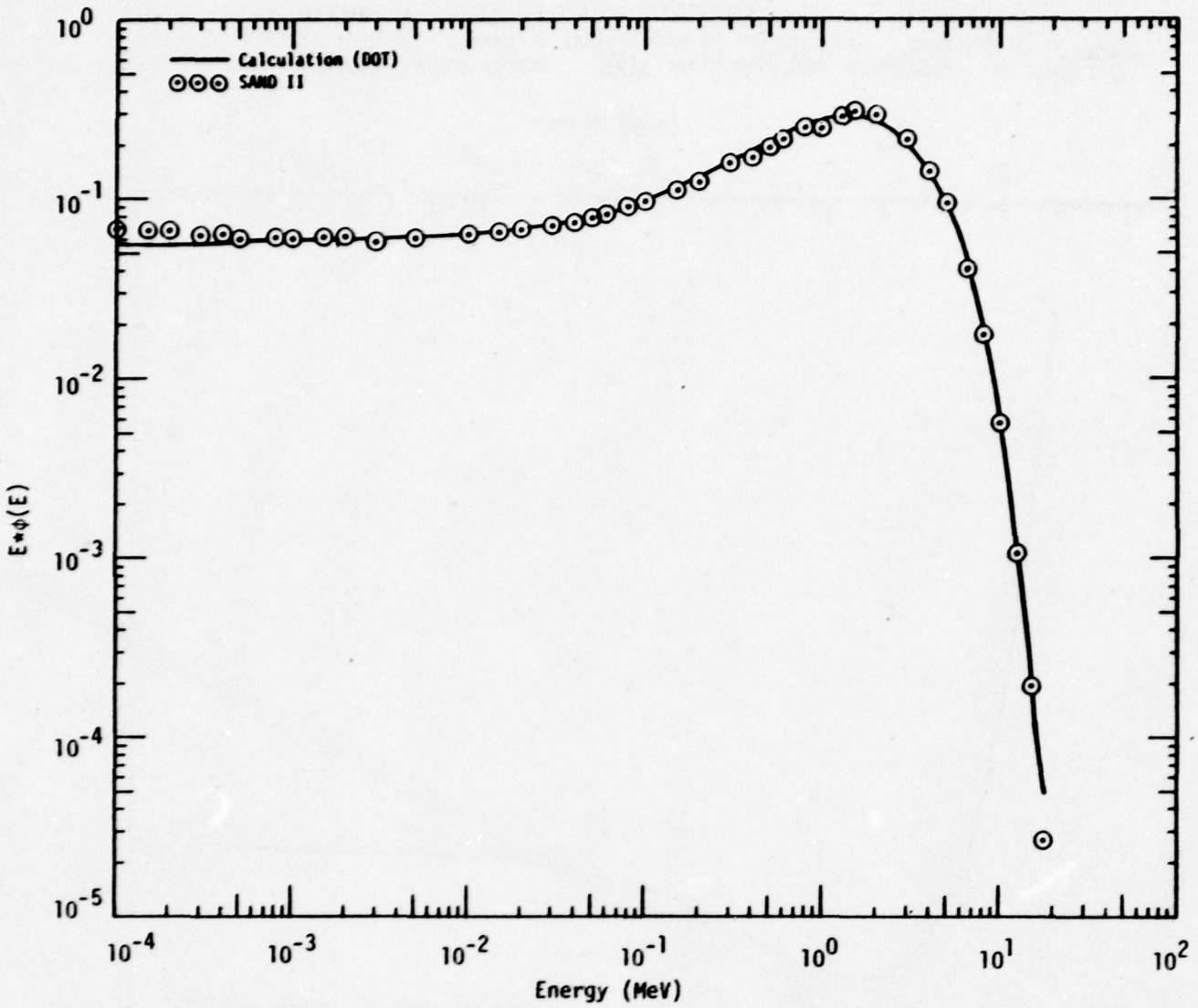

Figure 4. SANDIA ACPR Core. SAND II solution and trial spectrum (DOT calculation). Unfolded at SAI. Independent data with SANDIA foils and Ge(Li)detectors.

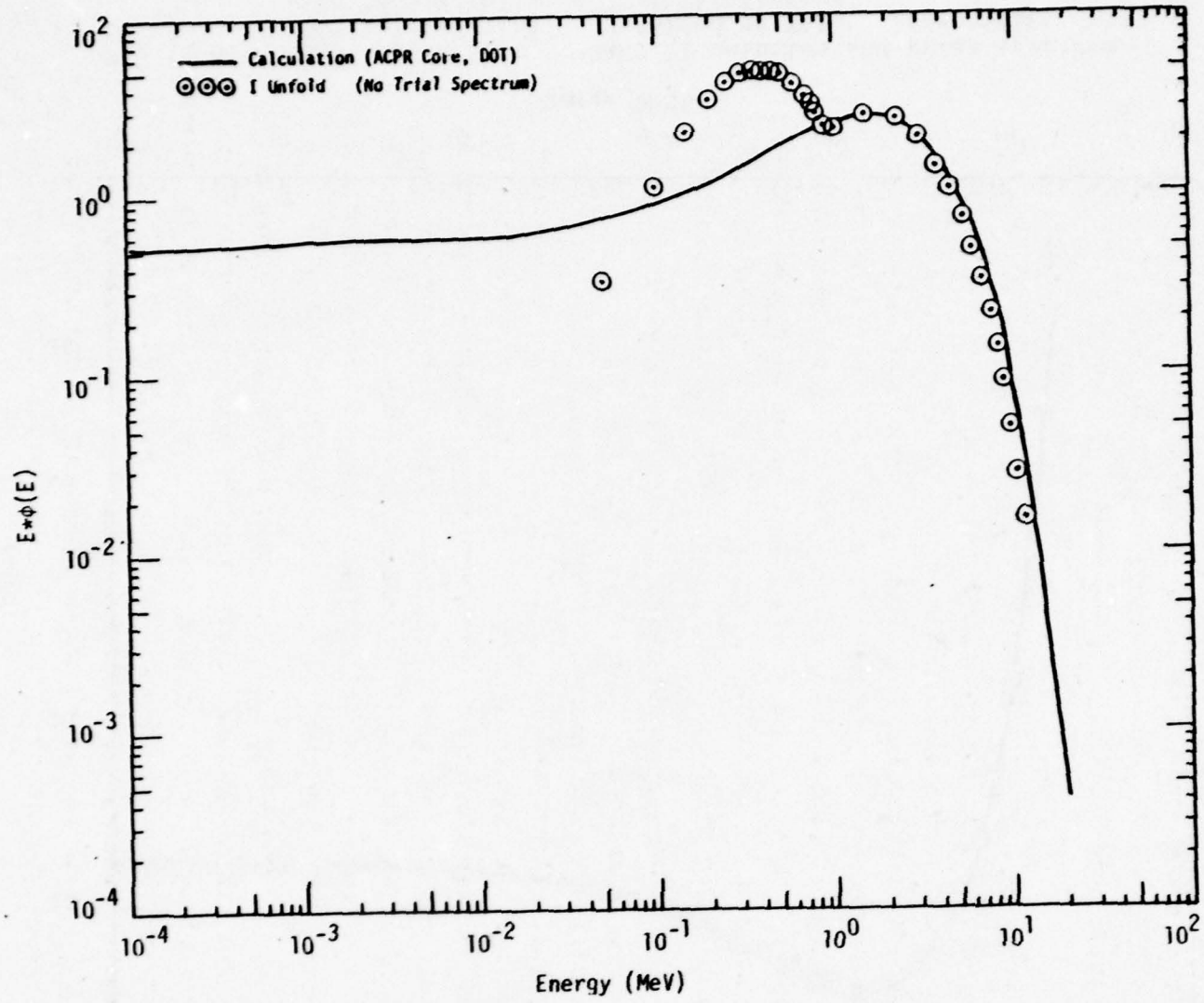

Figure 5. SANDIA ACPR Core. DOT calculation compared to IUNFOLD solution that was obtained without trial spectrum. Unfolded at SANDIA. This illustrates the need for the a priori data of a physically meaningful trial spectrum, especially below 1 MeV where few thresholds are available.

Figures 6 and 7 show the Northrop reactor spectrum just outside the boral wall in the exposure room adjacent to the reactor core. The shape factors ϕ_{eq}/ϕ are 1.18 and 1.10 for the data of Figure 6 (¼" boral next to the reactor core) and Figure 7 (¼" boral, 2" lead).

In Figure 8, the SPRII free field spectrum was passed through a 10-cm thick slab of polyethylene. This results in a highly moderated component below 1 MeV with the spectral shape looking much like that for a TRIGA reactor. However, careful examination shows that above 1 MeV the filtering has produced a harder spectrum due to the falling off of the C and H cross sections with increasing energy. This is seen by the larger value of ϕ_{eq}/ϕ, being equal to 1.38 which is much larger than the values of 1.03 to 1.18 for the four ACPR-core and TRIGA-leakage spectra.

A greatly distorted spectrum is shown in Figure 9. This was achieved with a 10-cm thick iron "filter". The inelastic scattering cross section is quite large for iron at just below 1 MeV and on up, which depletes the spectrum at high eneriges and builds it up a bit just above the 0.2 MeV "damage threshold" level where the silicon-damage cross section first becomes large. As a result, the neutrons above the 0.2 MeV "threshold" produce less damage, on the average. This is seen by the lowest value of ϕ_{eq}/ϕ observed for all these runs: i.e., $\phi_{eq}/\phi = 0.99$ (see Table 2 below).

The SPRII and APRF glory hole spectra, shown in Figures 10 and 11 respectively, have by far the hardest spectrum below 1 MeV. Yet, the respective ϕ_{eq}/ϕ values for these two spectra are 1.16 and 1.19; very much like the TRIGA reactor spectra. This is due to a very soft spectrum <u>above 1 MeV</u> which is due to the flux peaking at the core (glory hole) of the reactor. The neutrons reaching the glory hole

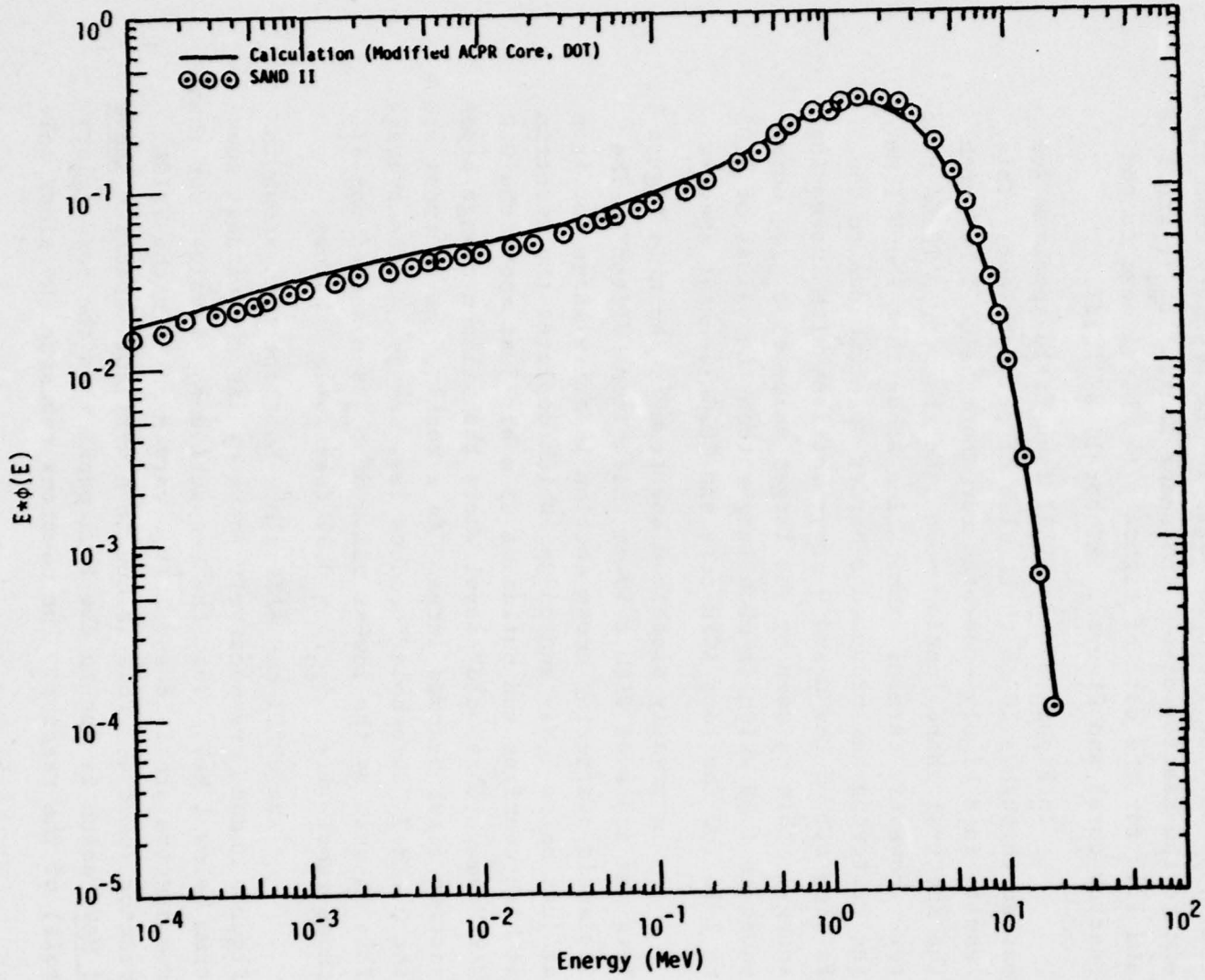

Figure 6. Northrop TRIGA, ¼-in Boral. SAND II solution and trial spectrum (1 DF calculation modified by boral absorption below 10^{-2} MeV).

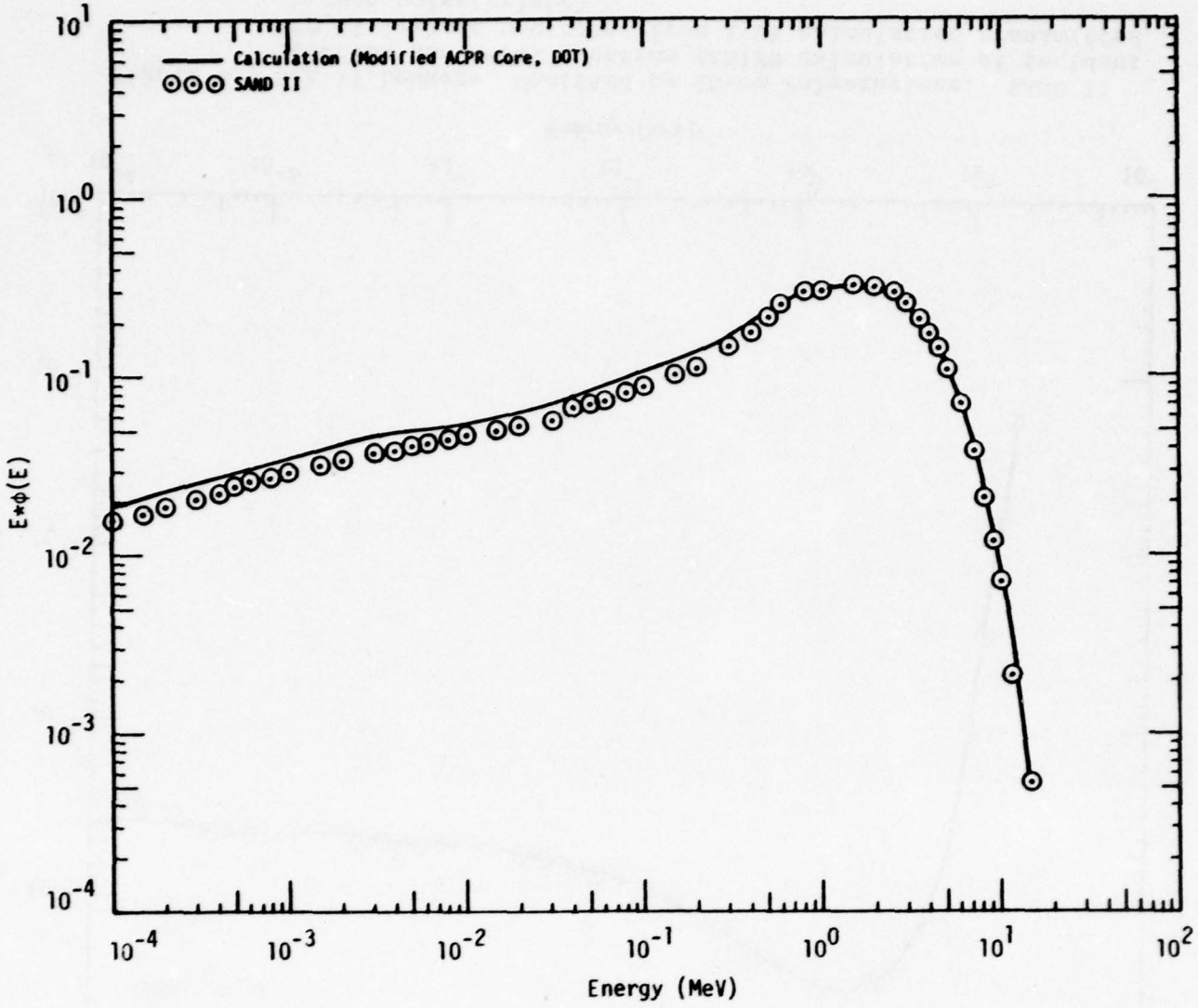

Figure 7. Northrop TRIGA, ½-in Boral and 2-in Lead. SAND II solution and trial spectrum (1 DF calculation modified by boral absorption below 10^{-2} MeV).

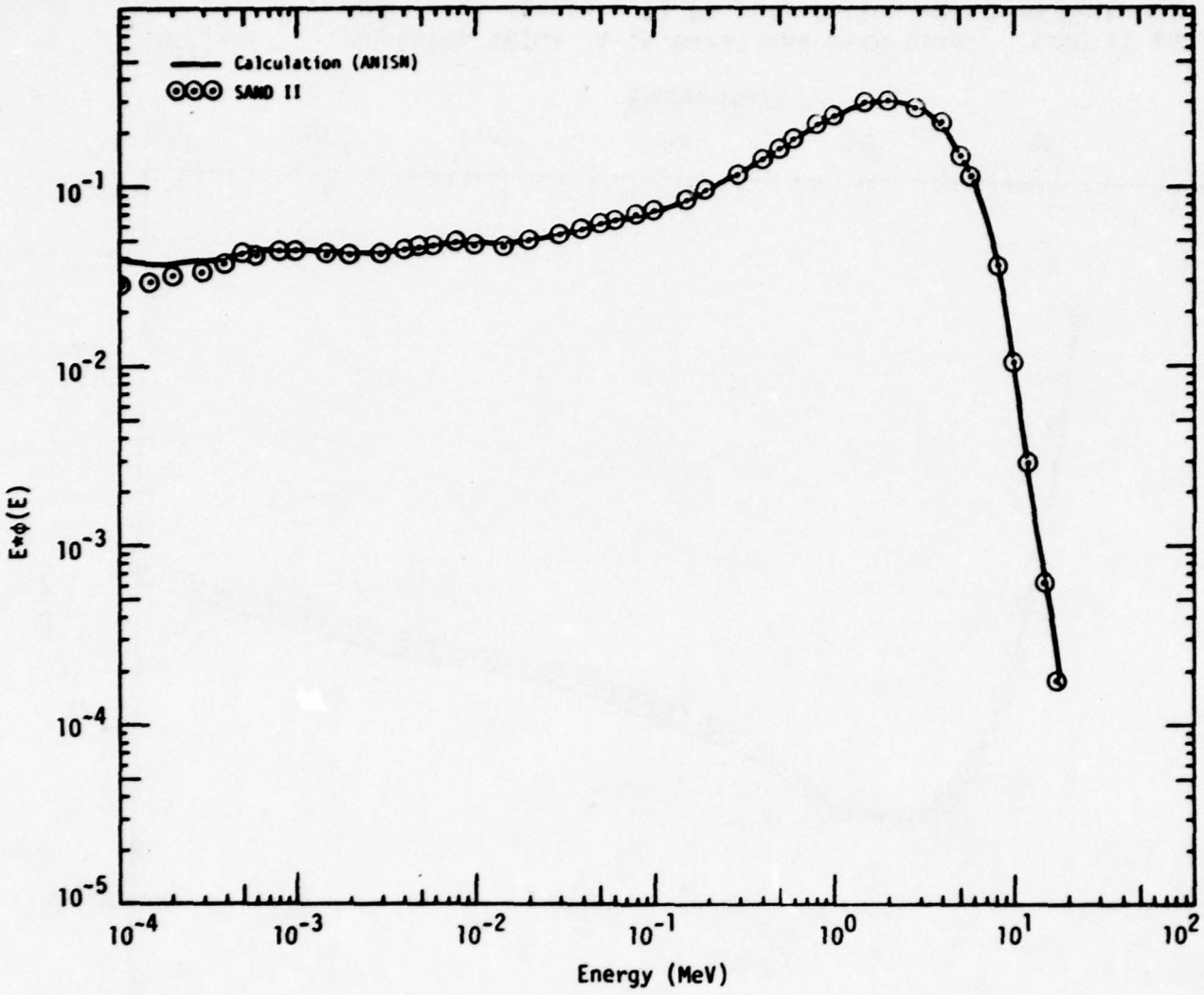

Figure 8. SPR II Leakage, Modified by 10-cm Polyethylene. SAND II solution and trial spectrum (ANISN calculation of incident SPR II leakage neutrons, from 1 DF calculation transmitted through polyethylene).

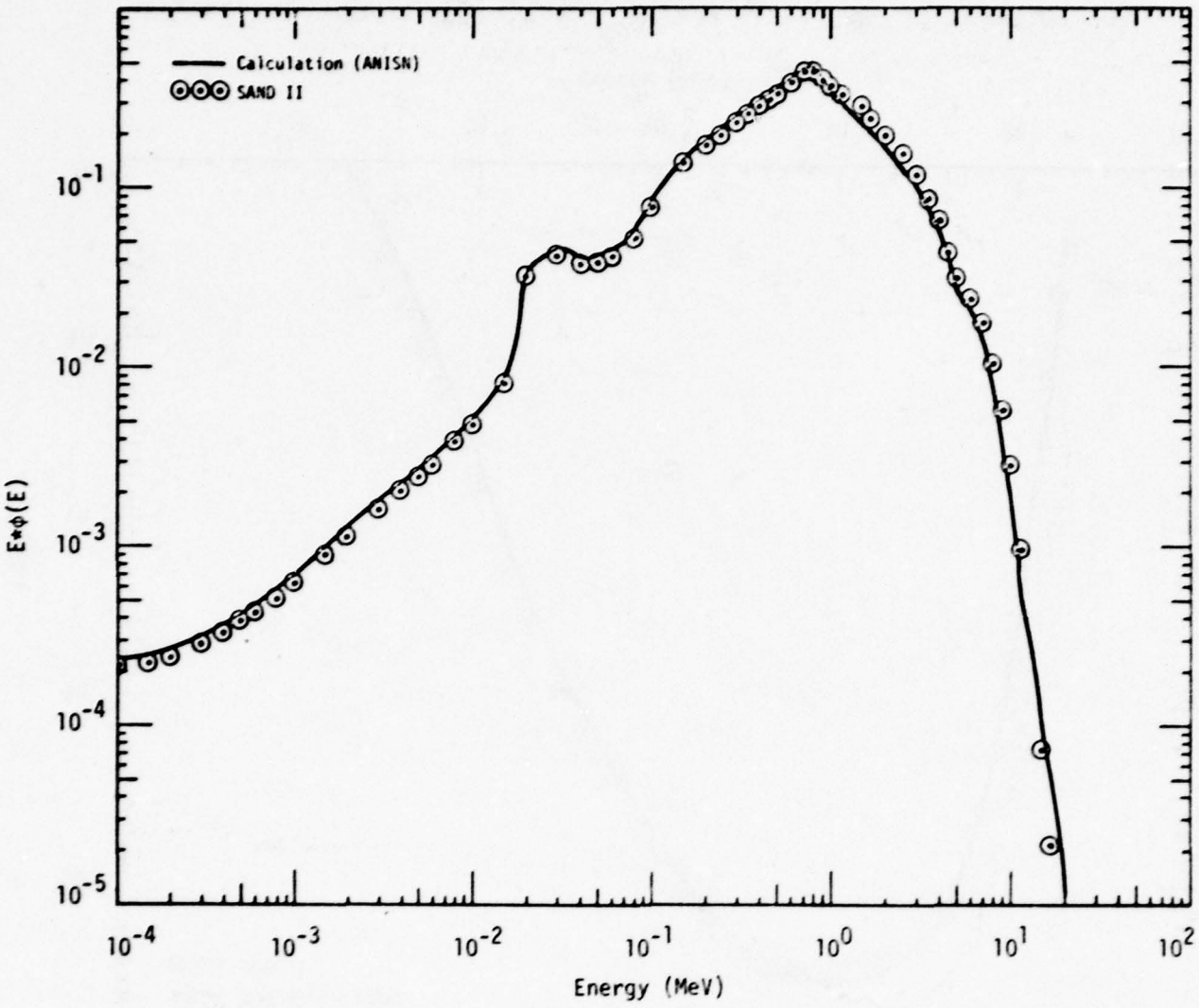

Figure 9. SPR II Leakage, Modified by 5-cm Iron. SAND II solution and trial spectrum (ANISN calculation of incident SPR II leakage neutrons, from 1 DF calculation, transmitted through iron).

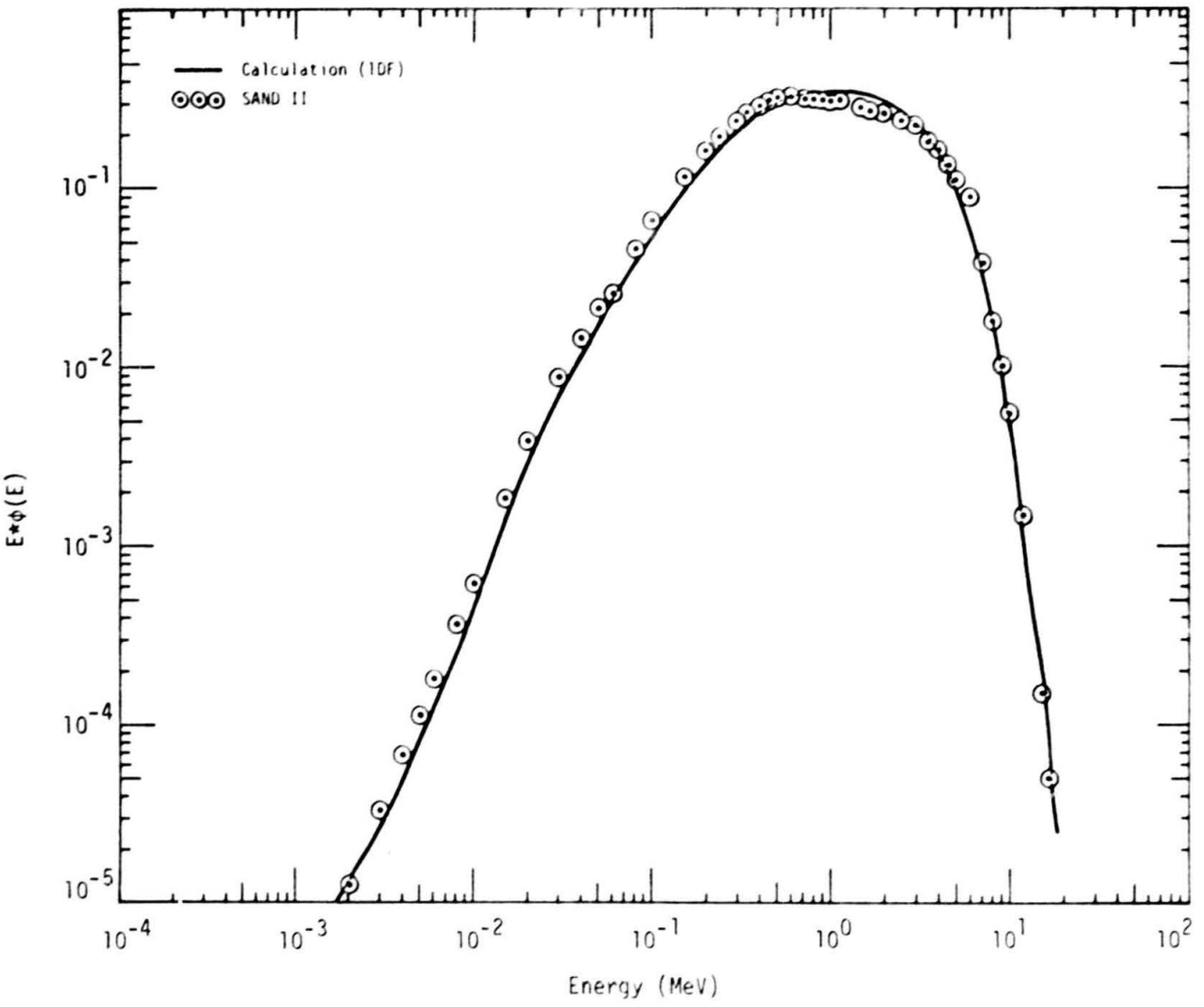

Figure 10. SPR II Glory Hole. Steady state SAND II solution and trial spectrum (1 DF calculation).

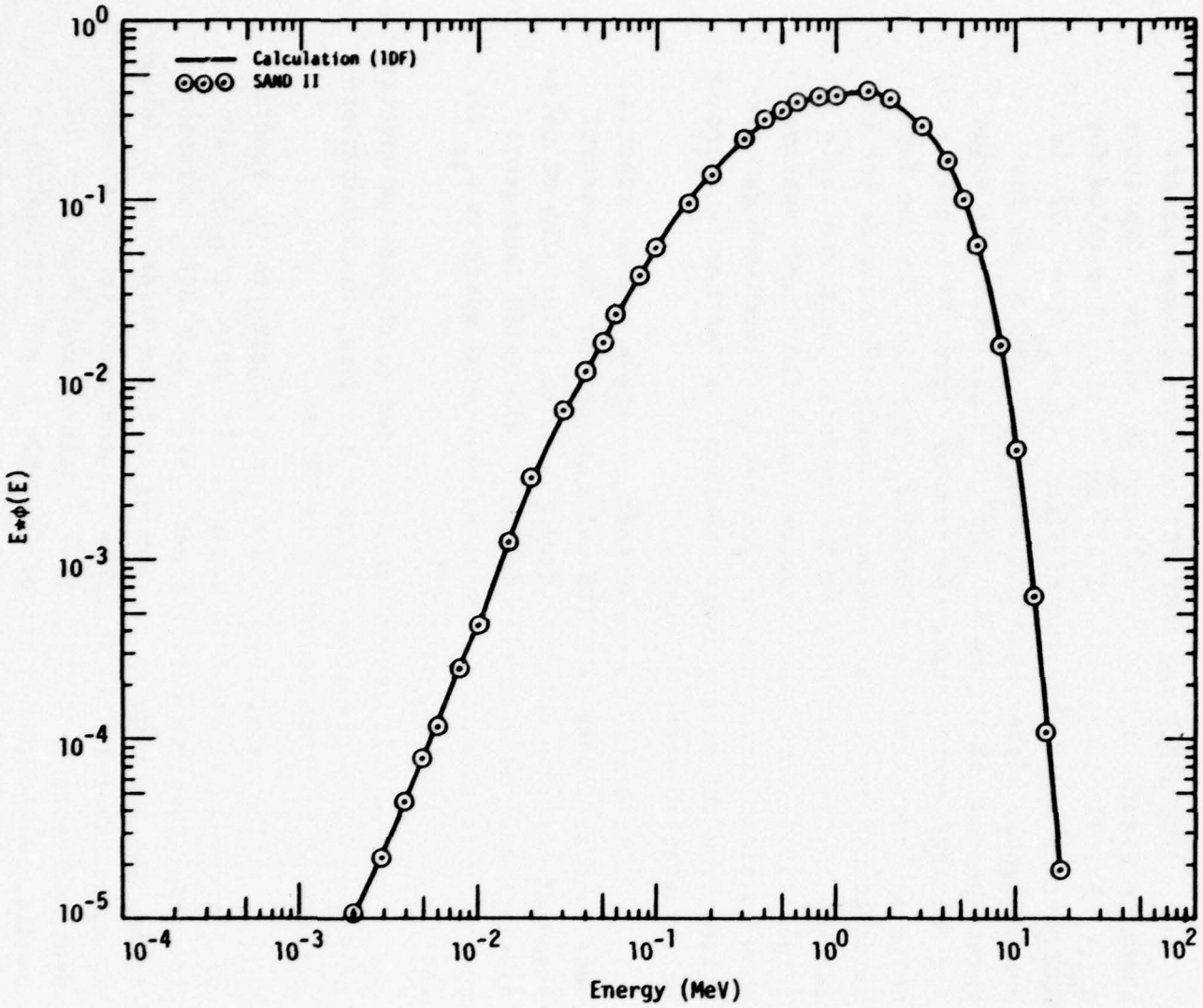

Figure 11. APRF Glory Hole. SAND II solution and trial spectrum (1 DF calculation).

have, on the average, passed through the least material of any of the neutron fields encountered in this series.

The SPRII and APRF FBR reactor leakage spectra shown in Figures 3, 13, 14, 15, and 16, yielded respective ϕ_{eq}/ϕ of 1.35, 1.42, 1.19, 1.42, and 1.41. The value for SPRII steady state spectrum of Figure 13, ϕ_{eq}/ϕ = 1.42, is only slightly higher than the value of 1.35 for the fast burst spectrum of Figure 12. On the other hand, the value for the APRF steady state spectrum of Figure 14 is only 1.19, which is lower than the value of ϕ_{eq}/ϕ = 1.41 for the fast-burst counterpart. This value is nearly the same as for the leakage spectrum measured at the hardness assurance table (Figure 15). Thus, the measurements of fast-burst spectra show no clear difference in hardness or silicon-damage capability from the steady state counterparts, either in ϕ_{eq}/ϕ or or in detailed spectral shape.

It should be noted that the above leakage spectra were used as inputs to ANISN calculations for the spectral shape of neutrons emerging from the 10 cm thick slab of polyethylene and the 5-cm slab of iron: the ANISN (emergent) spectra were in each case used as the trial spectrum ϕ_{tr} for the polyethylene and iron filter.

The foil activation data used to obtain the spectra of Figures 3-16 are given in Table 3. Here, the run numbers correspond to those described in Table 2.

The unfolding outputs corresponding to the spectra of Figures 3, 4, and 6-16 are given in Table 4, along with the trial spectrum used for each SAND II unfolding operation. Again, the run numbers correspond to those described in Table 2, except that Run 13 in Table 4 corresponds to the independent ACPR core data (Figure 4) obtained from Hugh Scott of Sandia. Although not stated in Table 2, all FBR leakage spectra were with the FBR $\sim$1½ m above the floor except for Run 12 (6 m).

Table 3. Activations Used for SAND II Unfolding

FOIL	$E_{Thr.}$(MeV)	$\lambda(sec^{-1})$	RUN 1	RUN 2	RUN 3	RUN 4	RUN 5	RUN 6	RUN 7	RUN 8	RUN 9	RUN 10	RUN 11	RUN 12
Au(Cd)		2.976-6	1.40-15*	8.91-18	4.75-17	5.36-17	1.85-15	-	-	-	-	-	1.24-16	1.98-17
Au		2.976-6	9.96-18	-	9.12-18	-	-	-	2.00-17	2.01-17	3.35-17	-	-	-
U235	0.01		1.46-11	2.71-11	2.71-11	3.48-11	1.92-11	7.88-11	2.82-11	2.81-11	9.36-11	7.60-11	1.11-10	3.08-11
Np237	0.5		7.99-12	2.15-11	-	2.87-11	1.27-11	4.92-11	2.03-11	2.08-11	7.74-11	7.09-11	8.09-11	2.49-11
In115	1.0	4.279-5	-	-	1.07-16	1.73-16	7.89-17	2.23-16	1.17-16	1.06-16	-	-	-	1.19-16
U238	1.45		1.53-12	3.62-12	3.72-12	5.55-12	-	6.37-12	4.32-12	3.82-12	1.39-11	1.24-11	1.37-11	4.34-12
Th232	1.75		4.08-13	9.63-13	1.01-12	-	6.76-13	1.64-12	-	1.01-12	3.66-12	3.00-12	3.86-12	1.20-12
Fe54	2.2	2.648-8	-	-	-	-	-	-	-	-	-	-	9.70-20	3.09-20
Ni58	2.9	1.125-7	5.82-20	1.54-19	1.57-19	2.26-19	1.23-19	1.84-19	1.66-19	1.45-19	5.49-19	4.03-19	5.23-19	1.69-19
Mg24	6.3	1.284-5	9.39-20	2.30-19	2.31-19	3.28-19	2.88-19	3.55-19	3.56-19	2.62-19	7.92-19	5.30-19	7.45-19	2.47-19
Fe56	7.5	7.551-5	-	1.17-18	1.00-18	1.33-18	-	1.33-18	-	-	3.63-18	2.39-18	3.27-18	1.08-18
Al27	8.7	1.284-5	4.45-20	1.16-19	1.21-19	-	1.46-19	1.73-19	1.90-19	1.28-19	3.67-19	2.58-19	-	1.18-19
Zr90	14.0	2.456-6	1.54-21	3.25-21	-	5.11-21	-	3.35-21	9.33-21	7.62-21	8.82-21	5.53-21	1.18-20	3.65-21

*1.40-15 ≡ 1.40×10^{-15}

NOTE: (1) for all foils except Au(Cd), ^{10}B cover (1.65 g/cm^2) was used except for runs 2, 10, and 11.
(2) Nλ is given for non-fission foils; N is given for all fission foils.

Table 4A. Tabulated SAND II values of $E*\phi_{trial}$ and $E*\phi(E)$. E is in MeV and $\phi(E)$ is in neutrons per cm^2 per MeV. $\phi(E)$ is normalized to unit fluence above .01 MeV. The multiplier given in the last row may be used to obtain the absolute fluence for each corresponding run.

		RUN 1	RUN 13		RUN 7	RUN 8
E_n(MeV)	$E*\phi_{tr}$ [1]	$E*\phi(E)$	$E*\phi(E)$	$E*\phi_{tr}$ [2]	$E*\phi(E)$	$E*\phi(E)$
1.0-4	4.95-2	3.60-2	6.88-2	1.60-2	1.50-2	1.54-2
1.5-4	5.00-2	3.84-2	6.78-2	1.77-2	1.66-2	1.70-2
2.0-4	5.04-2	4.14-2	6.73-2	1.93-2	1.80-2	1.85-2
3.0-4	4.96-2	4.20-2	6.34-2	2.13-2	1.99-2	2.05-2
4.0-4	5.15-2	4.50-2	6.49-2	2.31-2	2.16-2	2.22-2
5.0-4	5.20-2	4.60-2	6.09-2	2.47-2	2.31-2	2.37-2
6.0-4	5.20-2	4.57-2	6.53-2	2.60-2	2.43-2	2.49-2
8.0-4	5.23-2	4.57-2	6.24-2	2.81-2	2.63-2	2.70-2
1.0-3	5.25-2	4.64-2	6.143-2	2.98-2	2.79-2	2.86-2
1.5-3	5.25-2	4.67-2	6.18-2	3.24-2	3.03-2	3.11-2
2.0-3	5.41-2	4.87-2	6.30-2	3.47-2	3.25-2	3.34-2
3.0-3	5.11-2	4.79-2	5.66-2	3.77-2	3.52-2	3.62-2
4.0-3	5.40-2	5.06-2	6.20-2	3.98-2	3.72-2	3.82-2
5.0-3	5.48-2	5.16-2	6.27-2	4.16-2	3.90-2	4.00-2
6.0-3	5.52-2	5.21-2	6.31-2	4.30-2	4.03-2	4.14-2
8.0-3	5.57-2	5.31-2	6.34-2	4.54-2	4.25-2	4.36-2
1.0-2	5.67-2	5.51-2	6.44-2	4.72-2	4.42-2	4.54-2
1.5-2	5.80-2	5.70-2	6.57-2	5.00-2	4.68-2	4.81-2
2.0-2	6.03-2	5.98-2	6.82-2	5.27-2	4.93-2	5.07-2
3.0-2	6.38-2	6.41-2	7.18-2	5.70-2	5.34-2	5.49-2
4.0-2	6.71-2	6.80-2	7.53-2	6.71-2	6.29-2	6.47-2
5.0-2	7.09-2	7.22-2	7.94-2	7.09-2	6.65-2	6.84-2
6.0-2	7.39-2	7.57-2	8.27-2	7.39-2	6.93-2	7.12-2
8.0-2	8.13-2	8.38-2	9.08-2	8.13-2	7.62-2	7.83-2
1.0-1	8.76-2	9.12-2	9.93-2	8.76-2	8.22-2	8.45-2
1.5-1	1.02-1	1.07-1	1.13-1	1.02-1	9.62-2	9.89-2
2.0-1	1.17-1	1.24-1	1.30-1	1.17-1	1.11-1	1.14-1
2.4-1	1.29-1	1.37-1	1.42-1	1.29-1	1.22-1	1.26-1
3.0-1	1.46-1	1.56-1	1.60-1	1.46-1	1.39-1	1.44-1
3.4-1	1.57-1	1.69-1	1.72-1	1.57-1	1.52-1	1.57-1
4.0-1	1.61-1	1.75-1	1.73-1	1.61-1	1.60-1	1.67-1
4.5-1	1.69-1	1.86-1	1.80-1	1.69-1	1.73-1	1.81-1
5.0-1	1.86-1	2.06-1	1.97-1	1.86-1	1.95-1	2.05-1
6.0-1	2.08-1	2.34-1	2.17-1	2.08-1	2.26-1	2.39-1
7.2-1	2.31-1	2.63-1	2.40-1	2.31-1	2.58-1	2.72-1
8.0-1	2.41-1	2.76-1	2.54-1	2.41-1	2.73-1	2.87-1
9.2-1	2.36-1	2.71-1	2.48-1	2.36-1	2.71-1	2.84-1
1.0	2.34-1	2.69-1	2.48-1	2.34-1	2.72-1	2.82-1
1.2	2.51-1	2.90-1	2.74-1	2.51-1	2.99-1	3.05-1
1.5	2.57-1	3.05-1	3.14-1	2.57-1	3.25-1	3.22-1
1.7	2.58-1	3.03-1	3.14-1	2.58-1	3.30-1	3.20-1
2.0	2.47-1	2.92-1	3.00-1	2.47-1	3.19-1	3.07-1
2.5	2.32-1	2.72-1	2.60-1	2.32-1	3.02-1	2.87-1
3.0	1.98-1	2.32-1	2.18-1	1.98-1	2.61-1	2.45-1
3.5	1.61-1	1.89-1	1.81-1	1.61-1	2.13-1	2.00-1
4.0	1.35-1	1.56-1	1.44-1	1.35-1	1.80-1	1.66-1
4.5	1.13-1	1.30-1	1.19-1	1.13-1	1.51-1	1.39-1
5.0	9.23-2	1.06-1	9.51-2	9.23-2	1.24-1	1.13-1
6.0	5.85-2	6.16-2	5.51-2	5.85-2	8.08-2	6.84-2
7.0	3.55-2	3.14-2	3.08-2	3.50-2	5.03-2	3.71-2
8.0	2.10-2	1.75-2	1.73-2	2.10-2	2.97-2	2.10-2
9.0	1.22-2	1.01-2	1.01-2	1.22-2	1.77-2	1.22-2
10.0	6.94-3	5.72-3	5.70-3	6.94-3	1.01-2	6.94-3
12.0	2.12-3	1.74-3	1.73-3	2.12-3	3.11-3	2.11-3
15.0	3.16-4	2.34-4	1.97-4	3.16-4	6.23-4	5.14-4
17.0	8.07-5	5.96-5	5.01-5	8.07-5	1.60-4	1.33-4
(Multiplier)	-	(9.38+12)	(5.05+14)	-	(2.18+13)	(2.16+13)

1. ϕ_{tr} = ACPR core (DOT)

2. ϕ_{tr} = ACPR core modified below 3×10^{-2} MeV by boral attenuation

NOTE: Run numbers correspond to Table 2 except Run 13 is SANDIA independent foil data for ACPR

Table 4B. Tabulated SAND II values of $E*\phi_{trial}$ and $E*\phi(E)$. E is in MeV and $\phi(E)$ is in neutrons per cm^2 per MeV. $\phi(E)$ is normalized to unit fluence above .01 MeV. The multiplier given in the last row may be used to obtain the absolute fluence for each corresponding run.

		RUN 3	RUN 4	RUN 9	RUN 11		RUN 12
E_n(MeV)	$E*\phi_{tr}$ [3]	$E*\phi(E)$	$E*\phi(E)$	$E*\phi(E)$	$E*\phi(E)$	$E*\phi_{tr}$ [4]	$E*\phi(E)$
1.0-4	1.29-8	3.88-4	3.50-4	4.53-4	3.28-4	3.80-9	1.12-4
1.5	1.32-8	4.00-4	3.60-4	4.73-4	3.27-4	4.24-9	1.16-4
2.0	1.40-8	4.27-4	3.80-4	4.98-4	3.47-4	4.39-9	1.23-4
3.0	1.48-8	4.62-4	4.04-4	5.33-4	3.63-4	4.74-9	1.31-4
4.0	1.56-8	4.94-4	4.25-4	5.57-4	3.88-4	5.07-9	1.39-4
5.0	1.63-8	5.21-4	4.43-4	5.68-4	4.23-4	5.38-9	1.50-4
6.0	1.68-8	5.48-4	4.58-4	6.01-4	4.16-4	5.63-9	1.52-4
8.0	1.88-8	6.27-4	5.11-4	6.75-4	4.58-4	6.58-9	1.70-4
1.0-3	2.05-8	6.94-4	5.58-4	7.34-4	5.04-4	7.18-9	1.89-4
1.5	2.39-8	8.27-4	6.51-4	8.55-4	5.91-4	8.60-9	2.26-4
2.0	2.69-8	9.47-4	7.33-4	9.58-4	6.72-4	9.82-9	2.66-4
3.0	3.30-8	1.16-3	9.00-4	1.15-3	8.56-4	1.35-8	3.72-4
4.0	3.85-8	1.37-3	1.05-3	1.35-3	9.95-4	1.67-8	4.45-4
5.0	4.34-8	1.55-3	1.19-3	1.52-3	1.13-3	2.00-8	5.22-4
6.0	5.01-8	1.80-3	1.37-3	1.75-3	1.31-3	2.51-8	6.23-4
8.0	6.35-8	2.27-3	1.73-3	2.20-3	1.67-3	3.49-8	8.49-4
1.0-2	7.63-8	2.71-3	2.08-3	2.62-3	2.03-3	4.58-8	1.12-3
1.5	1.21-7	4.31-3	3.32-3	4.14-3	3.27-3	7.74-8	1.96-3
2.0	1.72-7	6.10-3	4.71-3	5.84-3	4.66-3	1.14-7	3.00-3
3.0	2.87-7	1.01-2	7.85-3	9.64-3	7.84-3	2.01-7	5.47-3
4.0	4.13-7	1.44-2	1.13-2	1.38-2	1.14-2	3.06-7	8.35-3
5.0	5.51-7	1.91-2	1.51-2	1.83-2	1.52-2	4.44-7	1.15-2
6.0	7.14-7	2.47-2	1.95-2	2.37-2	1.98-2	5.96-7	1.55-2
8.0	1.08-6	3.71-2	2.95-2	3.55-2	3.00-2	9.50-7	2.43-2
1.0-1	1.50-6	5.13-2	4.11-2	4.92-2	4.21-2	1.37-6	3.59-2
1.5	2.71-6	9.20-2	7.42-2	8.82-2	7.62-2	2.55-6	6.82-2
2.0	3.97-6	1.34-1	1.09-1	1.29-1	1.12-1	3.85-6	1.03-1
2.4	5.10-6	1.71-1	1.40-1	1.64-1	1.44-1	5.10-6	1.36-1
3.0	6.68-6	2.23-1	1.83-1	2.14-1	1.90-1	6.68-6	1.85-1
3.4	7.69-6	2.55-1	2.10-1	2.44-1	2.18-1	7.69-6	2.17-1
4.0	8.72-6	2.85-1	2.38-1	2.71-1	2.48-1	8.72-6	2.52-1
4.5-1	1.51-6	3.07-1	2.58-1	2.90-1	2.70-1	9.51-6	2.80-1
5.0	1.03-5	3.28-1	2.80-1	3.09-1	2.91-1	1.03-5	3.06-1
6.0	1.15-5	3.50-1	3.10-1	3.29-1	3.23-1	1.15-5	3.45-1
7.2	1.22-5	3.50-1	3.31-1	3.36-1	3.44-1	1.22-5	3.68-1
8.0	1.26-5	3.45-1	3.41-1	3.40-1	3.53-1	1.26-5	3.71-1
9.2	1.30-5	3.38-1	3.52-1	3.43-1	3.61-1	1.30-5	3.74-1
1.0	1.28-5	3.18-1	3.49-1	3.35-1	3.56-1	1.28-5	3.57-1
1.2	1.31-5	3.09-1	3.60-1	3.37-1	3.63-1	1.31-5	3.51-1
1.5	1.30-5	3.03-1	3.62-1	3.29-1	3.55-1	1.30-5	3.52-1
1.7	1.26-5	2.81-1	3.53-1	3.16-1	3.39-1	1.26-5	3.25-1
2.0	1.20-5	2.73-1	3.37-1	3.00-1	3.23-1	1.20-5	3.12-1
2.5	1.07-5	2.52-1	3.04-1	2.69-1	2.88-1	1.07-5	2.79-1
3.0	9.17-6	2.33-1	2.64-1	2.33-1	2.48-1	9.17-6	2.49-1
3.5	7.70-6	1.95-1	2.21-1	1.95-1	2.11-1	7.70-6	2.21-1
4.0	6.38-6	1.71-1	1.85-1	1.63-1	1.75-1	6.38-6	1.89-1
4.5	5.08-6	1.39-1	1.47-1	1.30-1	1.39-1	5.08-6	1.53-1
5.0	4.08-6	1.11-1	1.17-1	1.05-1	1.11-1	4.08-6	1.22-1
6.0	2.47-6	6.05-2	6.62-2	6.11-2	6.10-2	2.47-6	6.59-2
7.0	1.40-6	3.39-2	3.63-2	3.24-2	3.18-2	1.40-6	3.43-2
8.0	7.79-7	1.86-2	2.01-2	1.76-2	1.69-2	7.79-7	1.83-2
9.0	4.01-7	1.02-2	1.03-2	9.11-3	8.69-3	4.01-7	9.64-3
10.0	2.14-7	5.53-3	5.49-3	4.85-3	4.61-3	2.14-7	5.15-3
12.0	5.91-8	1.54-3	1.51-3	1.34-3	1.26-3	5.91-8	1.42-3
15.0	8.74-9	2.25-4	2.44-4	1.46-4	2.08-4	8.74-9	2.10-4
17.0	2.23-9	5.60-5	6.23-5	3.71-5	5.32-5	2.23-9	5.36-5
(Multiplier)	-	(2.35+13)	(2.96+13)	(8.41+13)	(7.86+13)	-	(2.46+13)

3. ϕ_{tr} = FBR leakage, FBR 1-1/2 m above floor (1DF calculation)

4. ϕ_{tr} = FBR leakage, FBR 6 m above floor (1DF calculation)

Table 4C. Tabulated SAND II values of $E*\phi_{trial}$ and $E*\phi(E)$. E is in MeV and $\phi(E)$ is in neutrons per cm^2 per MeV. $\phi(E)$ is normalized to unit fluence above .01 MeV. The multiplier given in the last row may be used to obtain the absolute fluence for each corresponding run.

		RUN 5		RUN 6		RUN 2	RUN 10
E_n(Mev)	$E*\phi_{tr}$ [5]	$E*\phi(E)$	$E*\phi_{tr}$ [6]	$E*\phi(E)$	$E*\phi_{tr}$ [7]	$E*\phi(E)$	$E*\phi(E)$
1.0-4	2.34-1	2.90-2	6.71-3	2.13-4	2.57-11	1.62-8	1.15-8
1.5	2.27-1	2.86-2	7.14-3	2.26-4	5.82-11	3.74-8	2.61-8
2.0	2.26-1	3.00-2	7.54-3	2.39-4	1.03-10	6.57-8	4.59-8
3.0	2.30-1	3.20-2	8.95-3	2.84-4	2.33-10	1.50-7	1.04-7
4.0	2.39-1	3.59-2	1.06-2	3.37-4	4.13-10	2.65-7	1.85-7
5.0	2.47-1	4.01-2	1.22-2	3.86-4	6.42-10	3.98-7	2.87-7
6.0	2.53-1	3.97-2	1.36-2	4.30-4	9.29-10	5.95-7	4.16-7
8.0	2.63-1	4.15-2	1.61-2	5.11-4	1.92-9	1.24-6	8.57-7
1.0-3	2.58-1	4.20-2	1.96-2	6.21-4	3.38-9	2.17-6	1.51-6
1.5	2.47-1	4.09-2	2.82-2	8.94-4	9.60-9	6.16-6	4.30-6
2.0	2.43-1	4.12-2	3.65-2	1.16-3	1.97-8	1.26-5	8.82-6
3.0	2.54-1	4.38-2	5.09-2	1.61-3	5.42-8	3.37-5	2.43-5
4.0	2.63-1	4.55-2	6.44-2	2.04-3	1.10-7	6.82-5	4.91-5
5.0	2.72-1	4.71-2	7.75-2	2.45-3	1.88-7	1.17-4	8.42-5
6.0	2.77-1	4.80-2	9.08-2	2.88-3	2.92-7	1.81-4	1.31-4
8.0	2.80-1	4.86-2	1.20-1	3.80-3	5.85-7	3.59-4	2.62-4
1.0-2	2.82-1	4.91-2	1.49-1	4.72-3	1.00-6	6.05-4	4.49-4
1.5	2.85-1	4.97-2	2.52-1	7.98-3	2.97-6	1.78-3	1.33-3
2.0	3.05-1	5.32-2	9.96-1	3.15-2	6.38-6	3.79-3	2.86-3
3.0	3.34-1	5.85-2	1.30+0	4.11-2	1.49-5	8.72-3	6.68-3
4.0	3.60-1	6.30-2	1.16+0	3.69-2	2.48-5	1.44-2	1.11-2
5.0	3.82-1	6.69-2	1.24+0	3.93-2	3.64-5	2.10-2	1.63-2
6.0	4.00-1	7.00-2	1.31+0	4.13-2	4.93-5	2.52-2	2.21-2
8.0	4.31-1	7.55-2	1.60+0	5.06-2	7.96-5	4.52-2	3.57-2
1.0-1	4.61-1	8.07-2	2.44+0	7.73-2	1.14-4	6.40-2	5.11-2
1.5	5.30-1	9.28-2	4.35+0	1.38-1	2.06-4	1.14-1	9.23-2
2.0	6.04-1	1.06-1	5.43+0	1.72-1	2.90-4	1.60-1	1.30-1
2.4	6.53-1	1.14-1	6.24+0	1.97-1	3.53-4	1.94-1	1.59-1
3.0	7.25-1	1.27-1	7.37+0	2.32-1	4.43-4	2.40-1	2.00-1
3.4	7.89-1	1.38-1	7.99+0	2.53-1	5.00-4	2.69-1	2.27-1
4.0	8.79-1	1.53-1	8.87+0	2.81-1	5.50-4	2.91-1	2.54-1
4.5-1	9.53-1	1.66-1	9.57+0	3.04-1	5.86-4	3.04-1	2.74-1
5.0	1.02+0	1.78-1	1.03+1	3.27-1	6.18-4	3.15-1	2.92-1
6.0	1.16+0	2.00-1	1.15+1	3.75-1	6.61-4	3.24-1	3.19-1
7.2	1.30+0	2.26-1	1.29+1	4.31-1	6.83-4	3.19-1	3.34-1
8.0	1.39+0	2.40-1	1.27+1	4.41-1	6.91-4	3.16-1	3.39-1
9.2	1.49+0	2.58-1	1.10+1	3.90-1	7.03-4	3.13-1	3.47-1
1.0	1.53+0	2.65-1	9.58+0	3.54-1	6.93-4	3.04-1	3.44-1
1.2	1.69	2.91-1	8.03+0	3.25-1	7.12-4	3.07-1	3.55-1
1.5	1.80	3.07-1	6.25+0	2.86-1	7.04-4	2.87-1	3.59-1
1.7	1.81	3.09-1	5.31+0	2.42-1	6.81-4	2.68-1	3.47-1
2.0	1.78	3.03-1	4.23+0	1.96-1	6.37-4	2.59-1	3.25-1
2.5	1.73	2.94-1	3.34+0	1.54-1	5.56-4	2.42-1	2.82-1
3.0	1.66	2.81-1	2.57+0	1.17-1	4.68-4	2.24-1	2.36-1
3.5	1.45	2.45-1	1.86+0	8.44-2	3.85-4	1.84-1	1.94-1
4.0	1.45	2.44-1	1.53+0	6.77-2	3.13-4	1.63-1	1.57-1
4.5	1.23	2.07-1	1.09+0	4.77-2	2.46-4	1.34-1	1.22-1
5.0	8.98-1	1.51-1	7.15-1	3.10-2	1.95-4	1.15-1	9.55-2
6.0	7.19-1	1.20-1	5.47-1	2.41-2	1.16-4	8.93-2	5.32-2
7.0	4.60-1	7.49-2	3.40-1	1.73-2	6.37-5	3.76-2	2.83-2
8.0	2.35-1	3.80-2	1.91-1	1.02-2	3.44-5	1.79-2	1.51-2
9.0	1.37-1	2.23-2	1.03-1	5.65-3	1.76-5	1.00-2	7.74-3
10.0	7.26-2	1.18-2	5.23-2	2.90-3	9.37-6	5.37-3	4.12-3
12.0	2.49-2	4.06-3	1.69-2	9.46-4	2.55-6	1.49-3	1.12-3
15.0	3.77-3	6.14-4	2.39-3	7.19-5	3.74-7	1.99-4	1.19-4
17.0	1.09-3	1.78-4	7.05-4	2.09-5	9.57-8	5.06-5	3.01-5
(Multiplier)	-	(1.33+13)	-	(6.52+13)	-	(2.19+13)	(6.53+13)

5. ϕ_{tr} = ANICN calculation of FBR leakage neutrons penetrating 10 cm polyethylene

6. ϕ_{tr} = ANICN calculation of FBR leakage neutrons penetrating 5 cm iron

7. ϕ_{tr} = Glory Hole spectrum (1DF calculation)

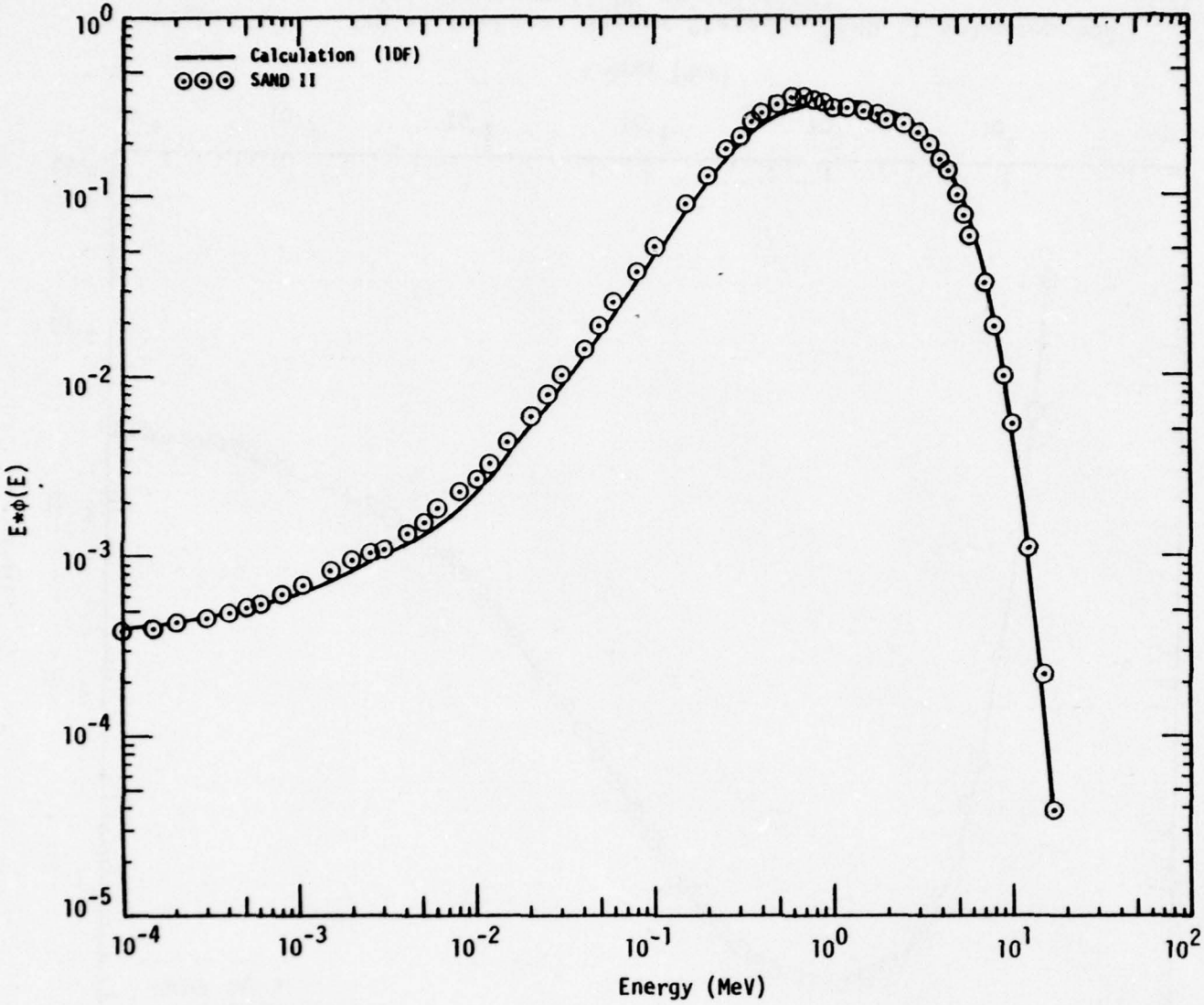

Figure 12. SPR II Leakage, Fast Burst. Sand II solution and trial spectrum (1 DF calculation).

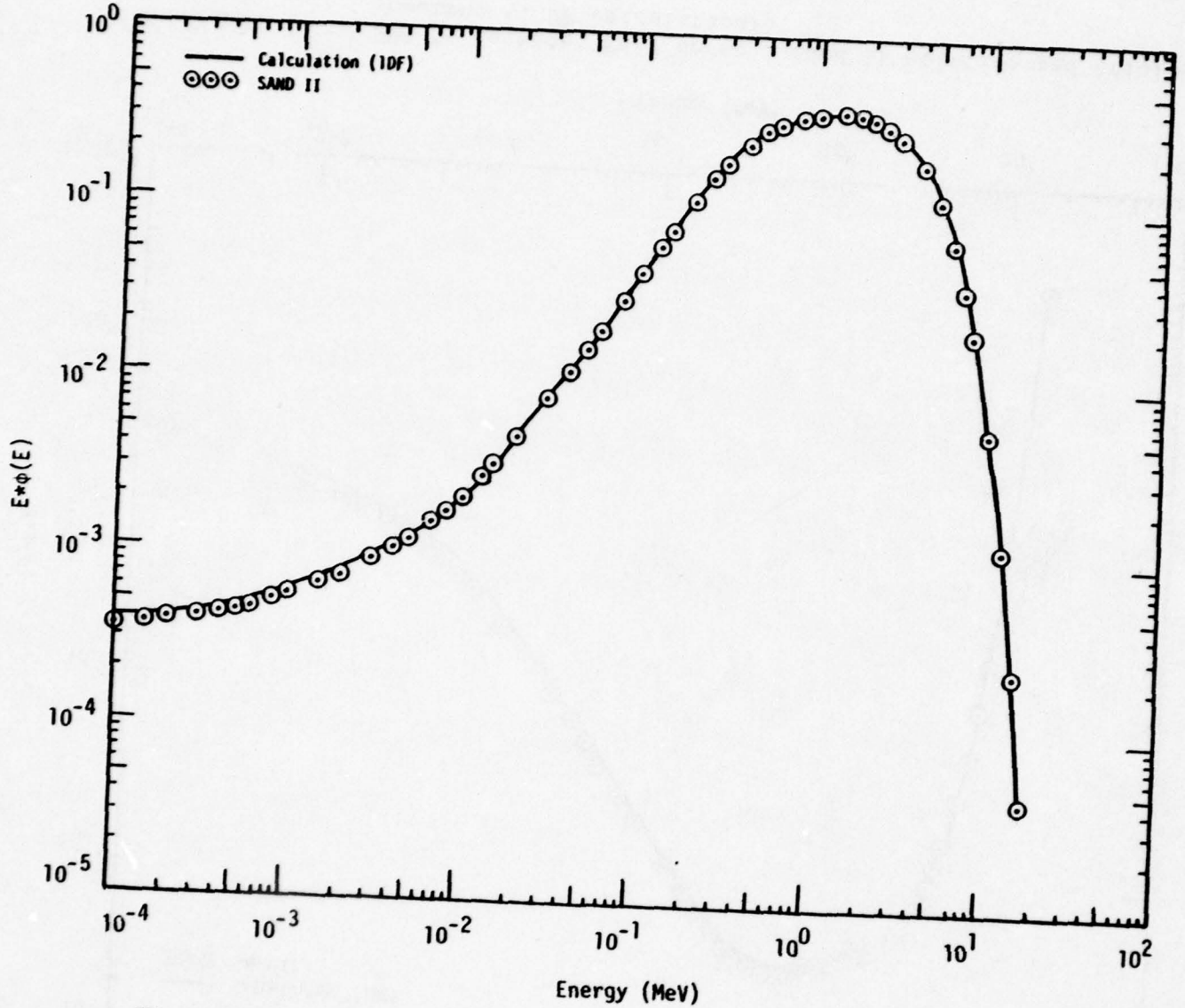

Figure 13. SPR II Leakage, Steady State. SAND II solution and trial spectrum (1 DF calculation).

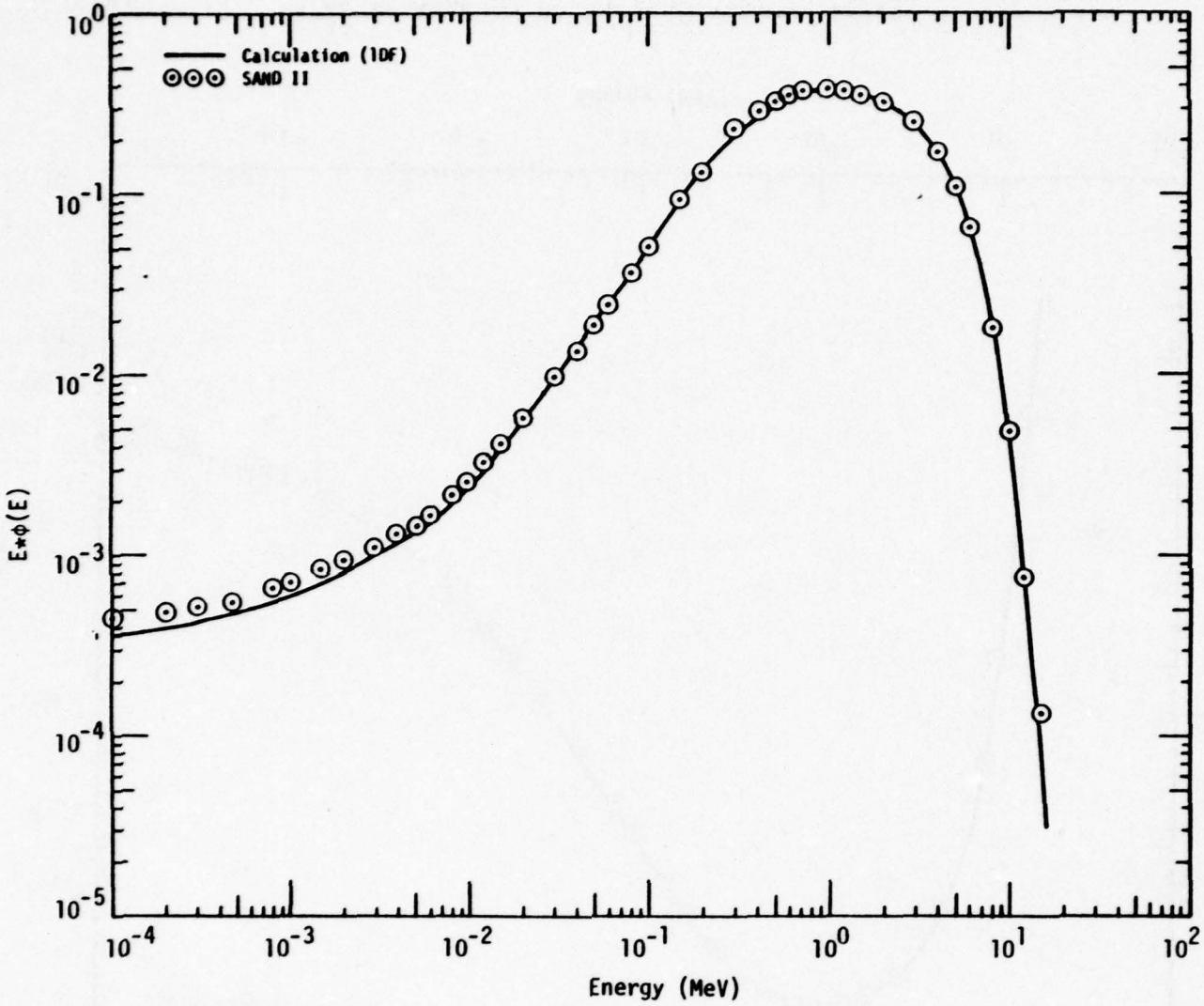

Figure 14. APRF Leakage Spectrum, Steady State.
SAND II solution and trial spectrum (1 DF calculation).

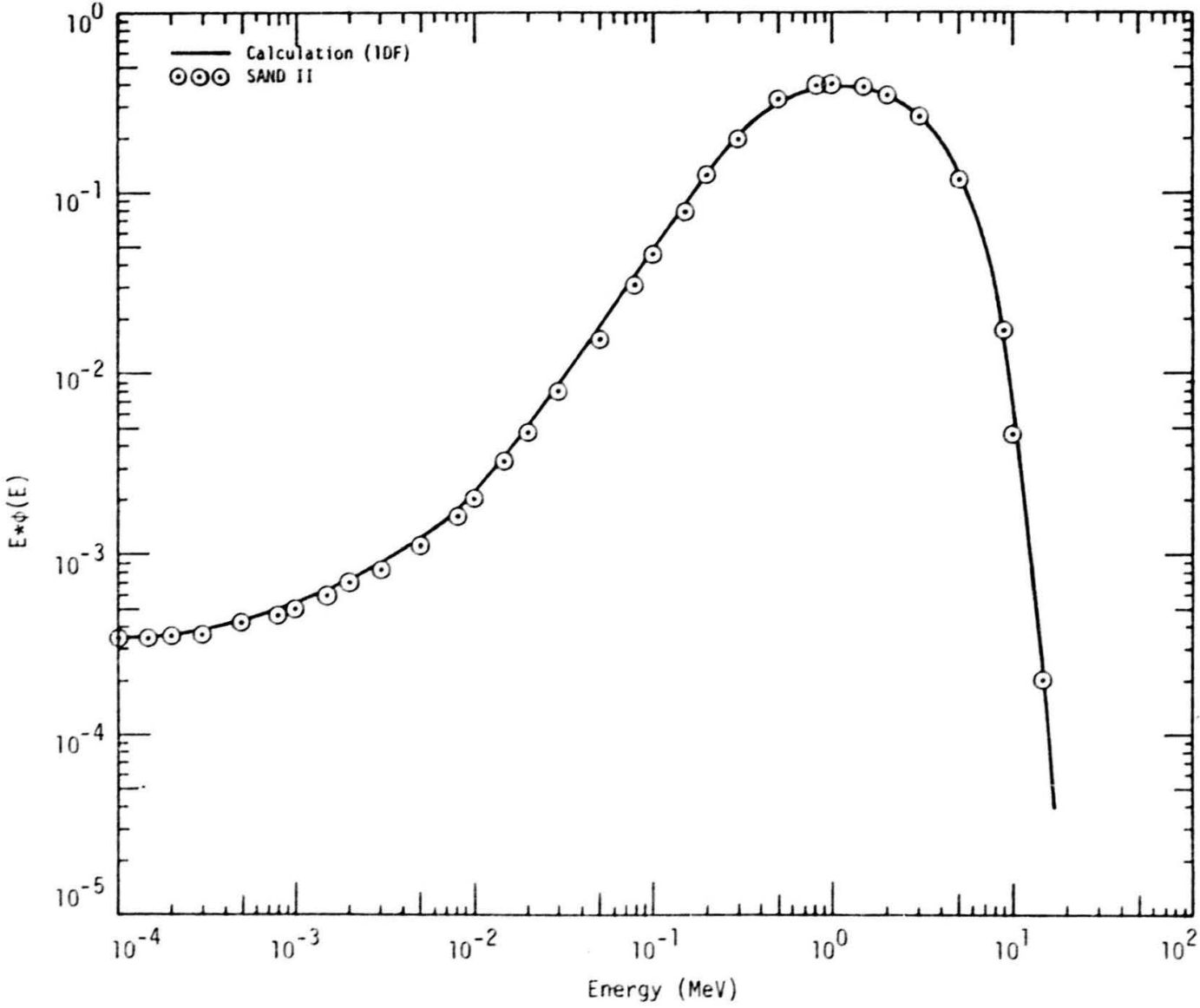

Figure 15. APRF Leakage on Hardness Assurance Table, Steady State. SAND II solution and trial spectrum (1 DF calculation).

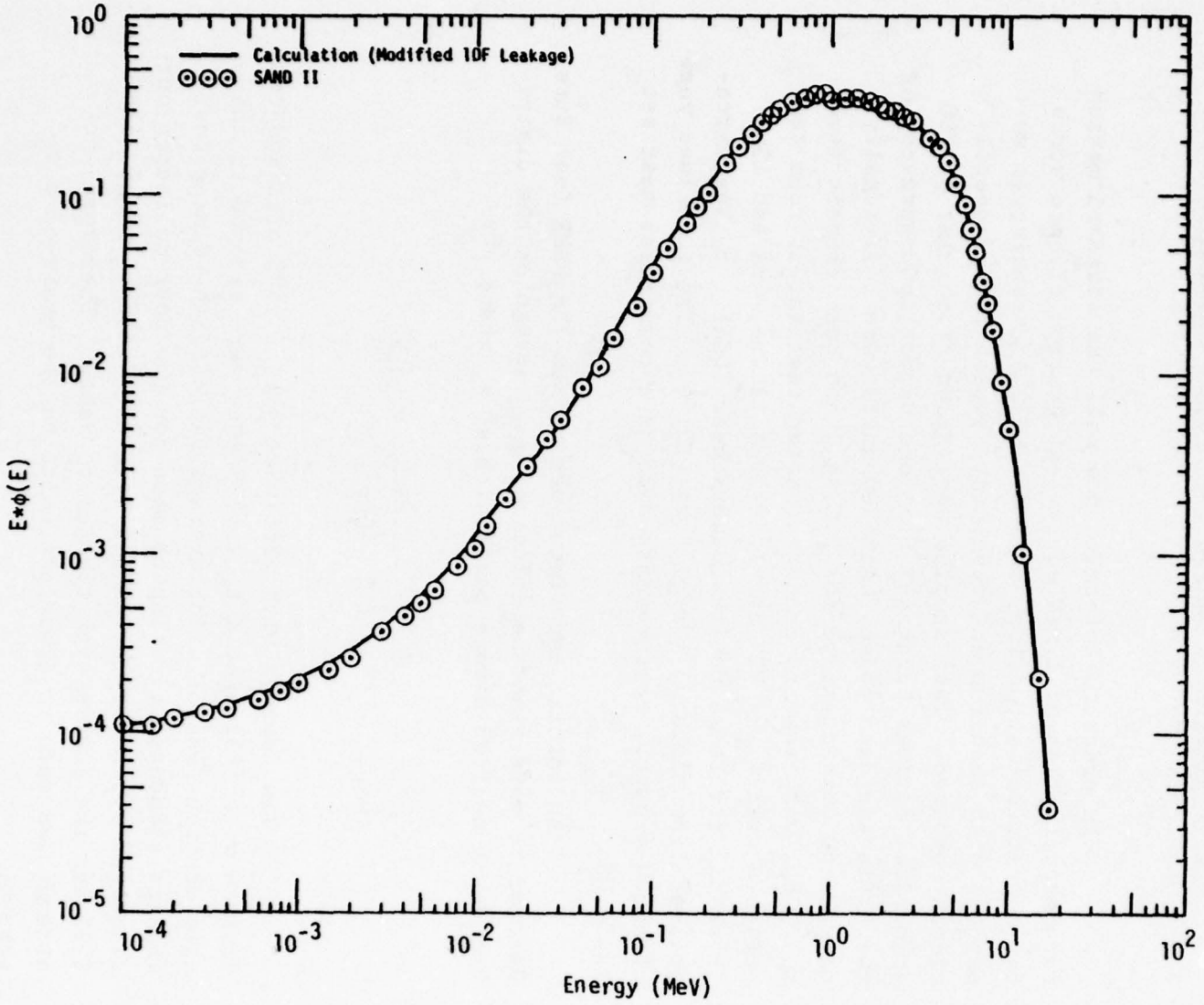

Figure 16. APRF Leakage, Burst, APRF 6 m Above Floor. SAND II solution and trial spectrum (1 DF calculation).

8. TRANSISTOR DAMAGE COEFFICIENT MEASUREMENTS

In order to determine how well the standard method for determination of 1 MeV equivalent neutron fluence works for a practical situation, sets of 2N2222A transistors were exposed with each run and resultant neutron damage coefficients compared. Test samples were drawn from a lot of 200 commerical devices purchased from one vendor and representing two different data codes. All 200 units were individually marked and characterized for D.C. h_{FE} and base transit time t_b. h_{FE} was measured on an automated test set at room temperature with V_{CE} = 10V and I_C = 10μA, 100μA, 1mA and 10mA. (Peak h_{FE} for these devices occurs near 10mA). t_b Was extrapolated from plots of $(2\pi f_T)^{-1}$ vs $(I_E)^{-1}$. The f_T values were obtained from h_{FE} measurements made on a commercial test set at 20 MHz.

An initial experiment was run on the WSMR Fast Burst Reactor to determine the effect of a t_b screen on the distribution of neutron damage coefficients, K, where

$$\Delta \frac{1}{h_{FE}} = \frac{1}{(h_{VE})_\phi} - \frac{1}{(h_{FE})_o} = t_b K \phi$$

Ten devices with .586 nSec $\leq t_b \leq$ .623 nSec and ten devices with .551 nSec $\leq t_b \leq$ .839 nSec were exposed to the same neutron fluence. The average ratio of the damage coefficient standard deviation to mean for the four collector currents was 6.3 % for the sample with the wider t_b range, and 8.3% for the sample with tighter t_b range. Therefore, no attempt was made to preselect units on the basis of a t_b screen.

A minimum of seven 2N2222A units was exposed with each set of activation foils and in four cases the units were both inside and outside the Boron-10 ball.

All units were exposed passively and each batch was tightly grouped to minimize spatial effects. Post irradiation h_{FE} measurements were made about one month after the final exposure. Measurements were made at room temperature on the same test set as the preirradiation h_{FE} measurements. Comparison of control samples indicated a repeatability of the h_{FE} measurements to within 2%.

A significant exposure to total ionizing (gamma) radiation resulted with some of the neutron exposures. Therefore, a correction was made for total (gamma) dose effects. The increase in base current from both neutron effects and total dose effects is additive, thus:

$$(\Delta 1/h_{FE})_{TOTAL} = t_b K \phi + (\Delta 1/h_{FE})_{\gamma}$$

The added $(\Delta 1/h_{FE})$ term can be subtracted out as a correction factor to give proper K values. In order to determine the $(\Delta 1/h_{FE})_{\gamma}$ term for each set of devices, exposures were made on a Co^{60} source. A total of 36 additional 2N2222A's from the same lot as used for the neutron exposures were passively exposed to $3x10^3$, 10^4, $3x10^4$, and 10^5 rad(Si), 9 devices at each level. The $(\Delta 1/h_{FE})_{\gamma}$ was determined for each device at V_{CE} = 10V and I_C = 10μA, 100μA, 1mA, and 10mA. A plot of the median $\Delta 1/h_{FE}$ vs γ was made for each collector current level and the value of $(\Delta 1/h_{FE})$ corresponding to the total dose level of each neutron exposure was subtracted from $(\Delta 1/h_{FE})_{TOTAL}$ to give the corrected K values. The maximum coefficient of variation $(\frac{\sigma}{ave})$ for the $(\Delta 1/h_{FE})_{\gamma}$ values ranged from ∿50% at 10 A to ∿30% at 10mA.

CaF_2 TLDS were used with each neutron exposure to determine the total ionizing dose. The correction factors ranged from less than 1% of $(\Delta 1/h_{FE})_{TOTAL}$ for most of the fast-burst reactor exposures, up to 10% for exposure #7 which was performed on the TRIGA Mark F behind 1/4" Boral. The total dose for this exposure was 9.5×10^4 rad(Si).

Table 2, shown on page 6 of Section 3, presents the results of the $K\phi$ measurements for the 2N2222A K's measured at I_c = 10μA, 100μA, 1mA and 10mA. The standard deviation for each set of 7 to 10 units is also given. Here,

$$K\phi = (\Delta 1/h_{FE}) / (t_b)$$

The values of $K\phi$ were divided by ϕ_{eq}, where the ϕ_{eq} were obtained from the spectrum measurements of $\phi(E)$, folded in with D(E) as per Equation 1. The values of K_1 through K_4 are given in Table 2, along with ϕ_{eq} and ϕ_{eq}/ϕ for each spectrum. Here, $K_1 \equiv K$ (10μA), $K_2 \equiv K$ (100μA), $K_3 \equiv K$(1mA), and $K_4 \equiv$ (10mA).

Note that for K_2 through K_4 the standard deviation on K is 4-5% (K_1, for 10μA, is perhaps of little interest) indicating that D(E) represents the damage function for 2N2222A's over a wide range of both unperturbed and "filtered" reactor spectra. This should make it possible quantitatively to interrelate the radiation damage work with, say, a TRIGA reactor and an FBR leakage spectrum. The value of ϕ_{eq} must easily be measurable for each irradiation, as is discussed in Section 9 below.

Since the observed damage coefficients are seen to be nearly constant over a range of spectral shapes where ϕ_{eq}/ϕ, the damage per neutron above 0.01 MeV, was made to range from 0.99 to 1.42, these data help establish, although not conclusively, the usefulness of D(E) and ϕ_{eq} in quantitatively

relating the damage induced by a basic (or modified) reactor spectrum to the damage expected of a threat spectrum. One would expect a good correlation at least in the case of larger volume transistors, where volume recombination effects predominate in the damage mechanism involved.

9. PRACTICAL METHOD FOR MEASUREMENT OF ϕ_{eq}

Table 2 lists values of ϕ_{eq}/S for all the measurements of basic and modified spectra carried out at the SANDIA SPRII and ACPR, the APRF FBR and the Northrop TRIGA facilities. In order to obtain ϕ_{eq} for any run (and thereby obtain a true measure of damagability), one measures the absolute sulfur activation S and multiplies by ϕ_{eq}/S to get ϕ_{eq}. Here S is the absolute disintegration rate ($N\lambda$) of ^{32}P, corrected back to the time at the end of the irradiation.

Two caveats must be interjected at this point. The first is that an absolute calibration (rigorous, yet possibly very simple) in units of disintegration rate per ^{32}S nucleus is needed. The second is that the ϕ_{eq}/S deduced from the earlier work presented in Appendix A should not be used for the WSMR FBR and the GA TRIGA. Since those data were obtained without the benefits of the recent improvements in foil counting (the cascade correction), and since all reactor spectra of a given type (e.g., all FBR's of roughly the same dimensions) are appreciably closer together than the error arising from the cascade correction, it is by far more accurate to use the SPRII leakage spectrum ϕ_{eq}/S (Table 1) for the WSMR FBR than to obtain it directly from the earlier work on the WSMR FBR of Appendix A.

The absolute ^{32}P activity per ^{32}S nucleus can be readily determined simply by the method alluded to in the text for getting the sulfur activation, or by the method suggested to us by H. Wright of WSMR. In the latter method, the sulfur foils and some aluminum foils are irradiated in the same 14 MeV neutron flux. The aluminum foils are counted for the 2.75 MeV ^{24}Na line with either a Ge(Li) or NaI detector calibrated against

some NBS standard foils (thorium and yttrium), and the absolute 14 MeV neutron flux is calculated from this measurement with the use of the $^{27}Al(n,\alpha)^{24}Na$ cross section at 14 MeV. With a knowledge of the 14 MeV flux and the $^{32}S(n,p)^{32}P$ reaction cross section at 14 MeV, the beta detector is calibrated absolutely. Both the $^{27}Al(n,\alpha)$ and $^{32}S(n,p)$ cross sections are known with reasonably good accuracy at 14 MeV.

With the method developed in this program and alluded to in the text, one simply activates a nickel foil and a sulfur foil together in the same reactor neutron field and counts the absolute nickel activation rate with a calibrated NaI or Ge(Li) detector (see Appendix B). The sulfur (^{32}P(activation rate per ^{32}S-target atom is then taken as 2.92 x the ^{58}Ni activation rate per ^{58}Ni foil atom. This approach was found to be good to an estimated accuracy of ±2% in the refolding calculations carried out with the SANDII code.

APPENDIX A

NUCLEAR SCIENCE AND ENGINEERING: 65, 316-330 (1978)

Threshold-Foil Measurements of Reactor Neutron Spectra for Radiation Damage Applications

Victor V. Verbinski,* Norman A. Lurie, and Vern C. Rogers

IRT Corporation, P.O. Box 80817, San Diego, California 92138

Received January 27, 1977
Accepted May 23, 1977

The accuracy of unfolding neutron spectra with threshold activation foils was investigated by comparing the unfolded spectra with "known" spectra obtained from calculations verified with more accurate spectrometry techniques. Because of the lack of spectral data below 1 MeV (only one useful activation threshold exists between 0.01 and 1 MeV), reliable results are generally obtained only with the a priori constraint of a physically complete trial spectrum. A family of trial spectra useful for reactor spectra [and any nuclear "evaporation" spectra, such as from high-energy (γ,n) reactions] has been formulated. The sensitivity of the solution φ(E) to the specific unfolding code used, to the threshold-foil cross sections and related nuclear data, and to foil-activation measurement accuracy was also investigated.

I. INTRODUCTION

This paper summarizes the results of a program in which a standard neutron spectrometry method was selected and evaluated as to accuracy. The program was carried out in support of a set of draft American Society for Testing and Materials (ASTM) Standards for characterizing neutron fields in terms of radiation damage effectiveness to silicon semiconductor electronic components. Such a characterization is of interest in planning irradiation schedules for parts screening or sample specification tests and in comparing the results of radiation damage studies carried out in different neutron fields.

The method provides the neutron spectral intensity $\phi(E)$ for general use, such as calculating radiation damage to materials other than silicon where the damage versus neutron energy, $D(E)$, is known or is calculable from known neutron cross sections.

II. SELECTION OF THE THRESHOLD-FOIL METHOD

Several candidate methods were considered for characterizing a neutron field in terms of bulk silicon radiation damage effectiveness. These included time-of-flight (TOF) spectrometry,[1,2] the proton-recoil scintillator,[3-5] the proton-recoil proportional counter,[6-8] ^{3}He and ^{6}Li coincidence-measurement techniques (sandwich counters),[9] the proton-recoil telescope, nuclear emulsions, threshold-foil-activation spectrometry, and the use of silicon itself as a dosimeter. The latter, although potentially the most straightforward, was

*Present address: Science Applications, Inc., P.O. Box 2351, La Jolla, California 92038.

[1]V. V. VERBINSKI and J. C. COURTNEY, *Nucl. Phys.*, **73**, 398 (1965).

[2]V. V. VERBINSKI, W. R. BURRUS, T. A. LOVE, W. ZOBEL, and N. W. HILL, *Nucl. Instrum. Methods*, **65**, 8 (1968).

[3]V. V. VERBINSKI, F. G. PEREY, J. K. DICKENS, and W. R. BURRUS, *Phys. Rev.*, **170**, 916 (1968).

[4]V. V. VERBINSKI and W. R. BURRUS, *Phys. Rev.*, **177**, 1671 (1969).

[5]W. R. BURRUS and V. V. VERBINSKI, *Nucl. Instrum. Methods*, **67**, 181 (1969).

[6]V. V. VERBINSKI and R. GIOVANNINI, *Nucl. Instrum. Methods*, **114**, 205 (1974).

[7]V. V. VERBINSKI, J. C. YOUNG, and J. M. NEILL, *Nucl. Sci. Eng.*, **52**, 330 (1973).

[8]E. F. BENNETT, *Nucl. Sci. Eng.*, **27**, 16 (1967); also, R. GOLD and E. F. BENNETT, *Nucl. Instrum. Methods*, **63**, 285 (1967); also, E. F. BENNETT and T. J. YULE, *Nucl. Instrum. Methods*, **98**, (1972).

[9]V. V. VERBINSKI and M. S. BOKHARI, *Nucl. Instrum. Methods*, **48**, 309 (1966).

0029-5639/78/0002-0316$02.00/0

eliminated because of difficulties in measuring the number of dislocation centers. The silicon would have to be kept at cryogenic temperatures during and after irradiation, and damage annealing from all sources would have to be correctly accounted for. The annealing can vary with the type of device used, the current drain, temperature, gamma-ray dose rate, and even the neutron dose rate.

The threshold-foil spectrometer was chosen for its versatility in measuring both pulsed and steady-state reactor spectra, its wide energy range (thermal through 14 MeV) and fluence range (3×10^{11} to 3×10^{15} n/cm^2), freedom from gamma-ray interference, good reproducibility, ease of access to remote regions in a reactor, and relatively good economy. It will not work at distances greater than ~50 cm from a reactor[10] in a low-Z shield such as LiH or H_2O, nor can it be used with a Linac source (in the forward direction) due to the significant number of (γ,fission) reactions. With a Linac-driven source, TOF methods are much more accurate.[11] However, for Linac-pulsed reactor assemblies, a long flight path, complex dieaway-time corrections, and a low k_{eff} (~0.9 or less) are required.[7,12,13]

III. INTERACTIVE OPERATION OF SAND-II

The method of threshold-foil spectrometry can be described as follows. A set of foils is selected with threshold energies, E_t, that vary from 0 to 14 MeV (see Table I). The foils are weighed, covered with cadmium or ^{10}B as necessary, and exposed to a neutron field having a spectral intensity $\phi_0(E)$. The resultant radioactivity is measured with a high-efficiency Ge(Li) or intrinsic germanium gamma-ray detector of good resolution to determine the number N of radioactive atoms produced during the irradiation of N_0 target atoms of the specific isotope. For each foil species x,

$$N_x = N_0 \int_{E_t}^{\infty} \sigma_x(E)\phi_0(E)dE \qquad (1)$$

where $\sigma_x(E)$ is the cross section for the reaction. The set of measured specific activities given by the ratio $R_m(x) = (N/N_0)_x$ is used as input to the SAND-II unfolding code, along with a trial spectrum $\phi_{tr}(E)$ that contains all the physical features (see Sec. IV).

Using Eq. (1) with $\phi_{tr}(E)$ in place of the unknown, $\phi_0(E)$, the SAND-II code calculates the various ratios $R_{tr}(x)$ that are consistent with $\phi_{tr}(E)$ by means of the SAND-II input library[14] of cross sections, $\sigma_x(E)$.

The fractional differences,

$$\Delta_0(x) = \frac{R_m(x) - R_{tr}(x)}{R_{tr}(x)} , \qquad (2)$$

for all the foils are calculated by the SAND-II code, and the standard deviation, S_0, is generated from the set of $\Delta_0(x)$. If S_0 is <0.05 (or any other value the user may input), then $\phi_{tr}(E)$ is the solution. If not, the code raises (lowers) the spectrum $\phi_{tr}(E)$ in the regions just above the threshold energy $E_t(x)$ for which the corresponding $\Delta_0(x)$ is large and positive (negative). The process is repeated to generate the sets $\phi_1(x), \ldots, \phi_n(x)$, $\Delta_1(x), \ldots, \Delta_n(x)$, and $S_1, \ldots, S_n$, where $S_n \leq 0.05$. If $n = 10$ or less, the probability that ϕ_n has little spurious structure is quite good.

If n is large and/or if considerable spurious structure is observed [as determined most sensitively by comparing $E \cdot \phi(E)$ plots of $\phi_{tr}(E)$ and $\phi_n(E)$], then the user must examine the $\Delta_0(x)$ set for a value (or values) that is appreciably different from the remainder of the set, eliminate the questionable value as not being consistent with the remainder of the set, and rerun SAND-II without the corresponding $R_m(x)$. Alternatively, the user can also restructure $\phi_{tr}(E)$ to yield a shape that results in a better set of $\Delta_0(x)$ and that therefore agrees with the measured activation set, $R_m(x)$.

IV. *A PRIORI* CONSTRAINTS

The limited information provided by the dozen or so measured foil-activity values, $R_m(x)$, means that the threshold-foil spectrometry method requires the *a priori* information of a meaningful trial spectrum, $\phi_{tr}(E)$. A simple one-dimensional mockup of the reactor and surrounding scattering material is usually adequate to provide a calculated spectrum, ϕ_c, that contains all the physics of the problem. Alternatively, the parameterized family of curves presented in Sec. VIII can be used for $\phi_{tr}(E)$ measurements of an unshielded reactor core.

[10] V. V. VERBINSKI, T. FUSE, J. D. KINGTON, and K. M. HENRY, "Transport of Fast Neutrons Through Lithium Hydride. Part II: Angular Distributions," ORNL-3360, Neutron Physics Division Annual Progress Report for Period Ending September 1, 1962, Oak Ridge National Laboratory (1962).

[11] V. V. VERBINSKI, M. S. BOKHARI, J. C. COURTNEY, and G. E. WHITESIDES, *Nucl. Sci. Eng.*, **27**, 283 (1967).

[12] J. M. YOUNG, J. M. NEILL, P. d'OULTREMONT, E. L. SLAGGIE, and C. A. PRESKITT, *Nucl. Sci. Eng.*, **45**, 141 (1971).

[13] P. d'OULTREMONT, D. H. HOUSTON, and J. C. YOUNG, "CAGE-BIRD-SPEC," Gulf-RT-10195, Gulf Radiation Technology (1970).

[14] For an early summary, see R. L. SIMONS and W. N. McELROY, "Evaluated Reference Cross-Section Library," BNWL-1312, Battelle-Northwest Laboratories (1970).

TABLE I

Activation Foils (1.27-cm diam)

Reaction	E_t (MeV)	E_γ (keV)	Gamma/Reaction (Fission Yield, %)	$T_{1/2}$	Foil Mass (g)	Isotopic Abundance (%)	Notes
$^{197}Au(n,\gamma)^{198}Au$	0	412	0.96	2.696 days	0.056	100	a
$^{59}Co(n,\gamma)^{60}Co$	0	1173 1333	1.00 1.00	5.258 yr	0.057	100	a,b
$^{55}Mn(n,\gamma)^{56}Mn$	0	847 1811	0.99 0.29	2.58 h	0.030	100	a,b
$^{238}U(n,f)^{140}La$	0(0.01)[c]	1596	0.96 (6.29)	40.23 h	0.281	100	a,d,e
$^{239}Pu(n,f)^{140}La$	0(0.01)[c]	1596	0.96 (5.24)	40.23 h	0.150	100	a,d,e
$^{237}Np(n,f)^{140}La$	0.5	1596	0.96 (5.69)	40.23 h	0.580	100	a,d,e
$^{237}Np(n,f)^{97}Zr$	0.5	743	0.92 (6.01)	16.8 h	0.580	100	a,f,e
$^{115}In(n,n')^{115m}In$	1.0	335	0.50	4.50 h	0.255	95.7	
$^{238}U(n,f)^{140}La$	1.45	1593	0.96 (6.02)	40.23 h	0.495	100	a,d,e
$^{232}Th(n,f)^{140}Ba$	1.75	537	0.256 (7.91)	12.8 days	1.066	100	a,g,e
$^{232}Th(n,f)^{97}Zr$	1.75	743	0.92 (4.12)	16.8 h	1.066	100	a,f,e
$^{54}Fe(n,p)^{54}Mn$	2.20	835	1.00	303 days	0.142	5.82	
$^{58}Ni(n,p)^{58}Co$	2.9	810	0.99	71.3 days	0.282	67.8	
$^{32}S(n,p)^{32}P$	2.9	Betas	1.00β	14.3 days	4.10	95.0	a
$^{26}Mg(n,p)^{26}Na$	6.3	1369	1.00	15.0 h	0.030	79	a
$^{56}Fe(n,p)^{56}Mn$	7.5	847 1811	0.99 0.29	2.58 h	0.142	91.7	a,i
$^{27}Al(n,\alpha)^{24}Na$	8.7	1369	1.00	15.0 h	0.257	100	a
$^{127}I(n,2n)^{126}I$	11.0	386 667	0.34 0.33	13.05 days	0.657	100	
$^{90}Zr(n,2n)^{89}Zr$	14	910	0.99	78.4 h	0.108	51.5	

[a] Cadmium cover 0.05 to 0.10 cm thick.

[b] Use ^{59}Co instead of ^{197}Au and ^{55}Mn for very long irradiations.

[c] $E_t \approx 0.01$ MeV with ^{10}B sphere (important for soft (TRIGA) spectra, where $\phi(E) < 0.01$ will otherwise dominate). When ^{238}U or ^{239}Pu foil is ^{10}B-covered, also cover ^{238}U and ^{237}Np foils so that accurate corrections can be made for ^{235}U and ^{239}Pu impurities in these high E_t foils.

[d] 40.23-h daughter of 12.80-day ^{140}Ba. Wait five days for maximum decay rate (ASTM E 393).

[e] Fission yields are for bombardment with fission-spectrum neutrons. For thermal and 14 MeV, see Ref. 5.

[f] Use ^{97}Zr for low fluence (3×10^{11} to 3×10^{12} n/cm^2). Use peak shape analysis or measure twice, seven days apart, to strip off 740-keV ^{99}Mo gamma ray ($T_{1/2}$ = 67 h).

[g] ^{232}Th radioactivity interferes with ^{140}La line.

[h] Requires separate detector, and calibration technique is complex.

[i] Maximum manganese impurity = 0.001%, cadmium-covered. Omit $^{56}Fe(n,p)^{56}Mn$ for long irradiations.

Note from Table I that a "fabricated" threshold appears at ~0.01 MeV as produced by a thick ^{10}B cover for the ^{238}U or ^{239}Pu fission foil. The only other useful threshold up to 1 MeV is that for the $^{237}Np(n,f)$ reaction, where the threshold energy $E_t \approx 0.5$ MeV. (Data below 0.01 MeV are usually of little use in radiation damage work.) Consequently, the output of SAND-II or any other code exhibits an extremely large "confidence interval" or "region of likely solutions" below 1 MeV, unless it is constrained to act as a small-perturbation calculation on a good trial spectrum to provide a final spectrum consistent with the foil activations.

The second constraint is that which is built into SAND-II. This is an improved version of the original iterative unfolding code[15] which was reprogrammed to retard the formation of spurious structure[16] while preserving the physically meaningful structure, i.e., a basic fission spectrum with varying strength of $1/E$ slowing down component attached at the low-energy side, a resonance "dip," a monoenergetic peak at ~14 MeV, or a broad thermal-neutron Maxwellian peak.

The third constraint is a user-interaction constraint of keeping the number of iterations, n, down to a low value (see Sec. III). This is accomplished by eliminating spurious foil activations and/or modifying $\phi_n(E)$ in regions above a foil threshold energy E_{th} for the foil yielding the largest disparity with the first $\phi_{tr}(E)$ used. These disparities [$\Delta_0(x)$ in Sec. III] are printed out in SAND-II for subsequent interactions as well [$\Delta_1(x)$]. Also, the energy "band" where 5 and 95% of the activation has occurred for each foil x is listed for each spectrum perturbation [$\phi_0(E) \equiv \phi_{tr}(E), \phi_1(E), \ldots, \phi_n(E)$] as an additional guide.

The final *a priori* constraint is that of accurate nuclear data, i.e., an evaluated consistent set of threshold-foil cross sections[14] input to the code, and of accurate half-lives and fluorescent yields (conversion coefficients, branching ratios, and fission yields) available for processing the foil-activity data.

V. CALCULATION OF $D(E)$ FOR SILICON

The damage function for silicon,[17] $D(E)$, used in the present work is shown in Fig. 1 (dotted line) and in Table II (10^{-5} to 2×10^7 eV). It was obtained with neutron cross sections for silicon from the ENDF/B-IV MAT1194 evaluation.[18] Details of the calculational method are described in Ref. 17. The results of a previous calculation,[19] also shown in Fig. 1, were based on neutron cross sections available in 1965 and 1966.

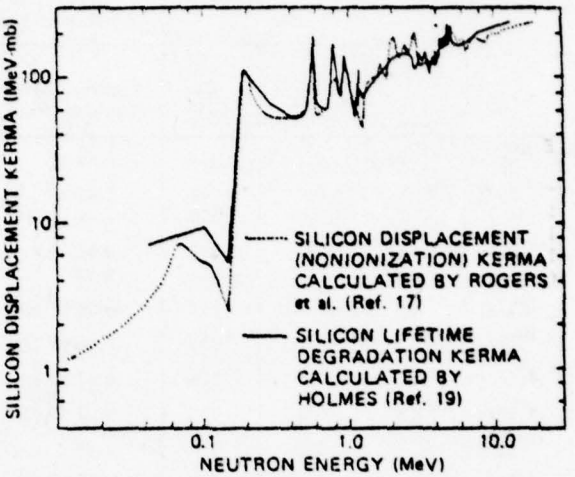

Fig. 1. Silicon kerma for displacement and lifetime degradation calculated for neutron energies from 0.01 to 20 MeV.

Although the uncertainty of the calculation of total energy [ionization, $I(E)$, and displacement, $D(E)$] is mainly governed by the neutron cross sections, the partition of total energy deposition between $I(E)$ and $D(E)$ is also limited by the accuracy of the Lindhard factor for determining the fraction of recoil-atom and charged-particle kinetic energy that is available to cause displacements, and by the Robinson[20] functional representation of the Lindhard factor. The Robinson representation needs to be improved by fitting to the very few data points presently available for energy partition and by future careful measurements. It is hoped that present $D(E)$ data will be updated when the work on the energy partition is accomplished.

VI. THE 1-MeV EQUIVALENT FLUX CHARACTERIZATION OF A NEUTRON FIELD

A neutron field can be characterized by ϕ_{eq} (1 MeV), which represents the fluence of 1-MeV neutrons required to produce the same radiation damage in bulk silicon. Since nearly all the neutron damage is produced by the neutrons above 0.01 MeV, even for a soft TRIGA spectrum (see below), we define ϕ_{eq} as

[15] W. N. McELROY et al., "A Computer-Automated Iterative Method for Neutron Flux Spectra Determination by Foil Activation," AFWL-TR-67-41, Vol. I, Air Force Weapons Laboratory (1967).

[16] S. BERG and W. N. McELROY, "A Computer-Automated Iterative Method for Neutron Flux Spectra Determination by Foil Activation," AFWL-TR-67-41, Vol. II, Air Force Weapons Laboratory (1967).

[17] V. C. ROGERS, L. HARRIS, Jr., D. K. STEINMAN, and D. E. BRYAN, *IEEE Trans. Nucl. Sci.*, NS-22, 5, 2326 (1975); *Erratum*, NS-23, 1, 875 (1976).

[18] D. C. LARSON and F. G. PEREY, "ENDF/B Evaluation of Neutron and Gamma-Ray Production Cross Sections for Silicon," published in ENDF/B Summary Documentation, BNL-17541 (ENDF-201), National Neutron Cross Section Center, Brookhaven National Laboratory (1973, plus updates).

[19] R. R. HOLMES, unpublished data (1970).

[20] M. T. ROBINSON, *Proc. Nuclear Fusion Reactors Conf.*, p. 364, British Nuclear Energy Society, Culham Laboratory (1969); see also, D. G. DORAN, *Nucl. Sci. Eng.*, 49, 130 (1972).

TABLE II

Calculated Silicon Displacement and Ionization Kerma

Energy (eV)	Silicon Kerma (MeV-mb)		Energy (eV)	Silicon Kerma (MeV-mb)		Energy (eV)	Silicon Kerma (MeV-mb)	
	Displacement	Ionization		Displacement	Ionization		Displacement	Ionization
1.000-5*	8.991+0	2.570+0	1.242+3	1.528-1	2.728-2	3.162+5	5.190+1	2.831+1
1.857-5	6.604+0	1.888+0	1.885+3	2.288-1	4.378-2	3.548+5	5.132+1	2.896+1
3.449-5	4.850+0	1.386+0	2.861+3	3.426-1	7.038-2	3.981+5	5.260+1	3.073+1
6.405-5	3.562+0	1.018+0	4.342+3	5.131-1	1.132-1	4.467+5	5.441+1	3.314+1
1.189-4	2.615+0	7.475-1	6.589+3	7.604-1	1.806-1	5.012+5	5.715+1	3.369+1
2.209-4	1.917+0	5.480-1	1.000+4	1.041+0	2.663-1	5.623+5	1.852+2	1.240+2
4.102-4	1.406+0	4.018-1	1.112+4	1.122+0	2.932-1	6.310+5	5.409+1	3.444+1
7.617-4	1.031+0	2.946-1	1.259+4	1.203+0	3.208-1	7.080+5	6.056+1	4.290+1
1.415-3	7.563-1	2.162-1	1.413+4	1.279+0	3.486-1	7.943+5	9.354+1	6.767+1
2.627-3	5.554-1	1.588-1	1.585+4	1.368+0	3.808-1	8.913+5	7.309+1	5.275+1
4.879-3	4.080-1	1.166-1	1.778+4	1.478+0	4.202-1	1.000+6	1.017+2	6.989+1
9.060-3	2.996-1	8.565-2	1.995+4	1.587+0	4.612-1	1.162+6	4.438+1	3.182+1
1.683-2	2.192-1	6.267-2	2.239+4	1.727+0	5.131-1	1.349+6	8.994+1	7.420+1
3.125-2	1.614-1	4.613-2	2.512+4	1.874+0	5.691-1	1.567+6	9.936+1	9.353+1
5.802-2	1.178-1	3.368-2	2.818+4	2.057+0	6.388-1	1.821+6	9.654+1	9.354+1
1.078-1	8.678-2	2.480-2	3.162+4	2.261+0	7.183-1	2.115+6	1.848+2	1.809+2
2.001-1	6.374-2	1.821-2	3.548+4	2.501+0	8.128-1	2.457+6	1.593+2	1.679+2
3.716-1	4.670-2	1.334-2	3.981+4	2.823+0	9.391-1	2.853+6	2.003+2	2.283+2
6.901-1	3.444-2	9.824-3	4.467+4	3.309+0	1.127+0	3.315+6	1.187+2	1.457+2
1.282+0	2.529-2	7.191-3	5.012+4	3.897+0	1.360+0	3.850+6	1.212+2	1.653+2
2.380+0	1.882-2	5.308-3	5.623+4	4.738+0	1.694+0	4.472+6	1.795+2	2.615+2
3.812+0	1.543-2	4.303-3	6.310+4	6.504+0	2.384+0	5.195+6	1.932+2	3.127+2
5.482+0	1.285-2	3.517-3	7.080+4	7.247+0	2.725+0	6.034+6	1.965+2	5.236+2
8.319+0	1.100-2	2.911-3	7.943+4	8.481+0	2.501+0	7.009+6	2.014+2	1.061+3
1.263+1	9.727-3	2.439-3	8.913+4	5.735+0	2.272+0	8.142+6	1.754+2	1.680+3
1.916+1	9.058-3	2.088-3	1.000+5	5.287+0	2.152+0	9.457+6	2.006+2	2.272+3
2.908+1	9.127-3	1.878-3	1.122+5	5.024+0	2.104+0	1.099+7	1.981+2	2.586+3
4.413+1	1.006-3	1.812-3	1.259+5	4.008+0	1.728+0	1.276+7	2.134+2	2.845+3
6.698+1	1.220-2	1.947-3	1.413+5	2.643+0	1.175+0	1.482+7	2.154+2	3.086+3
1.017+2	1.595-2	2.343-3	1.585+5	5.231+0	2.398+0	1.722+7	2.213+2	3.853+3
1.543+2	2.205-2	3.131-3	1.778+5	5.220+1	2.461+1	2.000+7	2.297+2	5.073+3
2.341+2	3.162-2	4.532-3	1.995+5	1.086+2	5.255+1			
3.553+2	4.628-2	6.883-3	2.239+5	7.566+1	3.748+1			
5.393+2	6.855-2	1.076-2	2.512+5	6.041+1	3.089+1			
8.184+2	1.022-1	1.707-2	2.818+5	5.423+1	2.863+1			

*Read as 1.000×10^{-5}.

$$\Phi_{eq} = \frac{\int_{0.01}^{18\ \mathrm{MeV}} \phi(E)D(E)dE}{D(1\ \mathrm{MeV})} \qquad (3)$$

Because of the rapid variation of $D(E)$ near 1 MeV, we define D (1 MeV) as the average value between 0.85 and 1.15 MeV.

It is also useful to define a neutron-spectrum-shape parameter Φ_{eq}/Φ, which is the number of 1-MeV neutrons per unit fluence of the neutron field being specified required to produce the same damage, i.e.,

$$\Phi_{eq}/\Phi = \frac{\int_{0.01}^{18\ \mathrm{MeV}} \phi(E)D(E)dE}{D(1\ \mathrm{MeV}) \int_{0.01}^{18\ \mathrm{MeV}} \phi(E)dE} \qquad (4)$$

By averaging $D(E)$ over the energy interval of 0.85 to 1.15 MeV, Φ_{eq}/Φ is slightly larger than unity for a GODIVA spectrum. This is intuitively preferable to a value less than unity [which would result from using D (1 MeV) instead of D (0.85 to 1.15 MeV)], considering that the average energy is

>1 MeV and that $D(E)$ increases with energy. By excluding the neutrons below 0.01 MeV (which contribute only ~1% to ϕ_{eq}/ϕ even for the soft TRIGA spectrum), the value of ϕ_{eq}/ϕ becomes independent of unimportant changes in neutron flux at sub-cadmium and sub-^{10}B energies.

VII. MEASUREMENTS OF THREE STANDARD SPECTRA

VII.A. Description of Measurements and Method of Accuracy Assessment

Measurements were made of three different reactor spectra, the glory-hole and leakage (50 cm from core) spectra of a bare GODIVA-type fast burst reactor (FBR) at White Sands Missile Range (WSMR) and the leakage spectrum from the General Atomic TRIGA reactor. The first two were measured by WSMR personnel[21] in 1974 and by IRT personnel in 1975 to obtain a measure of the precision of the threshold-foil spectrometry method. The two groups used different foil sets, Ge(Li) gamma-ray spectrometers, and National Bureau of Standards (NBS) calibrated gamma-ray reference standards.

Each spectrum was unfolded by using the corresponding "standard" spectrum (see the Appendix) as a trial spectrum, $\phi_{tr}(E)$, in the SAND-II unfolding code. Agreement between the SAND-II result, $\phi_s(E)$, and ϕ_{tr} in this case gives a measure of the accuracy of the foil activation measurements, the published branching ratios or fluorescent yields given in Table I, and the threshold-foil cross-section library provided with the SAND-II code.[22] The sensitivity of the threshold-foil method to ϕ_{tr}, to the type of unfolding code used, and to the individual foil cross sections (or foil activations) is discussed in Secs. VIII, IX, and X.

VII.B. Results

Table III lists the foil activations for the five measurements described above. The FBR foil activations measured by IRT were measured by WSMR personnel as well, using the same foil set but different detectors and NBS gamma-ray calibration standards. The two agreed with an average standard deviation of ~4.5%, although the wait (decay) times were appreciably different in most

[21] J. MEASON, H. WRIGHT, J. HOGAN, and J. HARVEY, *IEEE Trans. Nucl. Sci.*, NS-22, 6, 2330 (1975).

[22] SAND-II is available at the Radiation Shielding Information Center, Oak Ridge National Laboratory, Oak Ridge, Tennessee.

TABLE III

Foil Activations for Five Measurements: Fission Foils = Fission/Nucleus; Others = Disintegration/(s-nucleus) as Input to SAND-II in Time-Integrated Mode (i.e., corrected to instantaneous irradiation)

	FBR (IRT)		FBR (WSMR)		TRIGA (IRT)
	60 cm	Glory Hole	50 cm	Glory Hole	J-Tube
^{197}Au (n,γ)[a]	1.79-17[a]	8.05-17[a]	2.06-17[a]		4.55-17[a]
^{197}Au (n,γ)	2.83-17	8.00-17	3.76-17		1.13-16
^{238}U (n,f)	9.94-12[a]	2.34-10	1.24-11[b]	1.45-09[a]	5.91-12[a]
^{239}Pu (n,f)			1.71-11[b]	1.82-09[a]	
^{237}Np (n,f)	6.42-12[a]	1.49-10	9.58-12	1.03-09[a]	3.37-13[a]
^{115}In (n,n')	3.92-17	8.71-16	6.08-17		2.01-18
^{238}U (n,f)	1.29-12[a]	3.34-11	1.97-12[b]	1.88-10[a]	6.67-14[a]
^{232}Th (n,f)	3.81-13	8.05-12	4.85-13	3.93-11	1.83-14[a]
^{54}Fe (n,p)	1.05-20	2.58-19	1.54-20	1.37-18	
^{58}Ni (n,p)	5.77-20	1.49-18	9.18-20	8.07-18	3.01-21
^{32}S (n,p)	1.72-19		2.57-19		8.97-21[c]
^{24}Mg (n,p)	9.42-20	2.23-18	1.33-19	1.25-17	7.31-21
^{56}Fe (n,p)	4.90-19	9.24-18	5.95-19	5.36-17	
^{27}Al (n,α)	4.57-20	1.06-18	6.47-20		3.38-21
^{127}I $(n,2n)$	2.56-21		4.79-21	4.60-19	2.26-22
^{90}Zr $(n,2n)$				1.73-19	

[a] Cadmium-covered (~0.050 cm); read as 1.79×10^{-17}.
[b] ^{10}B-covered (~1.65 g/cm^2).
[c] Deduced, SAND-II run.

cases. This makes the comparison a "worst case" situation in that sense.

Figure 2 shows the results of the measured leakage spectrum at 60 cm from the center of the WSMR FBR (solid circles) using the 1975 IRT foil activation measurements as input to the SAND-II unfolding code. The spectrum calculated with the 1DF code (see the Appendix) was used as the trial spectrum (solid-line histogram Fig. 2). The agreement in shape between the SAND-II result and the 1DF calculation is quite good, indicating that the gamma-ray activation measurements, the gamma-ray and fission-fragment yields of Table I, and the SAND-II foil-activation cross-section library are reasonably accurate. The SAND-II spectrum was arbitrarily normalized to the 60-cm calculation at 0.5 to 1.5 MeV for shape comparison.

Table IV presents the values of ϕ_{eq}/ϕ for the WSMR measurements (spectrum A) as well as the IRT results (spectrum B). The two values of ϕ_{eq}/ϕ (1.080 and 1.060) bracket the 1DF value of 1.077, which shows good agreement in spectral shape for all three cases. The flux above 0.01 MeV per sulfur activation varied ~4% from the mean of 3.59×10^{-20} ^{32}P nuclei per ^{32}S nucleus per watt-second. This gives a measure of the accuracy of specifying the silicon-semiconductor radiation damage once the spectral shape is accurately known. If it is not, the sulfur pellet is a poor choice for monitoring radiation damage (see Sec. XIII.C).

The 1DF calculational results at 14 and 400 cm from the FBR center are also shown in Fig. 2 (both arbitrarily normalized to the 60-cm spectrum at 0.5 to 1.5 MeV for shape comparison) to illustrate the increasing importance of the moderated component due to wall and floor scattering as the distance from the reactor increases.

The measurement of the WSMR FBR glory-hole spectrum is shown in Fig. 3 along with the 1DF calculation used as ϕ_{tr} in the SAND-II unfolding code. The 1974 (WSMR) and 1975 (IRT) results were practically identical (Table IV, spectra C and D) yielding $\phi_{eq}/\phi = 1.037$ and 1.023, respectively. These values again bracket the 1DF result of $\phi_{eq}/\phi = 1.030$. The flux above 0.01 MeV per sulfur activation agreed within 2% for the two measurements in this case.

A measurement for the TRIGA swimming-pool reactor was made in the remote-access J-tube[23] that abuts the reactor core. A shield of 7.6-cm

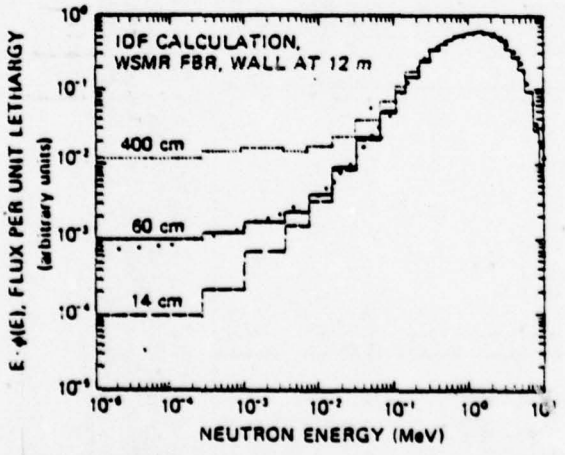

Fig. 2. Comparison of threshold-foil spectrum (SAND-II solid circles) with 1DF calculation (solid-line histogram) at 60 cm from the WSMR FBR center. The 1DF results are also shown at 14 and 400 cm to illustrate the importance of $1/E$ moderation component (flat line) due to wall scattering.

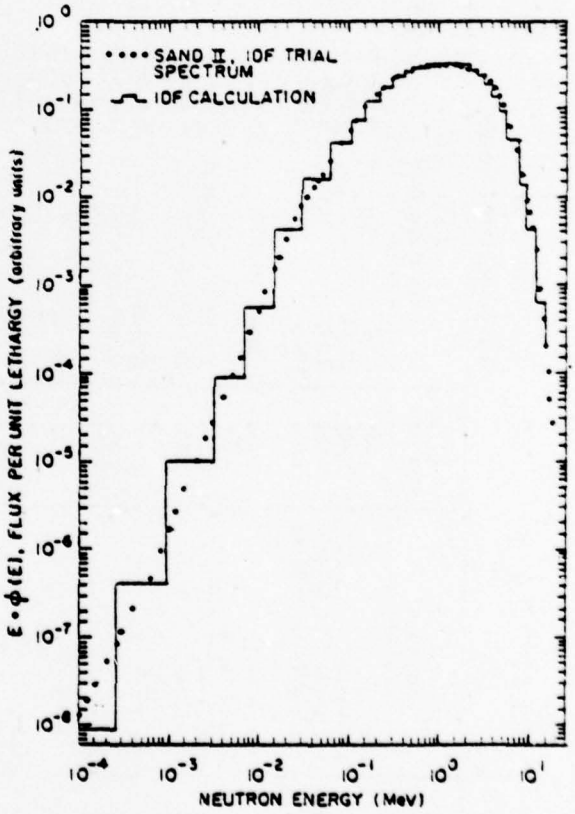

Fig. 3. The SAND-II results for the WSMR FBR glory-hole spectrum with $\phi_{tr}(E)$ = 1DF calculation (Table IV C and D).

[23]G. B. WEST, "Calculated Fluxes and Cross Sections for TRIGA Reactors," GA-4361, General Atomic Company (1963).

TABLE IV

Data for Individual Spectra

Spectrum	Foils Used[a]	ϕ_{cq}/ϕ Measured	ϕ_{cq}/ϕ Trial Spectrum		Iterations	ϕ_{cq}	Spectral Index	Variation
A(60 cm, 74)	1-9	1.080	(1DF)	1.077	2	1.25+13	7.30	---
B(60 cm, 75)	1-6, 10-16	1.060	(1DF)	1.077	9	7.45+12	6.42	---
C(glory hole, 74)	1-3, 5, 10-12, 15, 18, 20	1.037	(1DF)	1.030	3	1.16+15	7.86	---
D(glory hole, 75)	1, 2, 4-6, 13-16, 19, 21, 22	1.023	(1DF)	1.030	7	1.85+14	6.79	---
E(TRIGA)	1-4, 10-14, 16	1.019	(NIOBE, GAZE)	0.983	1	3.45+11	6.26	---
F(TRIGA)	1-4, 10-14, 16	0.992	(GAZE)	0.941	1	3.53+11	6.54	---
G(TRIGA)	1-4, 10-14, 17, 23	1.044	(NIOBE E_j = 0.2 MeV)	1.031	6	3.33+11	6.01	---
H(glory hole, 74)	1-3, 5, 10-12, 15, 18, 20	1.057	(GODIVA E_j = 0)	1.086	4	1.17+15	7.69	---
I(60 cm, 75)	1-6, 10-16	1.040	(GODIVA E_j = 0.005)	1.079	9	7.69+12	6.72	---
J(60 cm, 75)	1-6, 10-16	1.080	(GODIVA E_j = 0.01)	1.079	10	7.42+12	6.26	---
K(60 cm, 75)	1-6, 10-16	1.151	(GODIVA E_j = 0.02)	1.079	9	6.88+12	5.45	---
L(60 cm, 74)	1-3, 5-8, 16	1.087	(GODIVA E_j = 0)	1.086	2	1.28+13	7.47	---
M(60 cm, 74)	1-9	0.818	(GODIVA E_j = 0)	1.086	22	1.01+13	6.71	---
N(TRIGA)	1-4, 10-14, 17	0.659	(SPECTRA 1973)	0.843	5	3.68+11	10.99	---
O(glory hole, 74)[b]	1-3, 5, 10-12, 15, 20	1.037	(1DF)	1.030	16	1.17+15	8.01	---
P(60 cm, 74)	1-9	1.080	(1DF)	1.077	2	1.26+13	7.30	None
Q(60 cm, 74)	1-9	1.063	(1DF)	1.077	3	1.30+13	7.79	1.15 Pu
R(60 cm, 74)	1-9	1.048	(1DF)	1.077	10	1.37+13	8.01	1.25 Pu
S(60 cm, 74)	1-9	1.089	(1DF)	1.077	2	1.29+13	7.37	1.15 U8
T(60 cm, 74)	1-9	1.095	(1DF)	1.077	2	1.29+13	7.36	1.25 U8
U(60 cm, 74)	1-9	1.083	(1DF)	1.077	3	1.26+13	6.84	1.15 S
V(60 cm, 74)	1-9	1.084	(1DF)	1.077	5	1.26+13	6.37	1.25 S
W(60 cm, 74)	1-9	1.075	(1DF)	1.077	2	1.25+13	7.37	1.25 Mg
X(60 cm, 74)	1-9	1.070	(1DF)	1.077	8	1.24+13	7.15	1.25 Fe
Y(60 cm, 74)	1-9	1.102	(1DF)	1.077	3	1.29+13	7.32	1.25 U8, Mg
Z(60 cm, 74)	1-9	1.128	(1DF)	1.077	10	1.31+13	7.19	1.25 U8, 0.75 Mg

[a]Foil No. 1 = $^{58}Ni(n,p)$; 2 = $^{24}Mg(n,p)$; 3 = $^{127}I(n,2n)$; 4 = $^{197}Au(n,\gamma)$ (Cd); 5 = $^{56}Fe(n,p)$; 6 = $^{32}S(n,p)$; 7 = $^{238}U(n,f)$ (B); 8 = $^{235}U(n,f)$ (B); 9 = $^{239}Pu(n,f)$ (B); 10 = $^{234}U(n,f)$ (Cd); 11 = $^{235}U(n,f)$ (Cd); 12 = $^{237}Np(n,f)$ (Cd); 13 = $^{27}Al(n,\alpha)$; 14 = $^{115}In(n,n')$; 15 = $^{54}Fe(n,p)$; 16 = $^{232}Th(n,f)$; 17 = $^{232}Th(n,f)$ (Cd); 18 = $^{90}Zr(n,2n)$; 19 = $^{237}Np(n,f)$; 20 = $^{239}Pu(n,f)$ (Cd); 21 = $^{235}U(n,f)$; 22 = $^{238}U(n,f)$; 23 = $^{197}Au(n,\gamma)$.

[b]Unfolded with SPECTRA code (Radiation Shielding Information Center, Oak Ridge).

lead and 0.6-cm Boral (thermal-neutron transmission $\approx 5.6 \times 10^{-4}$) separates the core from the *J*-tube cavity used for radiation damage studies. The measured spectrum is shown in Fig. 4 along with the best available calculated spectrum that was used as $\phi_{tr}(E)$ in the SAND-II unfolding code. In this case, $\phi_{tr}(E)$ is a composite of the NIOBE code calculation, which had a low-energy cut-off of 0.8 MeV, and the GAZE calculation[23] (see Appendix). This measurement (spectrum *E* of Table IV) yielded a value of ϕ_{eq}/ϕ that was within ~3.4% of the calculational value. The SAND-II result using the GAZE code as $\phi_{tr}(E)$ was 5% higher in ϕ_{eq}/ϕ than the corresponding GAZE value (spectrum F of Table IV). Thus, the measurements are in best agreement with the composite calculated spectrum, which was experimentally verified above 0.8 MeV with an independent spectrometry method.

VIII. PARAMETERIZING $\phi_{tr}(E)$ FOR REACTOR SPECTRA

A GODIVA spectrum (spectrum 5 of the SAND-II library of trial spectra) is proposed as the basic reactor spectrum, but with a varying strength of $1/E$ moderating component that depends on the amount of moderator present. This GODIVA spectrum without any moderating component ($E_{join} = 0$) is adequate as $\phi_{tr}(E)$ for the glory-hole spectrum (Table IV.H). A comparison with the SAND-II result with $\phi_{tr}(E)$ = 1DF calculation shows agreement within 2% in ϕ_{eq}/ϕ and 1% in $\phi > 0.01$ MeV.

At 0.5 m from the reactor, neutron moderation from the concrete floor ~2 m below yielded a $1/E$ component that can be parameterized by E_{join} = 0.01 MeV. Figure 5 shows the results of three SAND-II runs with $\phi_{tr}(E)$ = GODIVA + $1/E$ moderation component joined at E = 0.005, 0.01, and 0.02 MeV (Table IV.I, J, and K). The best fit of the SAND-II output to $\phi_{tr}(E)$ occurs for E_{join} = 0.01 MeV, where ϕ_{eq}/ϕ = 1.080 for the SAND-II output versus 1.079 for $\phi_{tr}(E)$ with E_{join} = 0.01 MeV (Table IV.J). This compares to 1.060 for SAND-II with $\phi_{tr}(E)$ = 1DF, and ϕ_{eq}/ϕ = 1.077 for the 1DF spectrum. In addition, values of ϕ above 10 keV agree within 2%.

For the TRIGA *J*-tube spectrum, where the NIOBE calculation above 0.8 MeV agrees well with the GODIVA spectrum, we find E_{join} = 0.2 MeV (Table IV.G). Here, agreement with the baseline

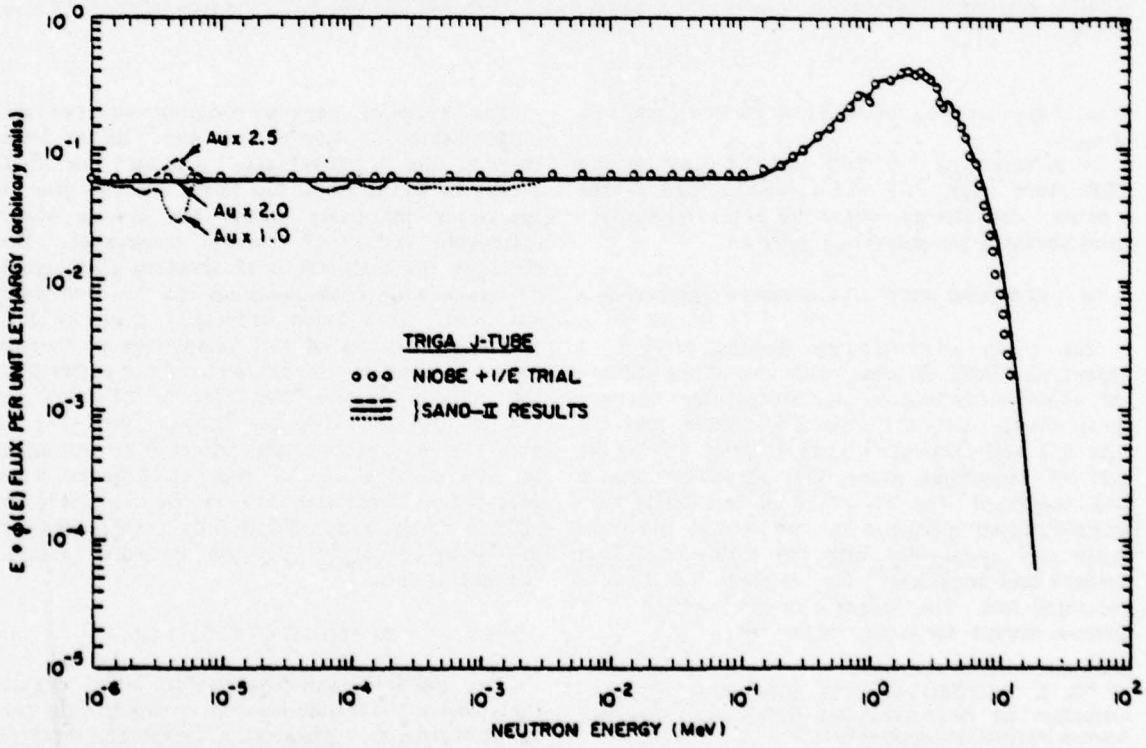

Fig. 4. The TRIGA *J*-tube spectrum SAND-II results with $\phi_{tr}(E)$ = NIOBE (>0.8 MeV) + GODIVA (0.2 to 0.8 MeV) + $1/E$; three gold foils (cadmium-covered). Corrections for foil thickness (0.0025 cm) are shown (Table IV.G).

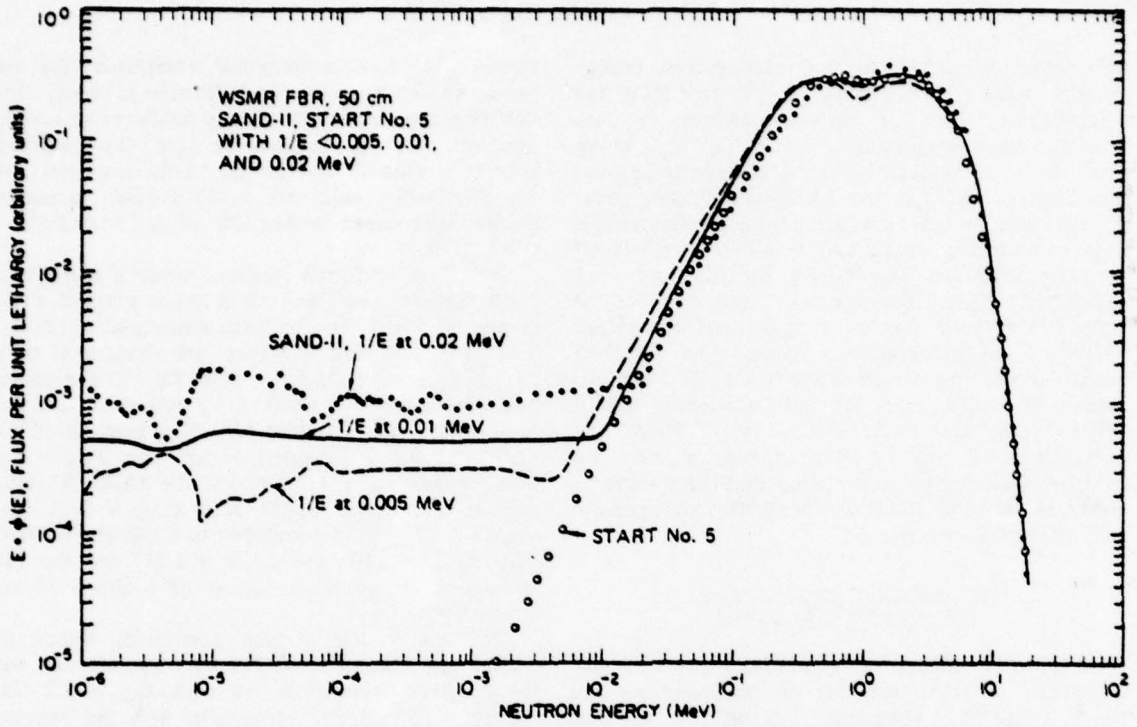

Fig. 5. Three unfolded results of the WSMR FBR leakage data with $\phi_{tr}(E)$ = "GODIVA" (Start number 5 of SAND-II library of trial spectra) and $1/E$ tail (flat line in above plot) joining at E_{join} = 0.005, 0.01, and 0.02 MeV. Note good agreement for E_{join} = 0.01 MeV.

case (Fig. 4 and Table IV.E) is 1% in ϕ_{eq} and 2½% in ϕ_{eq}/ϕ.

In summary, E = 0, 0.01, and 0.2 MeV for the FBR glory hole, FBR 0.5-m and TRIGA J-tube spectra, respectively, where the degree of moderation becomes progressively greater.

IX. PROBLEMS WITH LOW-ENERGY NEUTRONS

The three low-energy curves of Fig. 4 represent SAND-II runs with the three different gold-foil-resonance self-absorption corrections shown (1.0, 2.0, and 2.5). Note that the gold-foil self-absorption correction of 2.0 for the 4.95-eV resonance gives best agreement with a $1/E$ spectrum (Fig. 4). This is for nearly forward-directed neutrons in the J-tube and is in qualitative agreement with the factor of 2.5 of Sanford and Seckinger[24] for isotropic flux 0.0025-cm-thick foil. The isotropic flux correction is, of course, always the larger of the two.

[24]G. S. SANFORD and J. H. SECKINGER, "Thickness Corrections for Neutron-Activated Gold Foils," ANL-7545, Argonne National Laboratory (1969).

The ratio of bare-to-cadmium-covered gold foils (Table III) shows that the TRIGA J-tube thermal flux is appreciable. Although the TRIGA J-tube is Boral-lined, the Boral leakage plus the scattering materials inside the J-tube add a noticeable amount of thermal component. This stresses the importance of covering all thermal-activation foils with cadmium if a ^{10}B covering is not used. This holds especially true for foils where activations of foil impurities by thermal neutrons compete with finite-threshold activations, i.e., ^{23}Na in $^{27}Al(n,\alpha)^{24}Na$, ^{55}Mg in $^{56}Fe(n,p)^{56}Mn$, ^{238}U in $^{238}U(n,f)$, ^{239}Pu in $^{237}Np(n,f)$, etc. For the soft TRIGA spectrum, this effect is so serious as to rule out the use of most of these reactions unless the impurities are in the few parts per million range, and impurity foils are exposed with the same cover to provide reliable impurity correction data.

X. SENSITIVITY TO $\phi_{tr}(E)$

Two SAND-II unfolding results were obtained that illustrate that the solution does not, in general, converge to a physically meaningful spectral

shape unless $\phi_{tr}(E)$ brings the *a priori* constraint of a physically meaningful spectrum into the calculation.

Figure 6 shows the results of a SAND-II unfolding operation for the WSMR FBR leakage spectrum at 50 cm from the reactor. Using $\phi_{tr}(E)$ = GODIVA (solid line, Fig. 6) and omitting the low-energy gold foil data (cadmium-covered), the results obtained (represented by solid circles) agree with $\phi_{tr}(E)$ = GODIVA (Table IV.L) because the calculated ^{238}U and ^{239}Pu activations (5 to 95% points) are produced in the 0.16- to 4.3-MeV and 0.2- to 4.4-MeV bands, respectively. If the gold foil data are added, the spectrum designated by the symbol "X" results (Table IV.M). This is a clearly unreal spectrum. Here, ϕ_{eq}/ϕ has dropped from 1.090 (Table IV.A) to 0.818, the total flux is 8% high, and ϕ_{eq} has dropped to 80% of the proper value.

The next example illustrates that the unfolding process is not necessarily a converging process in that it may get progressively worse without the *a priori* constraint of a physically real spectrum for $\phi_{tr}(E)$. A comparison of the 1975 TRIGA J-tube measurement, as unfolded with SAND-II using $\phi_{tr}(E)$ = NIOBE + GAZE (Table IV.E), was made with some 1973 results [six-foil data unfolded with the SPECTRA code using $\phi_{tr}(E)$ = constant]. The value of ϕ_{eq}/ϕ for the 1973 spectrum is 0.843. When this spectrum was used as a trial spectrum for a SAND-II unfolding code run with the 1975 foil data, the resulting spectrum (Table IV.N) yielded ϕ_{eq}/ϕ = 0.659, which shows a further deterioration. This is compared to ϕ_{eq}/ϕ = 1.019 (Table IV.E). Also, the total flux above 10 keV is 65% high and ϕ_{eq} is 9% high.

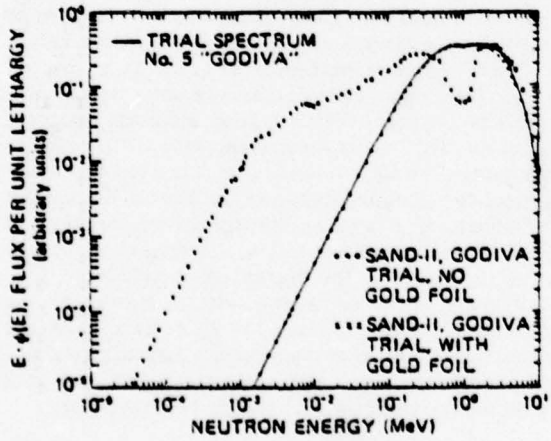

Fig. 6. Results of unfolding 50-cm WSMR FBR leakage spectrum with $1/E$ moderation component missing from $\phi_{tr}(E)$; i.e., $\phi_{tr}(E)$ = "GODIVA" (solid line). Without gold-foil data, SAND-II output agrees with glory-hole spectrum. When low-energy foil data are added (gold foil) and with no $1/E$ component in $\phi_{tr}(E)$, the SAND-II results are a catastrophic failure and show the need of good *a priori* data [$\phi_{tr}(E)$].

XI. SENSITIVITY TO UNFOLDING CODE

The WSMR FBR glory-hole data were unfolded with the SPECTRA code with $\phi_{tr}(E)$ = 1DF calculation. The results, presented as Fig. 7 and Table IV.O, are nearly identical to those of Fig. 3 and Table IV.C. The values of ϕ_{eq}/ϕ agree, and both fluxes ϕ and ϕ_{eq} are the same within 1%.

A comparison of Figs. 3 and 7 shows, however, that the feature of the SAND-II code designed to retard the formation of spurious structure is clearly evident. The SPECTRA result oscillates more about the 1DF calculation above 0.5 MeV.

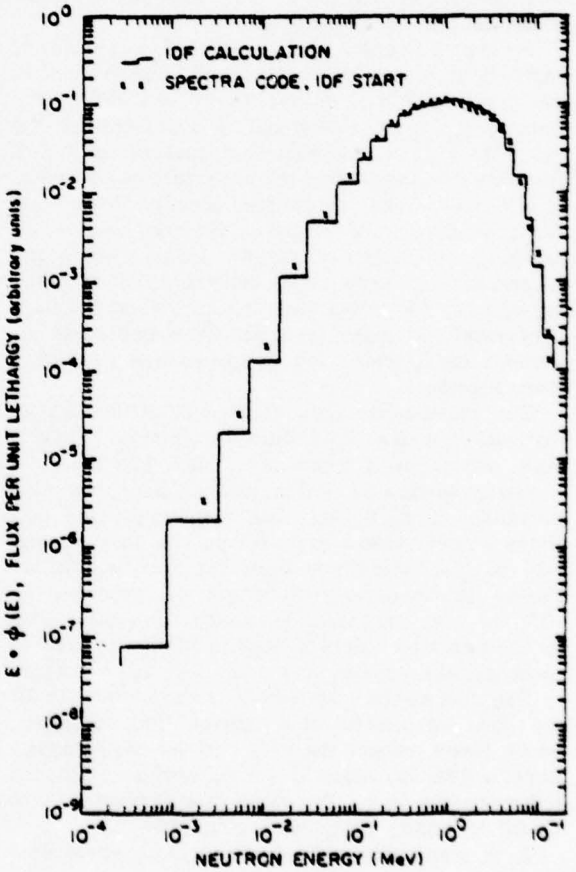

Fig. 7. Comparison of WSMR FBR glory-hole spectrum unfolded with SPECTRA code with $\phi_{tr}(E)$ = 1DF calculation.

XII. VARIATIONAL STUDY

A number of variational studies of the effects of cross-section uncertainties on unfolding have been made over the past several years.[25] In some of these studies, the reaction cross section for a given foil was varied at random over the neutron energy region above threshold. These showed that a random variation over many energy groups has almost no net effect on the output spectrum. In the work described here, the entire cross-section curve, $\sigma_x(E)$, was shifted bodily. This change can be representative of a cross-section normalization error, an incorrect gamma-ray branching ratio, or any uncertainty in the fission-fragment yield used in calculating back from count rate observed to activations actually produced. This cross-section change was simulated by changing the input activation number used in SAND-II. In fact, this variational study simultaneously evaluates the effects of counting, foil weighing, and self-absorption-correction errors, as well as cross-section uncertainties.

Figure 8 shows the result of a series of SAND-II unfolding operations with nine foils, with the cross sections varied by 15 and 25%, individually for most cases, and in pairs for the ^{238}U and ^{24}Mg foils. The perturbed spectra in Fig. 8 are shown compared to the unperturbed spectrum (solid line). The threshold energy of the foil cross section being varied is depicted by a vertical bar and horizontal arrow located below the corresponding curve. Note that the effect of varying one of the activations (or cross sections) is very local for those foils that have thresholds E_t above 1 MeV, where the E_t values are relatively close together.

The variational data (Tables IV.P through Z) indicate that for foils with thresholds below 2 MeV, where few thresholds exist, a 25% increase in cross section or foil activation produces ~2% decrease in ϕ_{eq}/ϕ; for foils with thresholds just above 2 MeV, where the neutron flux is still high and the thresholds are close together, a 25% increase in cross section of one foil produces an ~1% or less increase in ϕ_{eq}/ϕ; for foils with thresholds well above 2 MeV, a 25% increase in cross section results in a 0 to +0.4% ϕ_{eq}/ϕ change.

The flux above 0.01 MeV only varies by 0 to 3% for 25% variations in σ except for plutonium, which alone covers the 0.01- to 0.5-MeV region. Here, a 25% variation in cross section yielded a 10% variation in ϕ. The value of ϕ_{eq} varies by 0 to 4% for all cases except plutonium (8%).

It is clear that a flux-measuring method employing a large number of foils will provide greater accuracy than one employing one or two since error averaging and even error cancellation is involved with large numbers.

The threshold-foil method of flux (and radiation-damage) measurement is most sensitive to cross-section and counting errors in foils with thresholds below 2 MeV because few threshold values exist in this energy region. However, this energy region is covered by fission foils. Here, cross-section data are now approaching 5% in accuracy,[26] so that the contribution of these foils to the overall uncertainty in ϕ, ϕ_{eq}, and ϕ_{eq}/ϕ should be small compared to the importance of the *a priori* constraint of a good calculated value for the trial spectrum, $\phi_{tr}(E)$, used in the unfolding. Above a few MeV, where the cross-section errors are probably twice as large, there are several thresholds available, and appreciable cancellation of errors is expected. Also, the spectrum is rapidly falling there, so that the contribution to ϕ_{eq} is small.

XIII. SUMMARY AND CONCLUSIONS

XIII.A. Capabilities and Limitations of Foil Activation Spectrometry

Threshold-foil neutron spectrometry is a useful tool if enough information is input to the unfolding process. This consists of the *a priori* constraint of a good trial spectrum, $\phi_{tr}(E)$, especially below 1 MeV (but above 0.01 MeV), where at most two "windows" (intervals between successive E_t values) exist. In addition, a limited amount of operator interaction may be required to detect and eliminate any spurious activation value.

Thus, the threshold-foil activation method works well only when it carries out a small perturbation (correction) on a good spectral estimate to obtain $\phi(E)$ that is consistent with all threshold-foil data. The SAND-II code appears to be uniquely qualified to produce the minimum necessary perturbation, because this improved version of SAND retards the formation of spurious structure while preserving the known input structure (14-MeV peak, resonance dip, etc.). However, the version of SAND-II used for this work does not include the option of assigning a varying statistical weight to each foil activation, and this is a serious shortcoming that should be corrected.

XIII.B. Accuracy and Precision

The characterization of a neutron field in terms of its silicon radiation damage effective-

[25] W. N. McELROY, Hanford Engineering Development Laboratory, Private Communication (1975).

[26] *Proc. Consultants Mtg. on Nuclear Data for Reactor Neutron Dosimetry*, INDC (NDS)-56/U, September 10-12, 1973, International Atomic Energy Agency, Vienna (1973).

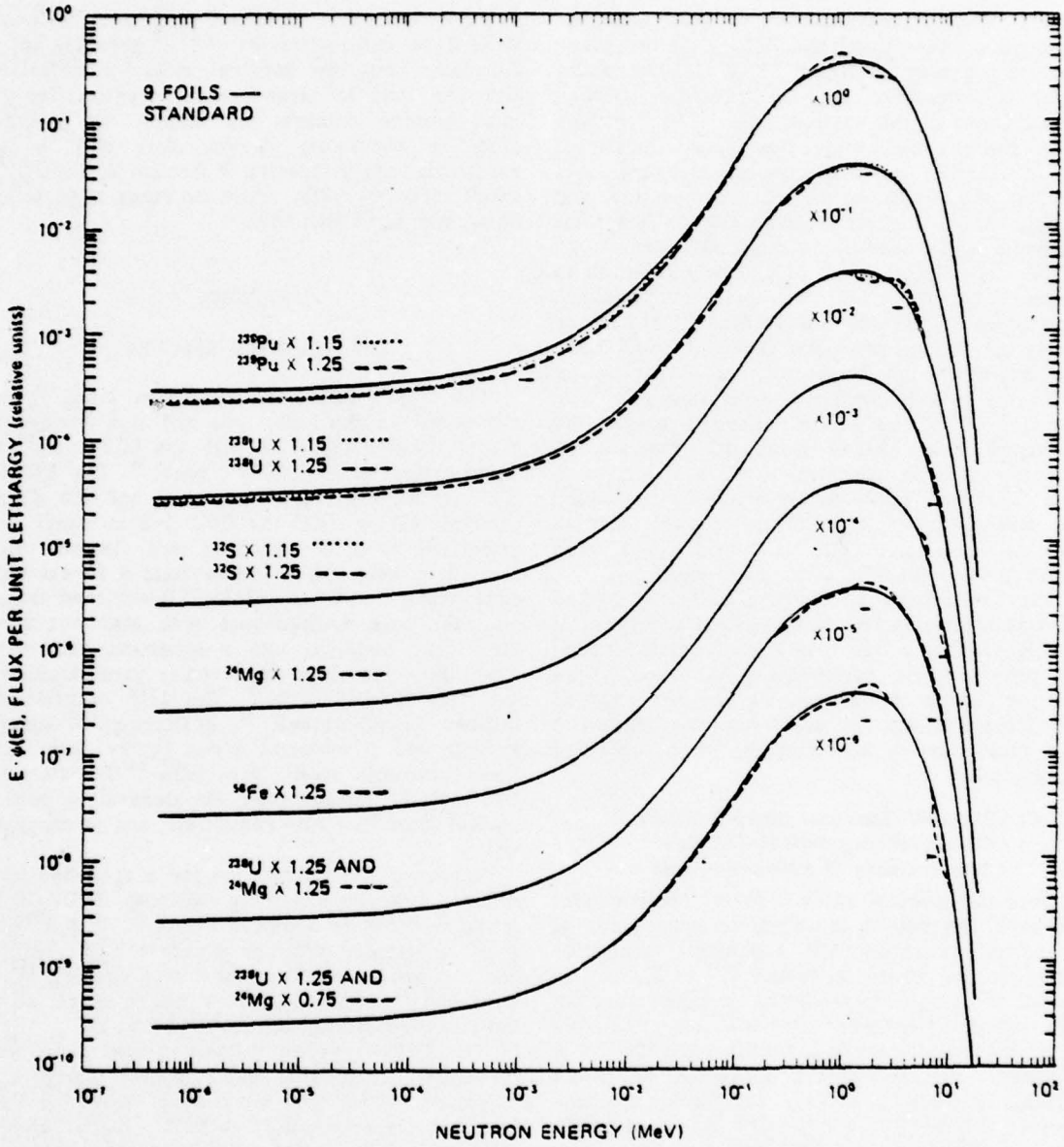

Fig. 8. Effect of varying foil activation or, equivalently, the cross section on SAND-II spectra. Solid curve is for unperturbed data in each case (the "standard" run).

ness is accomplished with an extensive parameter, Φ_{eq}, and an intensive parameter, Φ_{eq}/ϕ. The former quantifies the total radiation damage in terms of the equivalent fluence of 1-MeV (±15%) neutrons, and the latter quantifies the damage-producing capability of a unit of fluence, again in terms of the equivalent 1-MeV (±15%) fluence.

The definition of Φ_{eq} and Φ_{eq}/ϕ in Eqs. (3) and (4) involves only $\phi(E)$ and $D(E)$. Since $D(E)$ appears in the numerator and D (1 MeV ± 15%) in the denominator, only the shape of $D(E)$ is important for specifying the accuracy limitations of the present means of characterizing the neutron field. Thus, assuming the *shape* of $D(E)$ is correct [the

determination of the accuracy of $D(E)$ is beyond the scope of this paper], this leaves the measurement of the spectral flux $\phi(E)$ as the controlling factor in characterizing the radiation damage effectiveness of the neutron field. The accuracy of determining the spectral flux depends mostly on the accuracy of the foil activation measurements and data processing, on the foil cross sections and gamma-ray branching ratios, and on the trial spectrum $\phi_{tr}(E)$, used in the unfolding codes.

The cross-section set is probably known to an accuracy of 10 to 15% for nonfission foils and approaches 5% for the fission foils[28] that provide nearly all the spectral data from 0.01 to 2 MeV. The foil-activation measurements and branching ratios are given a suggested uncertainty of 15% or smaller. If a large number of foils are used, the variational study therefore indicates that ϕ_{eq} can be obtained to an accuracy of ~10% and ϕ_{eq}/ϕ to ~5%. This was independently checked by unfolding foil measurements of several "known" spectra with $\phi_{tr} = \phi_{calculated}$. The calculations ($\phi_c$) were known to better than 5% in terms of ϕ_{eq}/ϕ.

The precision of the threshold-foil method depends mostly on foil-measurement accuracy. It is only slightly better than the accuracy because the precision or repeatability is probably the limiting factor in determining the accuracy of specifying $\phi(E)$, ϕ_{eq}, and ϕ_{eq}/ϕ, once the constraint of a good starting spectrum, $\phi_{tr}(E)$, is accepted and applied.

XIII.C. Spectral Index and Other Methods of Characterizing Silicon-Damage Effectiveness of a Neutron Field

Once the spectral shape $\phi(E)$ of a neutron field has been determined, the absolute fluence can be measured accurately with any single threshold-activation foil whose threshold value, E_t, is low enough to sample the energies of importance yet high enough to receive negligible activation from the unimportant thermal and epithermal flux. For the three reactor spectra presented here, the fraction of the total damage sampled by a boron-covered ^{238}U or ^{239}Pu foil is 100% ($E_t \simeq 0.01$ MeV), $^{237}Np \cong 85\%$ ($E_t \simeq 0.5$ MeV), $^{238}U \simeq 50\%$ ($E_t \simeq 1.45$ MeV), and $^{32}S \simeq 15\%$ ($E_t \simeq 2.9$ MeV). While a boron-covered ^{235}U or ^{239}Pu foil can give a good measure of ϕ_{eq} and ϕ_{eq}/ϕ, because of a low threshold energy and flat cross section up to several MeV, the common practice of using ^{32}S foils (because of handling and licensing convenience and the economy of the required beta counter) to estimate the silicon radiation damage can lead to appreciable error if the neutron spectrum is not accurately known. Calculated spectra have often been used to obtain $\phi(E)$ which, in turn, was used to obtain the plutonium-to-sulfur ratio (spectral index of Table IV). However, most early calculations have underestimated $\phi(E)$ at energies above 2.9 MeV. Thus, the spectral-index characterization can lead to large errors in estimating the total neutron damage, ϕ_{eq}, unless the spectral shape is accurately known. Note that in the variational study (spectra P through Z, Table IV), the SI varied by ~25%, while the range of variation of ϕ_{eq} and ϕ_{eq}/ϕ was ~8%.

APPENDIX

THE STANDARD SPECTRA

The WSMR FBR spectrum (Figs. 2 and 3) was calculated in the glory hole and at a number of points outside the FBR with the 1DF code[27] (a modification of the DTF-IV code).[28] The ENDF/B-IV cross sections were used, and the slant-back-scattering from the floor (~2 m away) was simulated by a 4π concrete wall, 18 cm thick and 12 m away. The 20-cm-diam × 19-cm-high core, made of 10% Mo–93.2% ^{235}U-enriched uranium fuel, was homogenized with stainless-steel structural material into a spherical geometry. The flux-weighted cross sections were calculated with the GGC-5 code.[29] The 1DF calculations utilized S_8 quadrature, P_3 scattering, 30 energy groups, and 6 material zones [glory hole; air; liner (stainless steel); core (93%-^{235}U-enriched + 10% Mo + homogenized stainless-steel bolts); shroud (thin ^{10}B + Al + resin); air; and 4π concrete wall].

A recent 1DF calculation for a split-bed subcritical reactor assembly utilizing ENDF/B-IV cross sections is shown in Fig. A.1. It is in very good agreement with the accurate TOF (Ref. 7) and the proton-recoil proportional counter measurements[5,7] above 0.01 MeV where nearly all of the radiation damage occurs (see Fig. 1).

The TRIGA reactor "standard spectrum" was taken as a composite spectrum of a fine-group-structure NIOBE code calculation[11] above 0.8 MeV (verified experimentally with a ^6Li-^7Li diode-sandwich spectrometer utilizing shielded diodes[11]) overlapped with the GAZE-code reactor criticality

[27]The 1DF calculations and the GGC-5 calculation of the flux-weighted cross sections were carried out by C. Rindfleisch and D. Houston at IRT Corporation, San Diego, California.

[28]K. D. LATHROP, "DTF-IV Code, A FORTRAN-IV Program for Solving the Multi-Group Transport Equation with Anisotropic Scattering," LA-3373, Los Alamos Scientific Laboratory (1964). (1DF is an IRT modification of the DTF-IV code.)

[29]D. R. MATHEWS et al., "GGC-5, A Computer Program for Calculating Neutron Spectra and Group Constants," GA-8871, General Atomic Company (1971).

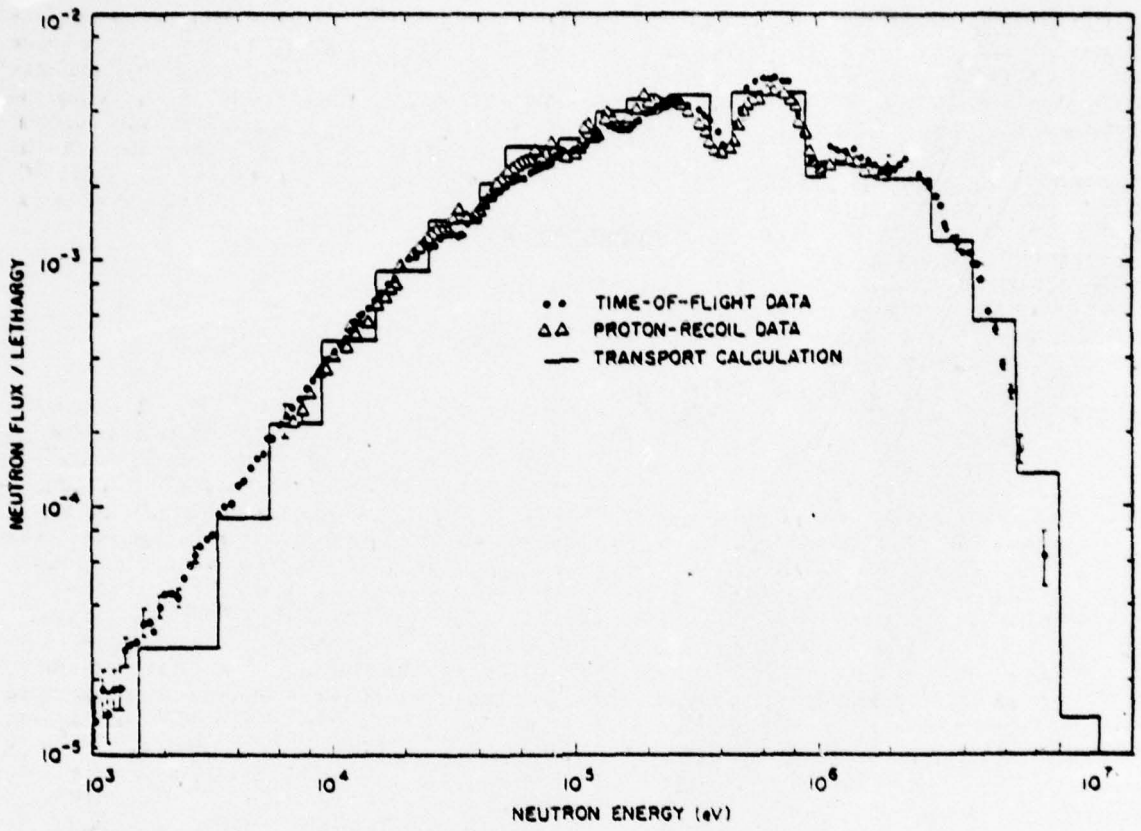

Fig. A.1. Time-of-flight and proton-recoil spectra for Linac-pulsed subcritical assembly compared to 1DF calculations (ENDF/B-IV cross sections).

calculation[23] in the 0.8- to 3-MeV region. The GAZE-code results were used below 0.8 MeV. The GAZE spectrum was checked independently with ^{239}Pu (^{10}B-covered), ^{237}Np, ^{238}U, and ^{32}S activation, with respective neutron threshold energies of ~0.01, 0.5, 1.45, and 2.9 MeV (Ref. 30). A comparison of measured neutron integral fluxes above each of the four respective thresholds with those given by the GAZE calculation yielded a constant ratio (within σ = 1.4%).

[30] J. A. SAYEG, Compiler, "Neutron and Gamma Dosimetry Measurements at the AFRRI-DASA TRIGA Reactor," AFFRI CR65-6, Air Force Radiobiology Research Institute, Defense Atomic Support Agency (1965).

ACKNOWLEDGMENTS

The authors gratefully acknowledge the assistance of H. Wright of WSMR for providing us with threshold-foil activation data from their 1974 FBR glory-hole and leakage spectra-foil activation data and reactor monitor data, for invaluable assistance in carrying out the 1975 IRT measurements at the WSMR FBR, and for performing an independent set of foil activation measurements with the IRT foils; of H. Wright and J. Meason (University of Arkansas) for help in getting the SAND-II code operational; of the Oak Ridge Radiation Shielding Information Center staff for providing the SAND-II and SPECTRA codes and cross-section tapes; of D. Houston for making the SAND-II and SPECTRA codes operational at IRT; of W. N. McElroy and B. F. Rider for helpful discussions; of D. Bryan and L. Harris for help with the $D(\delta)$ calculations; and of V. A. J. van Lint of Mission Research Corporation for help in correcting the $D(\delta)$ calculations.

This work was supported in part by the U.S. Defense Nuclear Agency.

APPENDIX B

DESIGNATION: E XX1

Standard Method for

IRRADIATING A STANDARD SET OF NEUTRON THRESHOLD ACTIVATION FOILS FOR RADIATION HARDNESS TESTING

1. SCOPE

1.1 This method describes a procedure for irradiating a standard set of threshold activation foils to be used for neutron spectrum unfolding covered in ASTM Method E XX3, "Standard Method for Unfolding Neutron Spectra for Radiation Hardness Testing." It is intended to be used in conjunction with ASTM Method E XX2, "Measuring Foil Activities for Radiation Hardness Testing," for providing the foil-activation data used as input to the SAND II neutron spectrum unfolding code.

1.2 This method presents a standard set of foils that have been used at many facilities, and describes the flux-uniformity, the neutron self-shielding, and flux-depression corrections that need to be considered in choosing the foil thickness, the covers, and the locations of the foils.

1.3 In this method, considerations that apply rather generally to neutron-activation detectors are discussed in ASTM Method E 261, "Measuring Neutron Flux by Radioactivation Techniques."

1.4 Background information on the detailed methods for individual threshold foil detectors of widest use is given in the following ASTM Methods.

E 262 Measuring Thermal Neutron Flux by Radioactivation Techniques

E 263 Measuring Fast-Neutron Flux by Radioactivation of Iron

E 264 Measuring Fast-Neutron Flux by Radioactivation of Nickel

E 265 Measuring Fast-Neutron Flux by Radioactivation of Sulfur

E 266 Measuring Fast-Neutron Flux by Radioactivation of Aluminum

E 343 Fast Neutron Flux by Analysis of Molybdenum-99 Activity from Uranium-238 Fission

E 393 Measuring Fast-Neutron Flux for Analysis for Barium-140 Produced by Uranium-238

E 419 Selection of Neutron Activation Detector Materials.

2. APPARATUS

2.1 Precision balance (0.1 mg accuracy).

2.2 Cadmium covers (0.05 to 1 mm thick).

2.3 ^{10}B cover ($\sim$1-1.8 g/cm^2 ^{10}B)

2.4 A 1.27 cm (0.5 inch) i.d. aluminum "cup" with cover for ^{127}I (as ICH_2CONH_2).

3. THRESHOLD ACTIVATION FOILS

3.1 Redundancy

3.1.1 The set of foils listed in Table I is part of the self-consistent set that resides in the SAND II cross-section library. These foils were selected in an experimental evaluation program (1) in which three different "known" spectra were compared to corresponding threshold-foil spectrometry measurements unfolded with the SAND II code. This set

contains two redundant 1/v foils {all three should be exposed, counted, and input to SAND II for a first-pass (ACTIVATION) run to select the average one}, and a redundant $E_t = 0$ fission foil. ^{235}U and ^{239}Pu have very similar cross-section shapes. The ^{235}U foil presents much less of a safety hazard than ^{239}Pu, and is cheaper. It is very useful, when measuring soft (TRIGA) spectra, in determining the correction for the ^{235}U impurity in the ^{238}U foil (readily available with ∿400 ppm ^{235}U impurity). Although the ^{32}S foil is widely used as a monitor foil, it is not part of the set because it requires an entirely different counter (for betas) and an involved calibration technique. It has about the same threshold as the $^{58}Ni(n,p)^{58}Co$ foil reaction, and should only be used when the Δ_o {the SAND II activation "error" as calculated for $\phi_{tr}(E)$ as input: see ASTM Method E XX3} of the two are within a few percent (≤5 percent) of each other; otherwise, SAND II may be driven to many iterations in trying to find a solution $\phi(E)$ that is compatible with both activations. This usually leads to an unacceptable solution.

3.2 Foil Impurities

3.2.1 Foil impurities are especially serious for a moderated source (TRIGA reactor) when the impurity leads to the same reaction product by way of thermal-neutron capture. Some of these foils (impurities) are $^{238}U(^{235}U)$, $^{27}Al(^{23}Na)$, $^{56}Fe(^{55}Mn)$. For a soft spectrum, such as the TRIGA J-tube spectrum (boral shielded), the ^{235}U fissions (Cd covered) were ≈100 times greater than the ^{238}U; therefore, the ^{238}U must have no more than ∿200 ppm of ^{235}U to reduce the error to 2 percent. Higher impurities can be tolerated for GODIVA-type reactors where the low-energy flux is much less intense, or with TRIGA-type reactors if the ^{235}U foil data are used for correcting the ^{238}U activity. In this case, the percent ^{235}U in ^{238}U must be accurately known. For the $^{56}Fe(n,p)^{56}Mn$

reaction the ^{55}Mn impurity must be no more than 10 ppm (with Cd cover) for use with a TRIGA spectrum, and 100 ppm at 50 cm from a GODIVA-type reactor (~2 meters off the concrete floor) for ≤2 percent background from the $^{55}Mn(n,\gamma)^{56}Fe$ reaction. Similarly, a manganese foil (Cd covered) can be used to correct the ^{56}Fe data if the impurity correction is small (≤20 percent of total n,p activation) and the percent Mn in Fe is accurately known.

3.3 The Influence of Nuclear Data on the Selection of Foils

3.3.1 Since the total number of interactions must be deduced from the absolute gamma-ray count with good accuracy (say 5 percent per foil), the foils selected must have gamma-ray yields known to a similar accuracy or better. These corrections include conversion-electron production, branching ratio to a given energy level, and fission yield.

3.3.2 The 1593-keV gamma-ray line from ^{140}La produced in ^{232}Th fission is not useful because of interference from ^{232}Th radioactivity. This has often led to the use of the 537-keV line from the ^{140}Ba precursor of ^{140}La, which is listed in the Table of Isotopes (2) as having an intensity of 0.34 gamma per ^{140}Ba decay. A recent evaluation (3) has shown this to be 25.7 percent, which is in much closer agreement with some work of Ref. 1, in which ^{235}U fission yields were compared by way of four fission-product gamma rays (1593 keV for ^{140}La, 537 keV for ^{140}Ba, 743 keV for ^{97}Zr, and 668 keV for ^{132}I).

3.3.3 The choice of gamma-ray line thus directly influences the accuracy of determining the specific activity produced during the neutron irradiation. It also influences the final choice of foil thickness, in that the selection of a low-energy gamma-ray line may lead to a large gamma-ray self-absorption correction in counting. For example, the ^{232}Th

foil of Table I has a maximum attenuation of 22 percent, or an average correction of ∿11 percent, for the 537 keV line. This represents an upper limit for foil thickness. Thus, the gamma scattering, as well as the neutron self-shielding discussed below, will influence the foil selection.

3.4 Foil Encapsulation

3.4.1 Fission foils may be encapsulated in a hermetically sealed container to avoid oxidation and loss of materials, and for health-hazard requirements. The ^{239}Pu foil, if used instead of the much safer ^{235}U foil, will require special encapsulation and periodic wipes to check for leakage of the material. Copper encapsulation has been found satisfactory for ^{235}U, ^{238}U, ^{237}Np, and ^{232}Th foils. It is made ∿0.1 to 0.25 mm thick at the flat surfaces and is soldered at the periphery.

3.5 Foil Diameter

3.5.1 All foils are to be 1.27 cm (0.5 inch) or smaller in diameter to simplify foil-size effects in calibrating against point gamma-source standards (see ASTM Method E XX2). A correction (small) can be made for this geometric effect.

4. IRRADIATION PROCEDURES

4.1 Foil Covers

4.1.1. Cadmium covers of 0.5 mm thickness are prescribed for all fission foils and 1/v detectors, and for detectors such as ^{238}U, ^{56}Fe, ^{60}Ni, and ^{27}Al, where traces of impurities (^{235}U, ^{55}Mn, ^{60}Co, and ^{23}Na) that yield the same reaction product via thermal-neutron capture can lead to unmanageably large corrections. When these corrections are greater than 5 percent, the irradiation should include cadmium-covered foils made of these impurities (^{235}U, ^{55}Mn, ^{60}Co, ^{23}Na, etc.). The corrections can then be made with good accuracy if the percent

impurity in the foil is accurately known. If not, a thermal-neutron activation-analysis type of irradiation will be required. Cadmium foils are not needed in the glory hole of a fast-burst reactor with little or no moderator material (<0.5 g, say) near or inside the cavity.

4.1.2. Covers of ^{10}B are useful on fission foils for the case of measuring a soft TRIGA spectrum, especially if a boral shield is used to surround the irradiation cavity. If the boral shield is a good 4π shield, and if a negligible amount of moderator is contained within the shield, the boral shielding can be properly accounted for by the SAND II unfolding code. In this case, the ^{10}B cover is not as important. The boral thickness is entered for each and every foil, and a 1/E spectrum is entered down to 3×10^{-7} MeV, the cadmium cutoff energy, or lower. If no ^{10}B cover is used, and if the cavity is only partially shielded, it will be difficult to predict the neutron spectrum from 10^{-3} MeV down to $\sim 3 \times 10^{-7}$ MeV, where the cadmium covers become effective. In this case, it is important to place all the 1/v foils, the foils with important 1/v impurities (see above), and all fission foils in a boral "box" or a ^{10}B cover. For best results, a ^{10}B cover of 1 to 1.8 g/cm^2 of (93 percent) ^{10}B is used. This cover thickness is then input to SAND II. In this way, the fraction of activations arising from 3×10^{-7} MeV to 10^{-2} MeV neutrons will be both greatly reduced and more accurately calculated for the SAND II unfolding process. The known spectrum outside the boral (a 1/E spectrum) is used down to 3×10^{-7} MeV or lower.

4.1.3 The ^{10}B covers may be replaced by cadmium covers for up to one meter from a GODIVA-type reactor that is a few meters above the concrete floor, or for the glory hole where no low-energy neutrons are found, and where the ^{10}B

covers generally cannot be placed in any case. If the covers are used with a directional source, such as outside the GODIVA reactor, the fission-foil activation will require a correction for scattering by ^{10}B. The correction can either be done experimentally, with pure finite-threshold fission foils (^{237}Np or ^{232}Th) that contain negligible zero-threshold impurities which yield the same gamma-ray lines, or with a sophisticated calculation that weights each inscattering by the track length through the material. These corrections are the order of 10 percent for a 1.65 g/cm^2 ^{10}B cover and a thin 1/2-inch-diameter fission foil (4).

4.2 Foil Interferences

4.2.1 A strong resonance absorber such as a thick ^{235}U foil cannot be placed in front of a 1/v absorber, and thick foils with their covers should not be stacked so as to result in a large and unmanageable scattering correction. For isotropic flux, the interfering foils should not scatter more than about 10 percent of the flux, as given by the simple hand calculation:

$$\phi = \phi_o e^{-\Sigma_t T} , \qquad (1)$$

where $\Sigma_t T$ is the sum of the products of the macroscopic total cross sections and thicknesses for those foils that are stacked in front of the deepest foil, i.e.,

$$\Sigma_t T = \Sigma_t(1)T_1 + \Sigma_t(2)T_2 + \cdots \qquad (2)$$

For a beam geometry, the corresponding "interference" must be held to no more than ∿4 percent because of the more complex scattering correction.

4.3 Foil Self Shielding

4.3.1.1 The correction for self shielding is appreciable only for the 0.0025-cm-thick gold foil (with its highly absorbing resonance at ∿5 eV), being about a factor of two for epicadmium neutrons (5,6). The effect on the unfolded spectrum, $\phi(E)$, of varying the gold-foil activation by a factor of two was mostly local, appearing as a dip or bump at the 5-eV resonance, and changing ϕ_{eq} by only 1 percent.

4.4 Flux Uniformity

4.4.1 If the foils cannot all be located in the same region, or in a region of uniform flux (as determined from symmetry considerations), they can be spread out over a larger volume of varying flux but of constant neutron-spectrum shape. If the flux varies by more than 3 percent from point to point, flux monitors should be used at the various cases. Around a GODIVA-type reactor, thick sulfur foils can be located near individual foils. Where space is more limited, thin nickel $\{^{58}Ni(n,p)^{58}Co\}$, iron $\{^{54}Fe(n,p)^{54}Mn\}$, or even aluminum $\{^{27}Al(n,\alpha)^{24}Na\}$, monitors can be used; considerations discussed in ASTM Method E 261 apply.

4.5 Flux Depression

4.5.1 At low energies, flux depression is important for bare thermal-neutron detectors near cadmium-covered discs, if both are embedded in a moderator. At high energies, it is important for the same situation if the moderator contains reactor fuel. However, in sizeable cavities used for radiation damage studies, the cadmium covers, as well as the foils, generally subtend a negligibly small solid angle at the point of any surrounding moderator of fuel. For a GODIVA reactor glory hole, the foil-interference considerations discussed in Sec. 4.2 will completely dominate.

5. FOIL WEIGHING

5.1 All foils should be weighed with a 0.1-mg precision balance that is checked against known weights over the range of the foil masses. The encapsulated foils are, of course, carefully weighed before encapsulation.

6. PURITY CERTIFICATION

6.1 The foil purity analysis results must be kept on permanent record for use in making foil impurity corrections. These impurities must be known to an accuracy dictated by the magnitude of the correction, which, in turn, will depend on the kind of neutron spectrum being measured (see Sec. 3.2). If, for example, the percentage impurity (say 400 ppm ^{235}U in ^{238}U) is known to an accuracy of 10 percent in a foil, and the separate impurity foil (^{235}U) is irradiated the same way as the other, then the impurity effect can be reduced to 10 percent of its stated value (40 ppm ^{235}U in ^{238}U, for this example) by calculating the correction. In this case, up to 2000 ppm of ^{235}U impurity could be tolerated for a TRIGA spectrum (see Sec. 3.2).

7. PRECISION

7.1 Foil weighing, neutron self shielding, and flux uniformity influence the precision of those aspects of the flux measurement to which this method is addressed. An estimated value of 3 percent is suggested as the effects of these corrections on the measurement of specific activities, assuming the scattering of the stack is kept to less than 10 percent for an isotropic flux, and to less than 4 percent for a directed flux. Assuming no thick ^{10}B covers are used in the directed-flux case, and secondary monitors such as thin $^{58}Ni(n,p)^{58}Co$ reaction foils are used when the foils are widely distributed in space, these factors will have only about a 1 percent effect on ϕ_{eq}.

8. ACCURACY

8.1 The factors that affect the precision (see Sec. 7) will directly impact the accuracy. In addition, the selection of the foils and the gamma-ray line to be measured for each foil impact the accuracy by way of the uncertainties in gamma-ray intensity (gamma/reaction) and fission yield. These may be as large as 10 percent in individual cases, but should, on the average, contribute no more than 5 percent to the uncertainty in the specific activations. Assuming a reasonable amount of foil-to-foil randomness in this error, the contribution to the uncertainty of specifying ϕ_{eq} is estimated to be no more than 2 to 3 percent.

REFERENCES

(1) Verbinski, V. V., Lurie, N. A., and Rogers, V. C., "Threshold-Foil Measurements of Reactor Spectra for Radiation Damage Applications" *Nuclear Science and Engineering* 65, 316 (1978).

(2) Lederer, C. M., Hollander, J. M., and Perlman, I., Table of Isotopes, John Wiley & Sons, Inc., New York, 6th Edition, 1967.

(3) Harvey, J. T., Meason, J. L., Hogan, J. C., and Wright, H. L., "Gamma-Ray Intensities for the Radioactive Decay of ^{140}Ba and ^{140}La, "*Nuclear Science and Engineering* 58, 431 (1975).

(4) Wright, H. L., Applied Sciences Division, White Sands Missile Range, New Mexico 88002 (private communication).

(5) ANL 5800, Reactor Physics Constants, Argonne National Laboratory, Argonne, Illinois 60439, Feb. 1969.

(6) Sanford, G. S., and Secksinger, J. H., "Thickness Corrections for Neutron-Activated Gold Foils," ANL-7545, Argonne National Laboratory, Argonne, Illinois 60439.

(7) *Proceedings of the Consultants' Meeting on Nuclear Data for Reactor Neutron Dosimetry,* INDC(NDS)-56/U, IAEA, Vienna, September 10-12, 1973.

(8) Meek, M. E., and Rider, B. F., "Compilation of Fission Product Yields," NEDO-12154-1, Vallecitos Nuclear Center, Pleasanton, California 94566.

TABLE I

Activation Foils (1.27-cm diam)

Reaction	E_t (MeV)	E_γ (keV)	Gamma/Reaction (Fission Yield, %)	$T_{1/2}$	Foil Mass (g)	Isotopic Abundance (%)	Notes
$^{197}Au(n,\gamma)^{198}Au$	0	412	0.95	2.696 days	0.056	100	a
$^{59}Co(n,\gamma)^{60}Co$	0	1173 1333	1.00 1.00	5.258 yr	0.057	100	a,b
$^{55}Mn(n,\gamma)^{56}Mn$	0	847 1811	0.99 0.29	2.58 h	0.030	100	a,b
$^{238}U(n,f)^{140}La$	0(0.01)[c]	1596	0.96 (6.29)	40.23 h	0.281	100	a,d,e
$^{239}Pu(n,f)^{140}La$	0(0.01)[c]	1596	0.96 (5.24)	40.23 h	0.150	100	a,d,e
$^{237}Np(n,f)^{140}La$	0.5	1596	0.96 (5.69)	40.23 h	0.580	100	a,d,e
$^{237}Np(n,f)^{97}Zr$	0.5	743	0.92 (6.01)	16.8 h	0.580	100	a,f,e
$^{115}In(n,n')^{115m}In$	1.0	335	0.50	4.50 h	0.255	95.7	
$^{238}U(n,f)^{140}La$	1.45	1593	0.96 (6.02)	40.23 h	0.495	100	a,d,e
$^{232}Th(n,f)^{140}Ba$	1.75	537	0.256 (7.91)	12.8 days	1.066	100	a,g,e
$^{232}Th(n,f)^{97}Zr$	1.75	743	0.92 (4.12)	16.8 h	1.066	100	a,f,e
$^{54}Fe(n,p)^{54}Mn$	2.20	835	1.00	303 days	0.142	5.82	
$^{58}Ni(n,p)^{58}Co$	2.9	810	0.99	71.3 days	0.282	67.8	
$^{32}S(n,p)^{32}P$	2.9	Betas	1.00β	14.3 days	4.10	95.0	a
$^{24}Mg(n,p)^{24}Na$	6.3	1369	1.00	15.0 h	0.030	79	a
$^{56}Fe(n,p)^{56}Mn$	7.5	847 1811	0.99 0.29	2.58 h	0.142	91.7	a,i
$^{27}Al(n,\alpha)^{24}Na$	8.7	1369	1.00	15.0 h	0.257	100	a
$^{127}I(n,2n)^{126}I$	11.0	386 667	0.34 0.33	13.05 days	0.657	100	
$^{90}Zr(n,2n)^{89}Zr$	14	910	0.99	78.4 h	0.108	51.5	

[a] Cadmium cover 0.05 to 0.10 cm thick.

[b] Use ^{59}Co instead of ^{197}Au and ^{55}Mn for very long irradiations.

[c] $E_t \simeq 0.01$ MeV with ^{10}B sphere [important for soft (TRIGA) spectra, where $\phi(E) < 0.01$ will otherwise dominate]. When ^{235}U or ^{239}Pu foil is ^{10}B-covered, also cover ^{238}U and ^{237}Np foils so that accurate corrections can be made for ^{238}U and ^{239}Pu impurities in these high E_t foils.

[d] 40.23-h daughter of 12.80-day ^{140}Ba. Wait five days for maximum decay rate (ASTM E 393).

[e] Fission yields are for bombardment with fission-spectrum neutrons. For thermal and 14 MeV, see Ref. 5.

[f] Use ^{97}Zr for low fluence (3×10^{11} to 3×10^{13} n/cm^2). Use peak shape analysis or measure twice, seven days apart, to strip off 740-keV ^{99}Mo gamma ray ($T_{1/2}$ = 67 h).

[g] ^{232}Th radioactivity interferes with ^{140}La line.

[h] Requires separate detector, and calibration technique is complex.

[i] Maximum manganese impurity = 0.001%, cadmium-covered. Omit $^{56}Fe(n,p)^{56}Mn$ for long irradiations.

DESIGNATION: E XX2

Standard Method for

MEASURING FOIL ACTIVITIES FOR
RADIATION HARDNESS TESTING

1. SCOPE

1.1 This method describes a standard procedure for measuring the absolute gamma-ray emission rate from a standard set of neutron threshold-activation foils used in spectrum measurements, and for calculating the specific activity of the foil from the gamma-ray data.

1.1.1 The measuring procedure takes into account corrections for finite foil size and thickness in detector calibration, count rate and pulse-pileup losses, and background measurements for complex decay schemes such as exist in some fission-foil lines.

1.1.2 The data processing takes into account complex background subtraction for fission-foil lines, corrections for irradiation, wait and count times, and corrections for gamma-ray branching ratios, conversion electrons, fission yields, and gamma-ray self absorption in the foils.

1.2 This method is intended to be used in conjunction with ASTM Method E XX1, "Irradiating a Standard Set of Neutron Threshold Activation Foils for Radiation Hardness Testing," for providing the foil-activation input data that are required in unfolding neutron spectra, as described in ASTM Method E XX3, "Unfolding Neutron Spectra for Radiation Hardness Testing." This method is part of the set of draft

standards which include ASTM Method E XX4, "Characterizing Neutron Spectra in Terms of 1-MeV Equivalent Fluence for Radiation Damage in Silicon," and ASTM Method E XX5, "Measuring the Relative 1-MeV Silicon-Equivalent Fluence with Fast Neutron Monitors."

1.3 In this method, considerations that apply rather generally to neutron-activation detectors are discussed in ASTM Method E 261, "Measuring Neutron Flux by Radioactivation Techniques," while background information on the detailed methods for the individual threshold-foil detectors of widest use is given in the following ASTM Methods.

E 262 Measuring Thermal Neutron Flux by Radioactivation Techniques

E 263 Measuring Fast-Neutron Flux by Radioactivation of Iron

E 264 Measuring Fast-Neutron Flux by Radioactivation of Nickel

E 265 Measuring Fast-Neutron Flux by Radioactivation of Sulfur

E 266 Measuring Fast-Neutron Flux by Radioactivation of Aluminum

E 343 Fast-Neutron Flux by Analysis of Molybdenum-99 Activity from ^{238}U

E 419 Selection of Neutron Activation Detector Materials

2. APPARATUS

2.1 Ge(Li) or Intrinsic Germanium Gamma-Ray Detector

2.1.1 Ten percent or greater photopeak efficiency for ^{60}Co, referred to a 7.62 cm by 7.62 cm (3 inch) diameter NaI(Tl) detector, both at 25 cm from source. Multichannel analyzer, about 4000 channels total, 100 mHz or faster, 2 to 2.5 keV resolution. Precision tail-pulser, ∿60 cps,

with inputs to gamma-ray detector preamplifier and to scaler.

2.2 Foil and Source Holders

2.2.1 For accurately positioning (and measuring) the center of each foil, and the center of the gamma-ray standard. Required precision is ∿0.2 mm or better in distance from face of detector, and 0.5 mm or better in lateral alignment. The apparatus must have provision for inserting a 1.27-cm-thick lead shield (see Sec. 2.3).

2.3 Lead Slab

2.3.1 A lead slab 1.27 cm thick, positionable against Ge(Li) or intrinsic germanium cryostat (flat face).

2.4 NBS 11-Line Gamma-Ray Standard

2.4.1 An NBS 11-line gamma-ray standard, less than one year old.

3. DETECTOR CALIBRATION

3.1 The detector must be calibrated to give the correct efficiency for gamma rays emitted from a 1.27-cm-diameter source, using a smaller diameter source as a standard. This is accomplished by measuring the count rate under each peak of the standard, first near the face of the detector cryostat, and then 10 cm farther back.

3.2 This measurement is made at both places with the 11-line NBS gamma-ray source. This gives the efficiency $\varepsilon(x)$ at some unknown distance x from the effective center of the detector, and $\varepsilon(10 + x)$ at 10 cm + x. (At 10 cm, the 1.27-cm-diameter foil size leads to a correction of <2 percent, as compared to the source which is ∿0.5 cm diameter.) Plot the efficiency at each position on log-log plotting paper and read off the efficiency at each position for an energy E_γ, corresponding to one of the hottest foils, say

$^{197}Au(n,\gamma)^{198}Au$ (412 keV), and calculate the ratio $R_{cal} = \varepsilon(x)/\varepsilon(10+x)$. Repeat the measurement at both positions with the gold foil and get R_{gold}. Multiply the $\varepsilon(x)$ by R_{gold}/R_{cal} to get the correct efficiency for a 1.27-cm-diameter foil at x. Repeat the procedure for one or two higher gamma-ray energies with another hot foil (say ^{56}Mn with gamma-ray lines at 847 and 1881 keV). Now slide the $\varepsilon(x)$ curve, as measured with the 11-line standard, to pass through these three corrected points. This represents the proper efficiency curve for a 1.27-cm-diameter foil at the distance x from detector "center."

3.3 From count-rate measurements at x and 10+x, it was found that the effective center of a particular 13 percent Ge(Li) gamma-ray detector (1) is 2.1 cm from the front face of the cryostat. Thus, the center of the standard source and of all the foils (the center being at half the foil thickness) must be located to within 0.2 mm to keep the positioning uncertainty down to 2%.

3.4 The above same calibration must be repeated for the ^{237}Np source behind the 1.27-cm lead shield.

3.5 A simpler approach can be used if the true axis of the detector is located. A careful measurement and x-y plot of count rate versus position at the cryostat face will accomplish this. The point source is then simply moved off axis, 0.7 of the way to the periphery of the 1.27-cm-diameter foil. The efficiency measured here is approximately the area-weighted efficiency over the 1.27-cm-diameter foil.

4. COUNTING PROCEDURE AND AREA ANALYSIS

4.1 Set the amplifier gain so that 2 MeV corresponds to 4000 channels on the analyzer, and the 1-MeV point at about 2000 channels so that the zero-channel offset is small. Set the precision pulser so that it falls at ∿1.9 to 1.95 MeV,

well above the ^{56}Mn 1811-keV line. Place the foil in the counting position. Run the analyzer on clock time with the pulser running. The ratio of the pulser events appearing in the peak at ∿1.9 to 1.95 MeV to the pulses generated gives the correction for the combination of analyzer deadtime and pulse-pileup losses from the peak. The analyzer can be run on live time instead, but in this case the true clock time must be measured. Alternatively, the pulser events can be counted with a scaler, care being taken that the analyzer and scaler are turned on and off together.

4.2 The peak analysis routine must be the same for pulses from the pulser as for those from both calibration and foil events. In one method, the counts are plotted for the peak and the nearby region (∿5 keV or more on each side). By fitting a straight line through the baseline, the baseline area can be subtracted from the peak area. In counting fission foils, the peak shape must be examined carefully for the presence of a very close neighboring peak, in which case peak-shape analysis must be used. The counting statistics must be very good for the peak-shape analysis to be accurate. The analysis can either be done by hand, or with the SAMPO code (2). The analyzer should be run, whenever possible, until the peak area is 10,000 counts or greater.

5. BACKGROUNDS

5.1 Room Background

5.1.1 This must be kept to a minimum by selecting a low-background counting area, stacking a lead shield of at least 5-cm thickness around the detector, and moving away all sources not being counted. A room-background run is taken and is definitely required for long (overnight) counts, such as for the $^{90}Zr(n,2n)^{89}Zr$ reaction, which has a threshold energy E_t at about 14 MeV, and consequently, a low specific activity, or for $^{60}Ni(n,p)^{60}Co$, where the half-life is very long.

5.2 Fission-Foil Background

5.2.1 Fission-foil backgrounds must be carefully measured because the foils are radioactive with a very complex gamma-ray emission spectrum, and because they are reused due to their high replacement cost. If they had been irradiated within several half-lives before the next planned irradiation (of at least the same or higher fluence), the background should be measured more than once to separate out the normal line {537, 743, or 1593 keV (see Table I)}, with relatively short half-life, from any long-lived radioactivity contribution due to natural radioactivity (or to other fission fragments). The background peak area that will still be present during the counting time after the next irradiation is then calculated by adding the time-dependent area of the gamma-ray line with known half-life to that of the steady-state component.

6. DATA ANALYSIS

6.1 Correct the peak areas for analyzer deadtime losses and pulse-pileup losses by multiplying the area by the ratio of the number of precision pulses generated during the counting period to the number found in the pulser peak at ∿1.9 MeV. Divide by detector efficiency, gamma-ray intensity (gamma/reaction, Table I), and fission yield (for fission foils). Correct for gamma-ray self absorption by using the approximate expression

$$\phi_o = \phi e^{+\Sigma_t (M/2)} \qquad (1)$$

where ϕ is the measured activation decay rate at the time of counting, ϕ_o the corrected activation, Σ_t the macroscopic gamma-ray total cross section (cm^2/g), and M the thickness

(g/cm^2) of the foil and encapsulation material. Equation (1) is accurate to ~1 percent in ϕ_o for $\phi_o/\phi < 1.2$. The number N of atoms made radioactive (or in the case of fission foils, the number of fissions induced) by the neutron irradiation is then given by:

$$N = \frac{N_A \lambda t(i)\, e^{\lambda t(w)} \left[1-e^{-\lambda t(i)}\right]^{-1} \left[1-e^{-\lambda t(c)}\right]^{-1}}{Y_\lambda Y_f} \qquad (2)$$

where N_A is the net peak area corrected for detector efficiency, t(i) the neutron irradiation time, t(w) the wait time between the end of the irradiation interval and the beginning of the counting interval, and t(c) is the duration of the counting interval, Y_λ is the λ/reaction, and Y_f is the fission yield.

6.2 For the 1593-keV line of ^{140}La ($T_{1/2}$ = 40.23 hours), which is produced by the ^{140}Ba decays ($T_{1/2}$ = 12.8 days), Eq. 2 becomes

$$N_B = \frac{N_L \lambda_B t(i)(\lambda_L-\lambda_B) \left[1-e^{-\lambda_B t(i)}\right]^{-1} \left[1-e^{-\lambda_B t(e)}\right]^{-1}}{\lambda_L Y_f * 0.96 \left[e^{-\lambda_B t(w)} - e^{-\lambda_L t(w)}\right]} \qquad (3)$$

where N_B, λ_B, and are the number of fissions produced, the decay constant for ^{140}Ba, and the fission yield for ^{140}Ba (see Table I), respectively, N_L is the peak area divided by detector efficiency for the 1593-KeV ^{140}La gamma rays, λ_L the decay constant for ^{140}La, and 0.96 is the (γ/reaction) for the 1593-keV gamma ray from ^{140}La.

6.3 For wait times of 10 days or more, Eq. 3 reduces to:

$$N_B = \frac{N_L \lambda_B t(i) * (0.869)\, c^{\lambda_B t(w)} \left[1-e^{-\lambda_B t(i)}\right]^{-1} \left[1-e^{-\lambda_B t(c)}\right]^{-1}}{Y_f * 0.96} \quad (4)$$

with ~1 percent error at 10 days.

6.4 The value of N or N_B (Eqs. 2, 3, or 4) is corrected for any significant neutron self shielding or flux depression during irradiation, and $R = N/N_o$ (radioactive atoms per target atom) is computed from the measured target mass and isotopic abundance for the reaction (Table I).

7. PRECISION

7.1 The precision is limited by the counting statistics, by the reproducibility of the NBS calibration source and of the location of the foils and the standard source with respect to the detector, and by the reproducibility of the peak-area-analysis routine used for the foil-counting and background measurement.

7.2 A calibration of one NBS 11-line source mix (88-, 122-, 165-, 279-, 392-, 514-, 662-, 898-, 1173-, 1333-, and 1836-keV lines) against another resulted in a standard deviation of 1 percent for the reproducibility of the calibration points. The source location (including source-size correction) leads to a precision uncertainty of ~3 percent (if a good alignment scheme is employed for both distance and lateral alignment); because of the nearness of the foils to the detector, the weaker foils must be counted next to the face of the detector cryostat. Peak-area analysis and background subtraction are somewhat inseparable. If ~1 percent or better

counting statistics can be achieved, the associated precision is ∿2 percent for non-fission foils and 2 to 5 percent for fission foils, depending on the line chosen, the irradiation fluence, and the magnitude of the background.

7.3 An overall precision of 5 to 6 percent is suggested as the best achievable precision, combining all the above factors. If the 16.8-hour ^{97}Zr line of 743 keV (4) is used for analysis of ^{232}Th and ^{237}Np fission, the error may be much greater, unless shape fitting is utilized and measurements are made at different times to subtract out the effect of the ^{99}Mo gamma-ray line (67 hour), which has nearly the same gamma-ray energy (740 keV).

8. ACCURACY

8.1 The accuracy of counting and data analysis reflects directly on the precision (see Sec. 7), and the accuracy of the nuclear data. At this time, it is felt that the uncertainty in the branching ratios of the gamma-ray decay schemes, including the conversion electron coefficients, is ∿5 percent for most cases, and may be as large as 10 percent for some individual cases. The fission yields are probably known to 5 percent. The half-lives are known to 1 percent for most cases, and will not be important except for waiting times of more than 2 to 3 half-lives. An overall accuracy of ∿10 percent is suggested as the value probably achievable for measuring specific activations, after some experience has been achieved with the source-location and area-analysis schemes and reliable methods have been developed; a value of 15 percent is more likely, and will have about a 5 percent effect on the accuracy of measuring ϕ_{eq} (see ASTM Methods E XX3 and E XX4).

REFERENCES

(1) Verbinski, V. V., Lurie, N. A., and Rogers, V.C., "Threshold-Foil Measurements of Reactor Spectra for Radiation Damage Applications," *Nuclear Science and Engineering* 65, 316 (1978).

(2) Routti, J. T., "SAMPO, A Fortran IV Program for Computer Analysis of Gamma Spectra from Ge(Li) Detectors, and Other Spectra with Peaks," UCRL-19452 (1969).

(3) Wright, H. L., Applied Sciences Division, White Sands Missile Range, New Mexico 88002 (private communication).

(4) The value of 743 keV, given in the "Chart of Nuclides" (ERDA, Division of Isotopes Development, 1970) agrees with measurements of Ref. 1. The value of 747 keV, listed in the "Table of Isotopes" does not, (Lederer, C. M., Hollander, J. M., and Perlman, I., John Wiley & Sons, Inc., New York, 1967).

(5) Meek, M. E., and Rider, B. F., "Compilation of Fission Product Yields," NEDO-12154-1, Vallecitos Nuclear Center, Pleasanton, California 94566

TABLE I

Activation Foils (1.27-cm diam)

Reaction	E_t (MeV)	E_γ (keV)	Gamma/Reaction (Fission Yield, %)	$T_{1/2}$	Foil Mass (g)	Isotopic Abundance (%)	Notes
$^{197}Au(n,\gamma)^{198}Au$	0	412	0.95	2.696 days	0.056	100	a
$^{59}Co(n,\gamma)^{60}Co$	0	1173 1333	1.00 1.00	5.258 yr	0.057	100	a,b
$^{55}Mn(n,\gamma)^{56}Mn$	0	847 1811	0.99 0.29	2.58 h	0.030	100	a,b
$^{238}U(n,f)^{140}La$	0(0.01)[c]	1596	0.96 (6.29)	40.23 h	0.281	100	a,d,e
$^{239}Pu(n,f)^{140}La$	0(0.01)[c]	1596	0.96 (5.24)	40.23 h	0.150	100	a,d,e
$^{237}Np(n,f)^{140}La$	0.5	1596	0.96 (5.69)	40.23 h	0.580	100	a,d,e
$^{237}Np(n,f)^{97}Zr$	0.5	743	0.92 (6.01)	16.8 h	0.580	100	a,f,e
$^{115}In(n,n')^{115m}In$	1.0	335	0.50	4.50 h	0.255	95.7	
$^{236}U(n,f)^{140}La$	1.45	1593	0.96 (6.02)	40.23 h	0.495	100	a,d,e
$^{232}Th(n,f)^{140}Ba$	1.75	537	0.256 (7.91)	12.8 days	1.066	100	a,g,e
$^{232}Th(n,f)^{97}Zr$	1.75	743	0.92 (4.12)	16.8 h	1.066	100	a,f,e
$^{54}Fe(n,p)^{54}Mn$	2.20	835	1.00	303 days	0.142	5.82	
$^{58}Ni(n,p)^{58}Co$	2.9	810	0.99	71.3 days	0.282	67.8	
$^{32}S(n,p)^{32}P$	2.9	Betas	1.00β	14.3 days	4.10	95.0	a
$^{24}Mg(n,p)^{24}Na$	6.3	1369	1.00	15.0 h	0.030	79	a
$^{56}Fe(n,p)^{56}Mn$	7.5	847 1811	0.99 0.29	2.58 h	0.142	91.7	a,i
$^{27}Al(n,\alpha)^{24}Na$	8.7	1369	1.00	15.0 h	0.257	100	a
$^{127}I(n,2n)^{126}I$	11.0	386 667	0.34 0.33	13.05 days	0.657	100	
$^{90}Zr(n,2n)^{89}Zr$	14	910	0.99	78.4 h	0.108	51.5	

[a] Cadmium cover 0.05 to 0.10 cm thick.

[b] Use ^{59}Co instead of ^{197}Au and ^{55}Mn for very long irradiations.

[c] $E_t \approx 0.01$ MeV with ^{10}B sphere (important for soft (TRIGA) spectra, where $\phi(E) < 0.01$ will otherwise dominate). When ^{235}U or ^{239}Pu foil is ^{10}B-covered, also cover ^{235}U and ^{237}Np foils so that accurate corrections can be made for ^{238}U and ^{240}Pu impurities in these high E_t foils.

[d] 40.23-h daughter of 12.80-day ^{140}Ba. Wait five days for maximum decay rate (ASTM E 393).

[e] Fission yields are for bombardment with fission-spectrum neutrons. For thermal and 14 MeV, see Ref. 5.

[f] Use ^{97}Zr for low fluence (3×10^{11} to 3×10^{12} n/cm^2). Use peak shape analysis or measure twice, seven days apart, to strip off 740-keV ^{99}Mo gamma ray ($T_{1/2}$ = 67 h).

[g] ^{232}Th radioactivity interferes with ^{140}La line.

[h] Requires separate detector, and calibration technique is complex.

[i] Maximum manganese impurity = 0.001%, cadmium-covered. Omit $^{56}Fe(n,p)^{56}Mn$ for long irradiations.

DESIGNATION: E XX3

Standard Method for

UNFOLDING NEUTRON SPECTRA
FOR RADIATION HARDNESS TESTING

1. SCOPE

1.1 This method describes a set of standard procedures for unfolding a neutron spectrum $\phi(E)$ with the SAND II code, using as input data a set of threshold-foil activations, with threshold energies E_t effectively ranging from cadmium cutoff ($\sim 3 \times 10^{-7}$ MeV) to $\sim$14 MeV.

1.2 The selection and exposure of a set of activation foils is covered in ASTM Method E XX1, "Method of Irradiating a Standard Set of Neutron Threshold Activation Foils for Radiation Hardness Testing." In addition, a minimum set of reliable foils is presented in that method.

1.3 The measurement of the specific activities of the threshold-activation foils is covered in ASTM E XX2, "Measuring Foil Activities for Radiation Hardness Testing."

1.4 The neutron spectrum $\phi(E)$ as measured by this method may have a wide variety of uses. Nevertheless, this method is specifically addressed to characterizing $\phi(E)$ for the purpose of comparing spectra used in radiation hardness testing. It is also possible to express $\phi(E)$ in terms of a single parameter ϕ_{eq} that gives a measure of its effectiveness in producing radiation damage in silicon semiconductor devices. This is discussed in ASTM Method E XX4,

"Characterizing Neutron Spectra in Terms of 1-MeV Equivalent Fluence for Radiation Damage in Silicon."

1.5 Periodic updating of nuclear data will improve the accuracy of the threshold-foil activation cross sections, branching ratios, and decay constants, as well as calculations of the damage function D(E). These must be utilized to update the input data for this method from time to time to improve its accuracy, which will require updating these standard methods.

1.6 All $E_t = 0$ foils (both 1/v and fission foils) are cadmium or ^{10}B covered, which excludes thermal-neutron measurements. This facilitates a more reliable solution at higher energies, where practically all of the radiation damage occurs in silicon.

1.7 Although codes other than SAND II, such as SPECTRA, CRYSTAL BALL, and OPTIMO {also available at Radiation Shielding Information Center (RSIC) (1)}, can give results, the SAND II code was chosen because of the built-in feature of retarding the formation of spurious structure (see Sec. 11.1). Also, it provides in convenient format the Δ_o's needed to evaluate the agreement between the foil data and the trial spectrum. This plays an important part in rejecting erratic foil data and in choosing a more realistic trial spectrum; a user interaction that is important to unfolding accuracy.

2. SIGNIFICANCE

2.1 This method provides the neutron fluence $\phi(E)$ for general use, such as for calculating radiation damage to materials other than silicon, where the damage versus neutron energy, D(E) is known or is calculable from known neutron cross sections.

2.2 This method and the supporting methods (Sec. 1) constitute a set of draft standards for characterizing diverse neutron fields. This characterization is of interest in planning irradiation schedules for parts screening or for sample-specification tests, and in comparing radiation damage studies carried out in different neutron fields.

3. DEFINITIONS

3.1 The description of terms relating to dosimetry are found in ASTM Definitions E 170, "Terms Relating to Dosimetry."

3.2 A_s is the saturated activity of the sample (in units of reciprocal time), as defined in ASTM Method E 261-70, "Standard Method for Measuring Neutron Flux by Radioactivation Techniques." R_m is the measured number of activations per nucleus produced by irradiating N_o target nuclei (of the isotope that can produce the reaction) for an irradiation time t_i. For constant reactor power, R_m is defined as the measured ratio $R_m = A_s t_i / N_o$.

4. SUMMARY OF THE METHOD

4.1 A set of foils is selected with thresholds E_t that vary from 0 to 14 MeV, the foils are weighed, covered with cadmium or ^{10}B as necessary, and exposed to a neutron field having a known spectral distribution $\phi(E)$. The resultant radioactivity is measured to determine the number N of radioactive atoms produced during the irradiation of N_o target atoms of the chosen isotope. For each foil species x,

$$N = N_o \int_{E_t}^{\infty} \sigma_x(E)\phi(E)\, dE, \qquad (1)$$

where $\phi_x(E)$ is the cross section for the reaction being

measured. The set of measured specific activities, given by the ratio $R_m(x) = (N/N_o)_x$, is used as input to the SAND II unfolding code, along with a trial spectrum $\phi_{tr}(E)$ that contains all the physical features. These features may include a "dip" due to a resonance, a peak, or a fission spectrum with 1/E moderated component (tail).

4.1.1 Using Eq. 1 with $\phi_{tr}(E)$ in place of $\phi(E)$, the SAND II code calculates the various $R_{tr}(x)$, utilizing the SAND II input library of cross sections $\sigma_x(E)$. In calculating the various $R_{tr}(x)$, the input spectrum $\phi_{tr}(E)$ is normalized so as to minimize the standard deviation S_o associated with the "zeroth iteration" differences $\Delta_o(x) = (R_m - R_{tr})/R_m$ between the measured and calculated specific activities.

4.1.2 For foils where $\Delta_o(x)$ is largest, the SAND II code adjusts the spectrum in the energy interval above $E_t(x)$, so as to produce a first-iteration solution, $\phi_1(E)$, with reduced $\Delta_1(x)$ and, consequently, with reduced S_1. These iterations are continued until the n-th iteration, where S_n <5 percent.

4.2 SAND II Limitations

4.2.1 The threshold-foil spectrometry method is not truly a spectrometry technique, but rather a mild perturbation technique. As such, it provides a reliable output only with considerable constraints applied, especially for the region below 1 MeV, where only one true threshold (^{237}Np, 0.5 MeV) exists. This constraint is that for reactor spectra, the epicadmium solution resembles a GODIVA spectrum with 1/E tail fitted (Sec. 6.1.2). Since this provides only one adjustable parameter, that of varying the 1/E fitting point until the solution resembles the trial spectrum, it is possible for this limiting case of reactor spectra to obtain a reliable solution with one real threshold, an

artificial one at 10 keV (^{235}U or ^{239}Pu in boron), and a 1/v detector providing information below 1 MeV. This is carried out with some interaction with the code.

5. INTERACTION WITH SAND II CODE

5.1 Examination of $R_m(x)$ and $\phi_{tr}(E)$ via the $\Delta_o(x)$ Set of Indicators

5.1.1 If the solution $\phi_n(E)$ is physically meaningful, it will have the same characteristics as ϕ_{tr}. This happens when no erroneous values of R_m are input to SAND II, and when the starting spectrum $\phi_{tr}(E)$ contains all the physical characteristics of the true spectrum. It is the task of the user to examine the set of $\Delta_o(x)$ to either reject single spurious values of the corresponding $R_m(x)$, or to adjust $\phi_{tr}(E)$ in regions above the threshold energy $E_t(x)$ where two or more corresponding values of $\Delta_o(x)$ are large and agree in sign and magnitude.

5.2 Choosing $\phi_{tr}(E)$ for Unfolding Reactor Spectra

5.2.1 Most reactor spectra used for radiation damage studies can be represented by a fission spectrum with properly normalized 1/E slowing-down component. The trial spectrum can be represented adequately in this case by a fission spectrum with a fitted 1/E tail. A trial fitting is first used, and if the $\Delta_o(x)$ for the cadmium-covered 1/v detector (^{197}Au, ^{59}Co, or ^{55}Mn) and the flat detector (^{239}Pu or ^{235}U boron-covered fission detectors) are large and positive (or negative), then the 1/E tail is normalized at a higher (or lower) energy to the fission spectru, and SAND II rerun. Prescribed values are given in Sec. 6.1 for the 1/E normalizing point for three different fission spectra commonly used in radiation damage work.

5.2.2 If $\phi_{tr}(E)$ is too low in the energy region above a few MeV, for a reactor spectrum, the $\Delta_o(x)$ will be positive and may increase with E_t of the foils. For this case, there are enough foils used in this prescription for SAND II to achieve a good solution in only a few iterations, so that $\phi_{tr}(E)$ need not be adjusted here. A more common problem here is that one of the $\Delta_o(x)$ is erroneous, requiring many iterations to achieve a solution. This is seen as a physically unreal oscillation in the solution $\phi_n(E)$, in which case the spurious activation $R_m(x)$ must be removed and SAND II rerun without this activation.

5.3 Recognition of a Well-Behaved Solution

5.3.1 When the $R_m(x)$ and $\phi_{tr}(E)$ are self consistent, the SAND II perturbation code will converge in a few iterations (n = 1 to 10), and $\phi_n(E)$ will be much like $\phi_{tr}(E)$.

5.3.2 The prescriptions set forth in Section 6 are designed to achieve such a solution. It is most easily recognized by comparing plots of $\phi_{tr}(E)$ and $\phi_n(E)$ on log-log paper, but with $E*\phi(E)$ plotted instead of $\phi(E)$. In this way, the 1/E slowing-down region appears as a flat line, and the slope of $\phi(E)$ above a few MeV is not nearly as steep. Deviations of $\phi_n(E)$ from $\phi_{tr}(E)$ are therefore much more apparent in the $E*\phi(E)$ plots.

6. SAND II OPERATING PROCEDURE

6.1 SAND II Inputs

6.1.1 The SAND II code is operated in the TIME INTEGRATED (time independent) mode, which standardizes the activation-foil input format for both fast-burst and steady-state irradiations. The inputs are the trial spectrum ϕ_{tr}, the specific activities $R_m(x)$ of the foils, and the foil-cover data.

6.1.2 Trial Spectrum ϕ_{tr}

6.1.2.1 For a GODIVA-type reactor, select spectrum No. 5 of the SAND II library of trial spectra for a glory-hole spectrum.

6.1.2.2 For a spectrum at 50 cm from a GODIVA-type reactor ~1.5 meters above a concrete floor, use trial spectrum No. 5 with a 1/E component fitted at 10^{-2} MeV (this will be compatible with the 1/v foil (^{59}Co, ^{55}Mn, or ^{197}Au) and the boron-covered ^{235}U or ^{239}Pu low-energy fission foil, and will avoid distortions in the solution $\phi(E)$ for E >0.01 MeV that result from omitting the 1/E component).

6.1.2.3 For a TRIGA spectrum, fit the 1/E component at 0.15 MeV.

6.1.2.4 To obtain the trial spectrum, first run SAND II with the trial spectrum No. 5 option called for. The SAND II output will include a printout of start spectrum No. 5 (620-point spectrum from 10^{-10} to 18 MeV). Normalize the 1/E spectrum at the proper point, as prescribed above and input the resulting hybrid spectrum at $\Delta E/E$ = 10 percent energy intervals above the normalizing point energy (i.e., at 0.15, 0.015, 0.0015 MeV, etc., down to $\sim 10^{-10}$ MeV). The hybrid spectrum is input as SPECTRUM TABULAR, as described in the input instructions.

6.1.2.5 For cases other than the three mentioned above, choose a normalizing point at 0.03 MeV for the 1/E tail, and proceed with the fitting operation as described in Sec. 5.2.

6.1.3 Threshold-Foil Data

6.1.3.1 The threshold-foil isotope, the type of reaction, the specific activity R_m, and the foil-cover data are required inputs to the SAND II code. For example,

U235F BORON 0.101

and

AU197G CADMIUM 0.00480

correspond to the $^{235}U(n,f)$ reaction with the ^{235}U foil covered with 1.68 g/cm^2 of ^{10}B, and the $^{197}Au(n,y)^{198}$ reaction with the ^{197}Au foil covered with a 0.1-cm-thick cadmium foil. A specific activation of 5.9-12 corresponds to $R_m(^{235}U) = 5.9 \times 10^{-12}$ fissions produced per ^{235}U atom present in the target. According to the structure of the code, whereas R_m is input for fission foils, for non-fission foils R_m is multiplied by $\lambda = 0.693/T_{\frac{1}{2}}$ of the radioactive species for input to SAND II. Three or more 1/v detector foils such as ^{197}Au, ^{59}Co, and ^{55}Mn can be used with a SAND II trial run, but the one with the value of Δ_o most nearly the average of the three should be chosen for the final run of SAND II, the others being rejected to keep the number of iterations of SAND II (and therefore the spurious structure) to a minimum.

6.2 Acceptance Criteria for a Good Solution $\phi_n(E)$

6.2.1 If an $E*\phi(E)$ plot of $\phi_n(E)$ shows the same general shape as a similar type plot of $\phi_{tr}(E)$, with $\phi_{tr}(E)$ selected as in Sec. 5.1.1, then $\phi_n(E)$ is likely to represent a good solution. This is usually accompanied by n being small, as mentioned in Sec. 5.4. If $\phi_n(E)$ exhibits a shape very much unlike ϕ_{tr}, the user must examine the $\Delta_o(x)$ (given by the SAND II printout) for spurious values of $\Delta_o(x)$, and, therefore, $R_m(x)$. Any spurious value is rejected and the SAND II code is rerun without this foil. On the other hand, when more than one foil in a given region of threshold energies $E_t(x)$ shows a large positive value of $\Delta_o(x)$ and these values agree in sign, the $\phi_{tr}(E)$ must be increased in that region for positive $\Delta_o(x)$, and vice versa. In some cases, such as at

high threshold energies where $\phi_{tr}(E)$ obtained from a calculation has often been found to be too low, the SAND II code may adjust the spectrum in very few iterations. This happens when the $\Delta_o(x)$ are progressively larger in magnitude with increasing $E_t(x)$ of the foil, and the activations $R_m(x)$ are consistent with a smooth, nonoscillating solution $\phi(E)$ in this region. In this case, the SAND II solution is valid {the code need not be rerun with $\phi_{tr}(E)$ adjusted}.

7. MINIMUM FOIL SET

7.1 Table I lists foils that have been successfully used. A 1/v foil is required for the low-energy region. ^{197}Au, cadmium covered, is suggested with appropriate epi-cadmium self-shielding correction. Use ^{235}U, or possibly ^{239}Pu, in ^{10}B as the "E_t = 10 keV" fission foil, along with ^{237}Np (E_t = 0.5 MeV), ^{238}U (corrected for ^{235}U impurity with the ^{235}U-foil data), ^{115}In, $^{54}Fe(n,p)^{54}Mn$, $^{60}Ni(n,p)^{60}Co$, $^{24}Mg(n,p)^{24}Na$, $^{27}Al(n,a)^{24}Na$, and $^{90}Zn(n,2n)^{89}Zr$.

8. AVAILABILITY OF THE SAND II CODE AND CROSS-SECTION LIBRARY

8.1 The SAND II program tape, including a large catalog of trial spectra, is available from RSIC. Documentation of the code is also available at RSIC (1).

9. THE SAND II CROSS-SECTION LIBRARY

9.1 The present cross-section library tape contains an evaluated self-consistent set of cross-section data. This is referred to as the 1974 evaluated cross-section library tape, and constitutes part of this standard. When this tape, or any other foil-activation data, becomes updated, it is understood that these ASTM standard methods will similarly require updating.

10. PRECISION

10.1 Using the prescriptions outlined above and in the two accompanying ASTM Methods (E XX1 and E XX2, mentioned in Sec. 1), both a glory-hole spectrum and a spectrum at 50 cm from a GODIVA-type reactor were measured (2,3) by two different experimental groups in an effort at evaluating the reproducibility of the method. Using different foil packets, but the same types of theshold foils, both spectra agreed within less than 2 percent in terms of the hardness parameter, ϕ_{eq}/ϕ (see ASTM Method E XX4). Different Ge(Li) gamma-ray detectors were used, each being cross calibrated with NBS standard gamma-ray sources having a quoted absolute accuracy of 2 percent. A standard consisting of an 11-line source mixture was used at both laboratories, indicating the precision of NBS standard-source intensities is 1 percent for the 11 lines. Assuming the prescriptions in these ASTM standard methods are carefully followed, a precision of 10 percent should be easily achievable in $\phi eq/\phi$, and 5 percent highly probably with additional work {such as checking activation ratios against those of similar spectra found in the literature (2) to help diagnose erratic foil activations}.

11. ACCURACY

11.1 The accuracy is specified here in terms of the 1-MeV equivalent flux, ϕ_{eq}, and the hardness parameter, ϕ_{eq}/ϕ, both of which are defined in ASTM Method E XX4. It was determined in a study wherein three different types of reactor spectra were measured (2). These spectra were found to belong to a parametric set, wherein they can be approximated by a GODIVA spectrum with 1/E tail fitted according to the degree of moderation present see Sec. 6.1.1, selecting $\phi_{tr}(E)$. The accuracy evaluation presented here is limited to spectra belonging to this set, which probably covers all

reactor spectra used for silicon radiation damage studies.

11.2 Comparison with Known Spectra

11.2.1 The SAND II results for ϕ_{eq}/ϕ as obtained from $\phi_{tr}(E)$ generated according to Sec. 6.1.1, agreed with ϕ_{eq}/ϕ as obtained from calculated values of $\phi(E)$ within better than 3 percent. The calculations were verified by time-of-flight measurements (2). In addition, the SAND II unfolding was carried out using the calculated $\phi(E)$ as the trial spectrum, ϕ_{tr}. In this case, the SAND II result agreed with the calculated spectrum to within $\sim$1 percent in ϕ_{eq}/ϕ, indicating that the threshold-foil data were consistent with the calculation. This and other data show that the accuracy is very sensitive to the choice of $\phi_{tr}(E)$, especially for E <1 MeV, where only one useful threshold exists {^{237}Np(n,f)} above 10 keV.

11.2.2 It is not possible to check the accuracy of ϕ_{eq} against calculations without doing more exact calculations, geometrically, and more absolute flux monitoring.

11.3 Sensitivity to Unfolding Method

11.3.1 A reactor spectrum was unfolded with both the SAND II and the SPECTRA {also available at RSIC (1)} codes. The results agreed within 2 percent in ϕ_{eq}/ϕ, and 3 percent in ϕ_{eq}, indicating that the choice of codes is not a major factor. Most of the difference came from some spurious structure in the SPECTRA solution that is relatively suppressed in the SAND II method.

11.4 Variational Studies on $\sigma_x(E)$ and $R_m(x)$

11.4.1 The SAND II unfolding of a GODIVA-type spectrum was carried out by varying the input activations of individual foils, $R_m(x)$, and of pairs of foils (2). This simulates a bodily shift (or renormalization) in the cross-section curve,

$\sigma_x(E)$. The results showed that for the spectrum at 50 cm from a GODIVA-type reactor, which was 165 cm above a concrete floor, a variation of 25 percent in the activation of any one foil (out of nine) with threshold below 2 MeV, where few thresholds exist, resulted in ~2 percent increase of ϕ_{eq}/ϕ. For foils with thresholds between 2 and 6.5 MeV, where the neutron flux is high and many thresholds exist, a 25 percent change in $\sigma_x(E)$ of any single foil produced a 1 percent change in ϕ_{eq}/ϕ. Above 6.5 MeV, where the neutron flux is very low, the corresponding sensitivity was 0.5 percent for one foil. With two values of $\sigma_x(E)$ varied by 25 percent, ϕ_{eq}/ϕ changed by as much as 4 percent in one case {+25 percent for $^{238}U(n,f)$ and -25 percent for $^{24}Mg(n,p)$}, and 2 percent in another (+25 percent for both ^{238}U and ^{24}Mg). A total of nine foils was used {$^{58}Ni(n,p)$, $^{24}Mg(n,p)$, $^{127}I(n,2n)$, $^{56}Fe(n,p)$, $^{239}Pu(n,f)$, $^{238}U(n,f)$, $^{235}U(n,f)$, $^{197}Au(n,\gamma)$, in Cd, and $^{237}Np(n,f)$}.

11.4.2 The variations in ϕ_{eq} were appreciably greater than the corresponding variations in ϕ_{eq}/ϕ. They were $\Delta\phi_{eq}$ = +12 percent for the ^{239}Pu foil, 2.7 percent for ^{238}U, and <0.5 percent for foils with thresholds above 2 MeV. The ^{238}U and ^{24}Mg foils produced a 2 percent increase in ϕ_{eq} when both were raised by 25 percent, but ϕ_{eq} changed only 0.3 percent when the ^{238}U activation was increased 25 percent and the ^{24}Mg foil decreased by the same amount. The large sensitivity to changes in ^{239}Pu (or, similarly, ^{235}U) activation (or cross section) arises from this being the foil with accuracy of 2 percent. A standard consisting of an 11-line source mixture was used at both laboratories, indicating the precision of NBS standard-source intensities is 1 percent for the 11 lines. Assuming the prescriptions in these ASTM standard methods are carefully followed, a precision of 10 percent should be easily achievable in ϕ_{eq}/ϕ, and 5 percent highly probably with additional work {such as checking activation ratios against those

of similar spectra found in the literature (2) to help diagnose erratic foil activations}.

11. ACCURACY

11.1 The accuracy is specified here in terms of the 1-MeV equivalent flux, ϕ_{eq}, and the hardness parameter, ϕ_{eq}/ϕ, both of which are defined in ASTM Method E XX4. It was determined in a study wherein three different types of reactor spectra were measured (2). These spectra were found to belong to a parametric set, wherein they can be approximated by a GODIVA spectrum with 1/E tail fitted according to the degree of moderation present {see Sec. 6.1.1, selecting $\phi_{tr}(E)$}. The accuracy evaluation presented here is limited to spectra belonging to this set, which probably covers all reactor spectra used for silicon radiation damage studies.

11.2 Comparison with Known Spectra

11.2.1 The SAND II results for ϕ_{eq}/ϕ as obtained from $\phi_{tr}(E)$ generated according to Sec. 6.1.1, agreed with ϕ_{eq}/ϕ as obtained from calculated values of $\phi(E)$ within better than 3 percent. The calculations were verified by time-of-flight measurements (2). In addition, the SAND II unfolding was carried out using the calculated $\phi(E)$ as the trial spectrum, ϕ_{tr}. In this case, the SAND II result agreed with the calculated spectrum to within ∿1 percent in ϕ_{eq}/ϕ, indicating that the threshold-foil data were consistent with the calculation. This and other data show that the accuracy is very sensitive to the choice of $\phi_{tr}(E)$, especially for E <1 MeV, where only one useful threshold exists {^{237}Np(n,f)} above 10 keV.

11.2.2 It is not possible to check the accuracy of ϕ_{eq} against calculations without doing more exact calculations, geometrically, and more absolute flux monitoring.

11.3 Sensitivity to Unfolding Method

11.3.1 A reactor spectrum was unfolded with both the SAND II and the SPECTRA {also available at RSIC (1)} codes. The results agreed within 2 percent in ϕ_{eq}/ϕ, and 3 percent in ϕ_{eq}, indicating that the choice of codes is not a major factor. Most of the difference came from some spurious structure in the SPECTRA solution that is relatively suppressed in the SAND II method.

11.4 Variational Studies on $\sigma_x(E)$ and $R_m(x)$

11.4.1 The SAND II unfolding of a GODIVA-type spectrum was carried out by varying the input activations of individual foils, $R_m(x)$ and of pairs of foils (2). This simulates a bodily shift (or renormalization) in the cross-section curve, $\sigma_x(E)$. The results showed that for the spectrum at 50 cm from a GODIVA-type reactor, which was 165 cm above a concrete floor, a variation of 25 percent in the activation of any one foil (out of nine) with threshold below 2 MeV, where few thresholds exist, resulted in ∿2 percent increase of ϕ_{eq}/ϕ. For foils with thresholds between 2 and 6.5 MeV, where the neutron flux is high and many thresholds exist, a 25 percent change in $\sigma_x(E)$ of any single foil produced a 1 percent change in ϕ_{eq}/ϕ. Above 6.5 MeV, where the neutron flux is very low, the corresponding sensitivity was 0.5 percent for one foil. With two values of $\sigma_x(E)$ varied by 25 percent, ϕ_{eq}/ϕ changed by as much as 4 percent in one case (+25 percent for ^{238}U and ^{24}Mg). A total of nine foils was used {$^{58}Ni(n,p)$, $^{24}Mg(n,p)$, $^{127}I(n,2n)$, $^{56}Fe(n,p)$, $^{239}Pu(n,f)$, $^{238}U(n,f)$, $^{235}U(n,f)$, $^{197}Au(n,\ )$, in Cd, and $^{237}Np(n,f)$}.

11.4.2 The variations in ϕ_{eq} were appreciably greater than the corresponding variations in ϕ_{eq}/ϕ. They were $\Delta\phi_{eq}$ = +12 percent for the ^{239}Pu foil, 2.7 percent for ^{238}U,

and <0.5 percent for foils with thresholds above 2 MeV. The ^{238}U and ^{24}Mg foils produced a 2 percent increase in ϕ_{eq} when both were raised by 25 percent, but ϕ_{eq} changed only 0.3 percent when the ^{238}U activation was increased 25 percent and the ^{24}Mg foil decreased by the same amount. The large sensitivity to changes in ^{239}Pu (or, similarly, ^{235}U) activation (or cross section) arises from this being the foil with the greatest sensitivity to neutrons between 0.01-MeV and the 0.5-MeV threshold of ^{237}Np. Fortunately, the cross-section data for fission foils such as ^{239}Pu and ^{235}U are accurately known, and a 25 percent uncertainty in either the cross section, or, equivalently, the foil count, is excessively large. Also, the specific activations are considerably greater than for the other fission foils, and are thus more accurately determined.

11.5 Overall Accuracy Assessment

11.5.1 The probable accuracy in ϕ_{eq} and ϕ_{eq}/ϕ, as estimated from the three contributing factors discussed above, is 10 percent for reactor spectra if the prescriptions outlined in these methods are carefully followed. An accuracy of 5 to 7 percent may be achievable with added effort, such as comparing activation ratios to those for similar spectra presented in the literature (2) to help detect erroneous values.

REFERENCES

(1) RSIC (Radiation Shielding Information Center), Oak Ridge National Laboratory, Oak Ridge, Tennessee 37830.

(2) Verbinski, V. V., Lurie, N. A., and Rogers, V. C., "Threshold-Foil Measurements of Reactor Spectra for Radiation Damage Applications," *Nuclear Science and Engineering* 65, 316 (1978)

(3) Meason, J. L., Wright, H. L. Hogan, J. C. and Harvey, J. T., "The Neutron Spectral Distribution From a GODIVA-Type Critical Assembly," IEEE Trans. Nucl. Sci. NS-22, No. 6, 2330 (1975).

TABLE I

Activation Foils (1.27-cm diam)

Reaction	E_t (MeV)	E_γ (keV)	Gamma/Reaction (Fission Yield, %)	$T_{1/2}$	Foil Mass (g)	Isotopic Abundance (%)	Notes
$^{197}Au(n,\gamma)^{198}Au$	0	412	0.95	2.696 days	0.056	100	a
$^{59}Co(n,\gamma)^{60}Co$	0	1173 1333	1.00 1.00	5.258 yr	0.057	100	a,b
$^{55}Mn(n,\gamma)^{56}Mn$	0	847 1811	0.99 0.29	2.58 h	0.030	100	a,b
$^{235}U(n,f)^{140}La$	0(0.01)[c]	1596	0.96 (6.29)	40.23 h	0.281	100	a,d,e
$^{239}Pu(n,f)^{140}La$	0(0.01)[c]	1596	0.96 (5.24)	40.23 h	0.150	100	a,d,e
$^{237}Np(n,f)^{140}La$	0.5	1596	0.96 (5.69)	40.23 h	0.580	100	a,d,e
$^{237}Np(n,f)^{97}Zr$	0.5	743	0.92 (6.01)	16.8 h	0.580	100	a,f,e
$^{115}In(n,n')^{115m}In$	1.0	335	0.50	4.50 h	0.255	95.7	
$^{238}U(n,f)^{140}La$	1.45	1593	0.96 (6.02)	40.23 h	0.495	100	a,d,e
$^{232}Th(n,f)^{140}Ba$	1.75	537	0.256 (7.91)	12.8 days	1.066	100	a,g,e
$^{232}Th(n,f)^{97}Zr$	1.75	743	0.92 (4.12)	16.8 h	1.066	100	a,f,e
$^{54}Fe(n,p)^{54}Mn$	2.20	835	1.00	303 days	0.142	5.82	
$^{58}Ni(n,p)^{58}Co$	2.9	810	0.99	71.3 days	0.282	67.8	
$^{32}S(n,p)^{32}P$	2.9	Betas	1.00β	14.3 days	4.10	95.0	a
$^{24}Mg(n,p)^{24}Na$	6.3	1369	1.00	15.0 h	0.030	79	a
$^{56}Fe(n,p)^{56}Mn$	7.5	847 1811	0.99 0.29	2.58 h	0.142	91.7	a,i
$^{27}Al(n,\alpha)^{24}Na$	8.7	1369	1.00	15.0 h	0.257	100	a
$^{127}I(n,2n)^{126}I$	11.0	386 667	0.34 0.33	13.05 days	0.657	100	
$^{90}Zr(n,2n)^{89}Zr$	14	910	0.99	78.4 h	0.108	51.5	

[a] Cadmium cover 0.05 to 0.10 cm thick.

[b] Use ^{59}Co instead of ^{197}Au and ^{55}Mn for very long irradiations.

[c] $E_t \approx 0.01$ MeV with ^{10}B sphere [important for soft (TRIGA) spectra, where $\phi(E) < 0.01$ will otherwise dominate]. When ^{235}U or ^{239}Pu foil is ^{10}B-covered, also cover ^{238}U and ^{237}Np foils so that accurate corrections can be made for ^{238}U and ^{239}Pu impurities in these high E_t foils.

[d] 40.23-h daughter of 12.80-day ^{140}Ba. Wait five days for maximum decay rate (ASTM E 393).

[e] Fission yields are for bombardment with fission-spectrum neutrons. For thermal and 14 MeV, see Ref. 5.

[f] Use ^{97}Zr for low fluence (3×10^{11} to 3×10^{12} n/cm^2). Use peak shape analysis or measure twice, seven days apart, to strip off 740-keV ^{99}Mo gamma ray ($T_{1/2}$ = 67 h).

[g] ^{232}Th radioactivity interferes with ^{140}La line.

[h] Requires separate detector, and calibration technique is complex.

[i] Maximum manganese impurity = 0.001%, cadmium-covered. Omit $^{56}Fe(n,p)^{56}Mn$ for long irradiations.

DESIGNATION: E XX4

Standard Method for

CHARACTERIZING NEUTRON SPECTRA IN TERMS OF 1-MeV EQUIVALENT FLUENCE FOR RADIATION DAMAGE IN SILICON

1. SCOPE

1.1 This method describes a standard procedure for characterizing a neutron field with spectrum $\phi(E)$ in terms of the ϕ_{eq}, the fluence of neutrons at $\sim$1 MeV required to produce the same radiation damage in some material x where the radiation damage function $D_x(E)$ is known.

1.2 This method describes a standard procedure for characterizing the shape of a neutron spectrum $\phi(E)$ in terms of the hardness parameter, ϕ_{eq}/ϕ. It is defined as the fluence of neutrons at $\sim$1 MeV required to produce the same radiation damage as one unit of fluence of neutrons of spectral distribution $\phi(E)$.

1.3 Although these standard procedures are applicable to characterizing the spectrum in terms of radiation damage to any material x where $D_x(E)$ is known, the prescriptions outlined here address themselves specifically to radiation damage in silicon; the damage function for silicon, $D_{Si}(E)$, is rapidly varying near 1 MeV. This method consequently prescribes an alternative definition for ϕ_{eq} (silicon).

1.4 This method is part of a set of standards dealing with neutron spectrometry, and is intended to serve as a means of characterizing different neutron spectra, $\phi(E)$, used in

radiation damage studies and parts testing of electronic components. A standard method of deducing $\phi(E)$ by unfolding neutron threshold-foil activation data is covered in ASTM Method E XX3, "Standard Method for Unfolding Neutron Spectra for Radiation Hardness Testing." The procedures for selecting, irradiating and counting the foils, the tabulation of some of the required nuclear constants, and the method of calculating specific activations of the foils are presented in ASTM Methods E XX1, "Irradiation a Standard Set of Neutron Threshold Activation Foils for Radiation Hardness Testing," and E XX2, "Measuring Foil Activities for Radiation Hardness Testing." Once ϕ_{eq} and ϕ_{eq}/ϕ have been measured and calculated, it is important for the user of a neutron irradiation facility to be able to measure ϕ_{eq} for subsequent irradiations. This is covered in ASTM Method E XX5, "Measuring the Relative 1-MeV Silicon-Equivalent Fluence with Fast-Neutron Monitors."

1.5 A flow chart shown in Figure 1 lists the sequence of operations that lead to $\phi(E)$, ϕ_{eq}, ϕ_{eq}/ϕ, and ϕ_{eq}/monitor.

2. SIGNIFICANCE

2.1 In neutron radiation damage studies, where the damage is neutron-energy dependent, it is convenient to parameterize a neutron field in terms of a single number called the 1-MeV equivalent fluence, $\phi_{eq} \pm \Delta\phi_{eq}$, which quantifies it by a single number and a standard deviation of that number. In addition, it is useful to assign a radiation-damage quality to a given spectral distribution, a parameter referred to here as the hardness parameter. This hardness parameter is simply ϕ_{eq}/ϕ, or the number of 1-MeV neutrons that produce the same radiation damage as a unit fluence of neutrons having the spectral distribution $\phi(E)$.

3. SUMMARY OF METHOD

3.1 The parameter ϕ_{eq} is defined as

$$\phi_{eq} = \frac{\int_{0.01\ MeV}^{\infty} \phi(E)\ D(E)dE}{D(1\ MeV)} , \qquad (1)$$

where $\phi(E)$ is the spectral distribution of the neutrons and D(E) the radiation damage per unit fluence. D(1 MeV) is taken as the average $\bar{D}$(0.85-1.15 MeV) because D(E) is rapidly varying near 1 MeV. The integral does not include neutrons below 0.01 MeV because even for a soft TRIGA spectrum, less than 1 percent of the damage in bulk silicon is contributed by neutrons below this energy. The 0.01-MeV cutoff greatly simplifies the computation of the hardness parameter, ϕ_{eq}/ϕ:

$$\phi_{eq}/\phi = \frac{\int_{0.01\ MeV}^{\infty} \phi(E)\ D(E)dE}{D(1\ MeV)\int_{0.01\ MeV}^{\infty} \phi(E)dE} . \qquad (2)$$

The "neutron count", given by the integral in the denominator of Eq. 2, includes only about half of the epicadmium neutron flux for a TRIGA-type reactor, and inclusion of the entire epicadmium flux would make ϕ_{eq}/ϕ very dependent on neutrons below 0.01 MeV, where almost no damage occurs. If the integral extended down very low energies, to include thermal neutrons, the situation would be much worse. The accurate assessment of the value of ϕ_{eq}/ϕ would then require an accurate measure of neutrons in the thermal region - an unnecessary complication and a great source of meaningless variation of ϕ_{eq}/ϕ, since a small amount of thermal-neutron shielding would change the parameter drastically without changing $\phi(E)$ above 0.01 MeV, where almost all the damage occurs.

4. CALCULATIONS

4.1 The output of the SAND II unfolding code is given as a 620-point spectrum, from 10^{-10} to 18 MeV, or 260 points in the region of 0.01 to 18 MeV. A recent calculation of the silicon displacement KERMA, D(E), has been carried out with the latest neutron cross sections for silicon (1,2), and is given at 200 energy points covering roughly the same neutron-energy interval. In folding $\phi(E)$ and D(E), a simple numerical integration is carried out as follows.

$$\int_{0.01}^{18\ \text{MeV}} \phi(E)\ D(E)dE = \sum_{i=361}^{620} \phi(E_i)\ D(E_i)\Delta E_i\ , \quad (3)$$

where i = 361 corresponds to E_i = 0.01 MeV of the SAND II output, and the $D(E_i)$ are the values given in Table I for the same energy mesh as the SAND II output above 0.01 MeV. They rperesent values obtained from the original table (1,2) by interpolation and some group averaging, where necessary.

4.2 The value given by Eq. 3 is divided by D(1 MeV)$\equiv$ $\bar{D}$(0.85-1.15 MeV = 84 MeV ·mb) to provide ϕ_{eq} as per Eq. 1. ϕ_{eq}/ϕ is calculated by simply carrying the summation

$$\sum_{0.01\ \text{MeV}}^{18\ \text{MeV}} \phi_i \Delta E_i \quad (4)$$

to obtain

$$\int_{0.01\ \text{MeV}}^{\infty} \phi(E)dE$$

in the denominator of Eq. 2. The error of the simple summation is less than 1 percent for the 620-point spectrum that vanishes at the upper limit of integration (18 MeV).

5. PROBLEMS

5.1 D(E) is strongly varying near 1 MeV. Its value, as given in Ref. 1, is 102 MeV·mb at 1 MeV, while the average value from 0.85 to 1.15 MeV is 84 MeV·mb. Although this difference does not impact inter-laboratory comparisons of silicon-damage effects if a standard value of D(1 MeV) is selected, it leads to an unrealistically small value for ϕ_{eq}/ϕ; a fluence of 0.89 neutrons of 1 MeV becomes equivalent to a unit fluence of GODIVA-type neutrons (50 cm from reactor). The GODIVA 50-cm spectrum is the hardest of three spectra measured in an evaluation program (2) supporting these draft specifications. If, however, $\bar{D}$ (0.85 to 1.15 MeV) is used in Eq. 2 instead of D(1 MeV), the 1-MeV equivalent fluence per unit fluence now becomes 1.06; a much more intuitively meaningful figure for neutrons whose average energy is greater than 1.0 MeV, weighted with a damage function $D_{Si}(E)$ that increases with E.

6. RECOMMENDED DEFINITION

6.1 Use $\bar{D}$(0.85 to 1.15 MeV) = 84 MeV·mb as D(1 MeV) in Eqs. 1 and 2.

6.2 Use Table I for $D(E_i)$, where the E_i mesh agrees with that of SAND II.

7. PRECISION

7.1 The estimated precision in calculating ϕ_{eq} and ϕ_{eq}/ϕ with the present method is appreciably better than 1 percent, assuming $\phi(E)$ and D(E) are exact, and that the SAND II 620-point spectrum is used in obtaining the fluence above 0.01 MeV (Eq. 2) (260 points above 0.01 MeV).

8. ACCURACY

8.1 The accuracy of the numerical integration is estimated to be better than 1 percent. The accuracy of D(E) can be usefully discussed in three parts.

8.2 Shape of D(E)

8.2.1 In the calculation of ϕ_{eq} and ϕ_{eq}/ϕ, only the shape of the D(E) curve is important, as related to inter-laboratory comparisons of these quantities, because D(E) appears in both the numerator and denominator of Eqs. 1 and 2. The shape of D(E) is probably known well enough to contribute no more than 3 to 5 percent to the relative values of ϕ_{eq} and ϕ_{eq}/ϕ obtained for different spectra $\phi(E)$.

8.3 The Absolute Value of D(E)

8.3.1 The latest D(E) data (1,2) were obtained with the most recent evaluated cross-section set for silicon, which provides the total energy deposited in Si to an accuracy that would, in itself, impact ϕ_{eq} and ϕ_{eq}/ϕ by no more than a few percent (say 2 to 3 percent) because of its effect on the shape of D(E). However, the calculation of the partition of this energy between ionization and displacement is much less well known. The partition was calculated with the Lindhard theory (3,4), which has not been modified to agree with experimental results (5). Consequently, the D(E) values may change by the order of 10 percent when appropriate adjustments are made to obtain good agreement with past and future measurements.

8.4 D(1 MeV)

8.4.1 The value of ϕ_{eq} and ϕ_{eq}/ϕ will vary about 20 percent, depending upon the interval over which $\bar{D}(1\ \text{MeV} \pm \Delta E)$ is averaged. There is a great deal of arbitrariness in the absolute value of ϕ_{eq} and ϕ_{eq}/ϕ in

this respect, in that the definition does not influence intercomparisons of these quantities for most reactor-type spectra used in radiation damage studies. The interval 0.85 to 1.15 MeV was chosen as a compromise between a very wide energy interval, over which $\phi(E)$ may encounter significantly large variations, and a delta function that results in an intuitively low value for ϕ_{eq}/ϕ because of the rapidly varying (and therefore unrepresentative) value of D(E) at or very near 1 MeV (see Discussion, Sec. 5).

REFERENCES

(1) Rogers, V. C., Harris, Jr., L., Steinman, D. K., and Bryan, D. E., "Silicon Ionization and Displacement KERMA for Neutrons from Thermal to 20 MeV," IEEE Trans. Nucl. Sci. NS-22, No. 6, 2326 (1975); Erratum, ibid., NS-23, No. 1, 875 (1976).

(2) Verbinski, V. V., Lurie, N. A., and Rogers, V. C., "Threshold-Foil Measurements of Reactor Spectra for Radiation Damage Applications," *Nuclear Science and Engineering* 65, 316 (1978)

(3) Radiation Effects in Semiconductors, edited by F. L. Vook, Plenum Press, New York, 1968 (*Proceedings of the Santa Fe Conference on Radiation Effects in Semiconductors*, October 3-5, 1967).

(4) Lindhard, J., Nielsen, V., Scharff, M., and Thompsen, P. V., *Kgl. Danske Vindenskab, Nat. Fys. Medd.* 33, No. 10 (1963).

(5) van Lint, V. A. J., private communication.

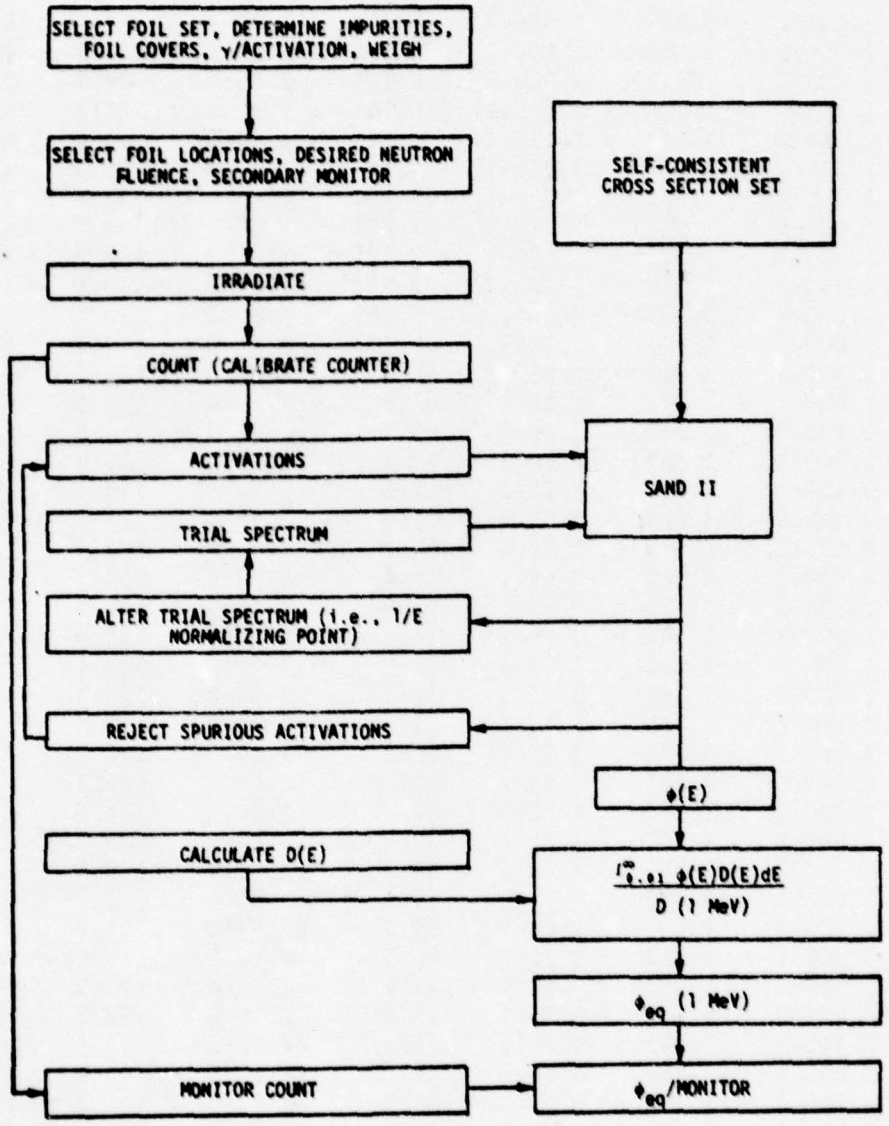

Figure 1. Flow Chart for Measuring $\phi(E)$ and Calculating ϕ_{eq} and ϕ_{eq}/Monitor.

TABLE I. D(E) in MeV·mb (E in MeV)

E	D	E	D	E	D	E	D
1.000-2	1.054	9.600-2	5.356	9.20-1	96.1	5.20+0	193.3
1.050-2	1.086	1.000-1	5.298	9.60-1	104.8	5.30+0	188.1
1.100-2	1.112	1.050-1	5.269	1.00+0	72.5	5.40+0	182.5
1.150-2	1.144	1.100-1	5.182	1.10+0	62.6	5.50+0	176.4
1.200-2	1.164	1.150-1	4.803	1.20+0	44.0	5.60+0	170.6
1.275-2	1.208	1.200-1	4.367	1.30+0	69.9	5.70+0	175.5
1.350-2	1.252	1.275-1	3.784	1.40+0	92.6	5.80+0	181.9
1.425-2	1.287	1.350-1	3.202	1.50+0	98.7	5.90+0	188.6
1.500-2	1.322	1.425-1	2.911	1.60+0	101.9	6.00+0	196.5
1.600-2	1.377	1.500-1	2.911	1.70+0	120.5	6.10+0	189.2
1.700-2	1.429	1.600-1	7.569	1.80+0	96.6	6.20+0	177.6
1.800-2	1.479	1.700-1	16.30	1.90+0	168.8	6.30+0	166.5
1.900-2	1.563	1.800-1	66.95	2.00+0	177.0	6.40+0	155.7
2.000-2	1.572	1.90-1	101.9	2.10+0	184.8	6.50+0	147.3
2.100-2	1.630	2.00-1	105.7	2.20+0	142.6	6.60+0	151.4
2.200-2	1.688	2.10-1	91.1	2.30+0	133.0	6.70+0	155.7
2.300-2	1.747	2.20-1	81.5	2.40+0	154.3	6.80+0	161.0
2.400-2	1.805	2.30-1	71.3	2.50+0	157.2	6.90+0	165.3
2.550-2	1.913	2.40-1	64.6	2.60+0	142.6	7.00+0	170.9
2.700-2	1.965	2.55-1	59.4	2.70+0	157.2	7.10+0	175.0
2.800-2	2.038	2.70-1	55.6	2.80+0	197.9	7.20+0	177.3
3.000-2	2.140	2.80-1	54.4	2.90+0	185.4	7.30+0	179.3
3.200-2	2.212	3.00-1	53.0	3.00+0	142.6	7.40+0	181.1
3.400-2	2.387	3.20-1	52.1	3.10+0	127.5	7.50+0	183.4
3.600-2	2.515	3.40-1	51.5	3.20+0	123.4	7.60+0	183.1
3.800-2	2.678	3.60-1	51.2	3.30+0	118.8	7.70+0	181.4
4.000-2	2.887	3.80-1	52.1	3.40+0	122.3	7.80+0	180.2
4.250-2	3.057	4.00-1	52.7	3.50+0	124.6	7.90+0	178.7
4.500-2	3.348	4.25-1	53.6	3.60+0	123.4	8.00+0	177.3
4.750-2	3.581	4.50-1	54.7	3.70+0	122.6	8.10+0	176.1
5.000-2	3.930	4.75-1	55.6	3.80+0	121.7	8.20+0	175.0
5.250-2	4.221	5.00-1	59.7	3.90+0	121.7	8.30+0	174.7
5.500-2	4.512	5.25-1	80.1	4.00+0	123.1	8.40+0	174.4
5.750-2	5.094	5.50-1	147.0	4.10+0	124.3	8.50+0	173.8
6.000-2	5.706	5.75-1	113.5	4.20+0	129.8	8.60+0	173.2
6.300-2	6.404	6.00-1	61.1	4.30+0	148.5	8.70+0	172.9
6.600-2	6.986	6.30-1	55.0	4.40+0	168.8	8.80+0	173.2
6.900-2	7.248	6.60-1	56.8	4.50+0	180.2	8.90+0	177.3
7.200-2	7.132	6.90-1	59.4	4.60+0	185.4	9.00+0	181.6
7.600-2	6.783	7.20-1	64.6	4.70+0	188.6	9.10+0	186.6
8.000-2	6.462	7.60-1	78.6	4.80+0	192.7	9.20+0	190.4
8.400-2	6.171	8.00-1	92.6	4.90+0	195.0	9.30+0	195.0
8.800-2	5.822	8.40-1	96.0	5.00+0	194.5	9.40+0	198.2
9.200-2	5.560	8.80-1	82.7	5.10+0	193.9	9.50+0	200.3

TABLE I (Continued)

E	D	E	D
9.60+0	199.4	1.41+1	214.8
9.70+0	198.8	1.42+1	214.8
9.80+0	198.0	1.43+1	214.8
9.90+0	197.1	1.44+1	214.8
1.00+1	196.5	1.45+1	215.1
1.01+1	195.6	1.46+1	215.1
1.02+1	195.0	1.47+1	215.1
1.03+1	195.3	1.48+1	215.4
1.04+1	195.6	1.49+1	215.7
1.05+1	196.2	1.50+1	216.3
1.06+1	196.5	1.51+1	216.6
1.07+1	196.8	1.52+1	217.2
1.08+1	197.1	1.53+1	217.5
1.09+1	197.4	1.54+1	218.0
1.10+1	198.0	1.55+1	218.6
1.11+1	199.1	1.56+1	218.9
1.12+1	200.6	1.57+1	219.5
1.13+1	202.0	1.58+1	219.8
1.14+1	203.5	1.59+1	220.1
1.15+1	204.9	1.60+1	220.6
1.16+1	206.4	1.61+1	220.7
1.17+1	207.8	1.62+1	220.7
1.18+1	209.6	1.63+1	220.7
1.19+1	210.5	1.64+1	220.7
1.20+1	210.8	1.65+1	220.9
1.21+1	211.0	1.66+1	220.9
1.22+1	211.6	1.67+1	220.9
1.23+1	211.9	1.68+1	220.9
1.24+1	209.6	1.69+1	221.2
1.25+1	212.5	1.70+1	221.2
1.26+1	212.8	1.71+1	221.2
1.27+1	213.1	1.72+1	221.2
1.28+1	213.4	1.73+1	222.1
1.29+1	213.7	1.74+1	222.7
1.30+1	213.7	1.75+1	223.3
1.31+1	213.7	1.76+1	223.9
1.32+1	214.0	1.77+1	224.4
1.33+1	214.0	1.78+1	224.7
1.34+1	214.2	1.79+1	225.3
1.35+1	214.2	1.80+1	226.2
1.36+1	214.5		
1.37+1	214.5		
1.38+1	214.8		
1.39+1	214.8		
1.40+1	214.8		

DESIGNATION: E XX5

Standard Method for

MEASURING THE RELATIVE 1-MeV
SILICON EQUIVALENT FLUENCE
WITH FAST-NEUTRON MONITORS

1. SCOPE

1.1 This method describes the measurement of ϕ_{eq}/Monitor, the 1-MeV equivalent-neutron fluence per unit monitor count, for a neutron field where the spectrum $\phi(E)$ has been measured and the 1-MeV equivalent fluence for silicon radiation damage has been calculated.

1.2 This method is part of, and follows as a corollary to, the four ASTM methods that are addressed to measuring the neutron spectrum $\phi(E)$, and with it, calculating ϕ_{eq}. These are as follows:

E XX1 Irradiating a Standard Set of Neutron Threshold Activation Foils for Radiation Hardness Testing

E XX2 Measuring Foil Activities for Radiation Hardness Testing

E XX3 Unfolding Neutron Spectra for Radiation Hardness Testing

E XX4 Characterizing Neutron Spectra in Terms of 1-MeV Equivalent Fluence for Radiation Damage in Silicon

2. SIGNIFICANCE

2.1 This method is user oriented, in that it is addressed to measuring ϕ_{eq}/Monitor for neutron irradiations

subsequent to the one in which $\phi(E)$ was measured. It provides ϕ_{eq}/Monitor for a variety of options, depending on (a) the access to the results of the SAND II code used to deduce $\phi(E)$ from the threshold data, and (b) the availability of the apparatus and facilities required for calibrating various types of monitor foils.

3. APPARATUS

3.1 Nickel or iron foils and gamma-ray detector as in ASTM Method E XX2.

3.2 Sulfur foils, beta counter, aluminum foil, Ge(Li) or intrinsic germanium detector, NBS gamma-ray sources (calibration standards), and access to 14-MeV neutron generator.

4. DETERMINING ϕ_{eq} PER UNIT MONITOR COUNT

4.1 By Measurement

4.1.1 During the course of measuring $\phi(E)$ to obtain ϕ_{eq}, a monitor foil may be placed in the same neutron field as the set of threshold activation foils, or in some more convenient location, thus obtaining ϕ_{eq}/Monitor directly. Subsequent monitor counts will then predict the absolute flux in terms of ϕ_{eq} if no shields or nearby moderators or scatterers are changed. Thus, a "retractable" GODIVA-type reactor, calibrated at, say 2 meters above the floor, must be subsequently relocated in height to within 0.1 meter if the monitor foils are located at the same distance from the reactor as the irradiation samples ($\sim$50 cm), and within a few centimeters if the monitors are approximately a factor of two nearer (or farther). Nearby scatterers must not be moved so as to change the flux by more than a few percent. An upper limit on the inscattering effect of any materials,

such as sample holders or nearby stands, can be estimated (a) by using a rough average of the total cross section in the vicinity of 1 MeV for reactor neutrons, (b) by assuming isotropic scattering, and (c) by taking into account the flux at the scatterer and the solid angle subtended at the detector. For thick materials such as concrete, a fast neutron albedo of 10 percent can be used.

4.1.2 Most shielding materials in front of either sample or monitor must be kept constant in thickness within ∿2 mm for less than a 5 percent change in flux {2 mm for polyethylene and water (1)}.

4.1.3 While 2 or 3 grams of additional moderator alongside a fast neutron monitor will make little difference, a few tenths of a gram of moderator adjacent to the cadmium-covered zero-threshold detectors can be important (i.e., 1/v detectors, and ^{235}U or ^{239}Pu foils).

4.1.4 The monitor is generally chosen with a threshold high enough to make it insensitive to neutrons below 0.01 MeV whose contribution to the radiation damage is negligibly small. Sulfur $^{32}S(n,p)^{32}P$ is usually selected because of the high threshold value for the reaction, the sensitivity, the convenient half-life of the resultant ^{32}P radioactivity (beta rays), and the ease of purifying sulfur. Detailed considerations for using sulfur are described in ASTM Method E 265-70, "Measuring Fast Neutron Flux by Radioactivation of Sulfur." However, the $^{54}Fe(n,p)^{54}Mn$ or $^{58}Ni(n,p)^{58}Co$ reactions are preferable if a Ge(Li) or intrinsic germanium detector is available; the absolute activations can then be measured by simply cross calibrating against NBS standard gamma-ray sources, providing the absolute value of $\phi(E)$ if a spectral-shape measurement is available.

4.1.5 The ϕ_{eq}/Monitor may be measured at a different time, if either a reliable secondary monitor is used (such as a fission chamber in a steady-state reactor, or a thermometer in a fast-burst irradiation). If not, one of the threshold foils used in measuring $\phi(E)$ can be used for calibration during exposures subsequent to measuring $\phi(E)$.

4.2 By Calculation

4.2.1 If a standard monitor foil such as sulfur is not included in the set of foils irradiated to measure $\phi(E)$, then the ^{32}S activation can be calculated with the SAND II code. The code is rerun with a trial value of $R_m(^{32}S)$ added, and $R_m(^{32}S)$ is adjusted until Δ_o (see Method E XX3) becomes zero. If the $^{58}Ni(n,p)^{58}Co$ reaction had been used in determining $\phi(E)$, the ^{32}S activation can be estimated from the resultant ^{58}Co activity. The two reactions have nearly the same threshold, and it was found that $R_m(^{32}S) \cong 2.92\ R_m(^{58}Ni)$ for three different reactor spectra (fast burst reactor glory hole, 50 cm from the FBR, and TRIGA J-Tube). Once $R_m(^{32}S)$ is calculated, the sulfur-foil counter must be calibrated in terms of absolute ^{32}P beta-ray activity resulting from the $^{32}S(n,p)^{32}P$ reaction. One such technique utilizes 14-MeV neutrons to irradiate Al and S, the absolute 14-MeV neutron flux (and therefore the absolute ^{32}P activity) being given by the $^{27}Al(n,\alpha)^{24}Na$ reaction. The cross sections for both reactions are accurately known at 14 MeV. Alternatively, a known amount of ^{32}P (NBS source) can be mixed in with a sulfur pellet. This cross calibration of ^{32}S is, of course, unnecessary if the $^{58}Ni(n,p)^{58}Co$ reaction, the $^{54}Fe(n,p)^{54}Mn$ reaction, or some other well-known reaction leading to a gamma-ray emitter is used for monitoring ϕ_{eq}.

5. PRECISION

5.1 The precision for measuring ϕ_{eq}/Monitor is the combination of the precision of measuring ϕ_{eq} and of measuring the monitor count. The accuracy of measuring ϕ_{eq} is treated in ASTM Method E XX4, and will not be covered here. The precision of measuring the $^{58}Ni(n,p)^{58}Co$ and $^{54}Fe(n,p)^{54}Mn$ activations is about 3 percent if counting statistics and calibration techniques allow. The foil location, the fluence of each irradiation, and the counting times will determine the counting statistics, and these factors are largely subject to the choice of the user. The precision for beta counting of sulfur foils is about the same as for the nickel and iron monitor foils, if the sulfur foils are thick enough to make the count-rate independent of thickness. Many of the sulfur counting considerations are discussed in ASTM Method E 265-70, "Measuring Fast-Neutron Flux by Radioactivation of Sulfur."

6. ACCURACY

6.1 If ^{58}Ni and ^{54}Fe foils are used, an accuracy of $\sim$5 percent can be achieved on the absolute activation if counting statistics are not a consideration (see Sec. 5). For sulfur monitoring, the accuracy is $\sim$5 percent if the sulfur is exposed simultaneously with the threshold activation foils. If not, and the sulfur activation must be calibrated indirectly, the accuracy is in this case estimated to be 10 percent.

REFERENCES

(1) Goldstein, Herbert, Fundamental Aspects of Reactor Shielding, Addison Wesley (1959).

DISTRIBUTION

Department of Defense

Assistant to the Secretary of Defense
Atomic Energy
Washington, DC 20301
ATTN Executive Assistant

Director
Command & Control Technical Center
Department of Defense
The Pentagon, Rm BE 685
Washington, DC 20301
ATTN C-362 Mr. Adkins

Defense Documentation Center
Cameron Station
Alexandria, VA 22314
ATTN TC

Commander
Defense Electronic Supply Center
1507 Wilmington Pike
Dayton, OH 45444
ATTN DESC-EQE J. Counsil
ATTN DESC-ECS J. Dennis
ATTN DESC-ECS D. Droege
ATTN DESC-EQE R. Grillmeier
ATTN DESC-ECS D. Hill
ATTN DESC-ECT J. Niles
ATTN DESC-ECP B. Nunke

Director
Defense Logistics Agency
Cameron Station
Alexandria, VA 22314
ATTN DLA-SE
ATTN DLA-QEL J. Slattery

Defense Material Specifications and
Standards Office
Room 105 Dwyer Bldg.
3320 Duke Street
Alexandria, VA 22314
ATTN L. Fox

Director
Defense Nuclear Agency
Washington, DC 20305
ATTN DDST
ATTN TITL
ATTN TISI Archives
ATTN RAEV H. Fitz, Jr.
ATTN RAEV Maj. M. Kemp

Commander
Field Command
Defense Nuclear Agency
Kirtland AFB, NM 87115
ATTN FCPR

Chief
Livermore Division Fld Command DNA
Department of Defense
Lawrence Livermore Laboratory
P.O. Box 808
Livermore, CA 94550
ATTN FCPRL

Under Secy of Def for Rsch & Engrg
Department of Defense
Washington, DC 20301
ATTN AE
ATTN SSS

Director
National Security Agency
Ft. Meade, MD 20755
ATTN T. Brown
ATTN G. Daily

Director
Defense Supply Agency
DSAH/SE 4A586
Cameron Station
Alexandria, VA 22314

Department of the Army

Commander
Aberdeen Proving Ground
Department of the Army
Aberdeen Proving Ground, MD 21005
ATTN S. Harrison

Director
BMD Advanced Technology Center
Huntsville Office
Department of the Army
P.O. Box 1500
Huntsville, AL 35807
ATTN ATC-T
ATTN BMDSC-TEN R. DeKalb

Deputy Chief of Staff for
Rsch Dev and Acq
Department of the Army
Washington, DC 20310
ATTN LTC G. Ogden

Commander
Harry Diamond Laboratories
Department of the Army
2800 Powder Mill Road
Adelphi, MD 20783
ATTN DEHLD-NP
ATTN DEHLD-RBH F. Balicki
ATTN DEHLD-RBH H. Eisen
ATTN DEHLD-RBH J. Halpin
ATTN DELHD-RB J. McGarrity
ATTN DELHD-RBH E. McGarry
ATTN DELHD-RBH S. Rattner
ATTN DELHD-RBH C. Wenger

Commander
Redstone Scientific Information CTR
U.S. Army R & D Command
Redstone Arsenal, AL 35809
ATTN Chief, Documents

Commander
U.S. Army Armament Research &
Development Command
Dover, NJ 07801
ATTN DRDAR-LCA-PD

Project Officer
U.S. Army Electronics Rsch & Dev Command
Fort Monmouth, NJ 07703
ATTN D. Huewe

Commander
U.S. Army Materiel Development
and Readiness Command
5001 Eisenhower Avenue
Alexandria, VA 22333
ATTN J. Corrigan

Commander
U.S. Army Nuclear & Chemical Agency
7500 Backlick Road
Building 2073
Springfield, VA 22150
ATTN MONA-WE Maj A. Lind
ATTN Nuc Surv Cmte Col A. Lowrey

Commander
White Sands Missile Range
Department of the Army
White Sands Missile Range, NM 88002
ATTN STEWS-TE-AN T. Leura
ATTN STEWS-TE-NT M. Squires
ATTN R. Williams

Department of the Navy

Chief of Naval Operations
Department of the Navy
Washington, DC 20350
ATTN OP985F

Chief of Naval Research
Ballston Center Tower #1
800 N. Quincy Street
Arlington, VA 22217
ATTN Code 220 D. Lewis
ATTN Code 427 L. Cooper

Commander
Naval Air Systems Command
Washington, DC 21360
ATTN Air 350F

Commander
Naval Electronic Systems Comd
Department of the Navy
Washington, DC 20360
ATTN 5045.11 C. Suman

Commander
Naval Ocean Systems Center
San Diego, CA 92152
ATTN Code 4471 (Tech Lib)

Superintendent (Code 1424)
Naval Postgraduate School
Monterey, CA 93940
ATTN Code 2124 Tech Rpts Librarian

Commanding Officer
Naval Research Laboratory
Washington, DC 20375
ATTN Code 6701 J. Brown
ATTN Code 5210 J. Davey
ATTN Code 6627 C. Guenzer
ATTN Code 5216 H. Hughes
ATTN Code 6600 J. McElhinney
ATTN Code 6650 A. Namenson
ATTN Code 6601 E. Wolicki

Commander
Naval Sea Systems Command
Washington, DC 20362
ATTN SEA-9931 R. Lane

Commander
Naval Ship Engineering Center
Washington, DC 20362
ATTN Code 6174D2

Commander
Naval Surface Weapons Center
White Oak, Silver Spring, MD 20910
ATTN J. Downs
ATTN R. Jenkins
ATTN Code WA52 R. Smith

Commander
Naval Weapons Center
China Lake, CA 93555
ATTN Code 533 (Tech Lib)

Commanding Officer
Naval Weapons Evaluation Facility
Kirtland Air Force Base
Albuquerque, NM 87117
ATTN Code AT-6

Commanding Officer
Naval Weapons Support Center
Crane, IN 47522
ATTN Code 7024 T. Ellis
ATTN Code 7024 J. Munarin
ATTN Code 7024 J. Ramsey

Director
Strategic Systems Project Office
Department of the Navy
Washington, DC 20376
ATTN Code 2015
ATTN Code 230 D. Gold
ATTN Code 2701 J. Pitsenberger
ATTN Code 2730 P. Spector

Department of the Air Force

Commander
Air Force Aero-Propulsion Laboratory, AFSC
Wright Patterson AFB, OH 45433
ATTN POD P. Stover

Commander
Air Force Avionics Laboratory, AFSC
Wright-Patterson AFB, OH 45433
ATTN TEA R. Conklin
ATTN DHE H. Hennecke

Commander
Air Force Institute of Technology
Wright-Patterson AFB, OH 45433
ATTN ENP C. Bridgman

Commander
Air Force Materials Laboratory, AFSC
Wright-Patterson AFBV, OH 45433
ATTN LTE

Headquarters
Air Force Systems Command
Andrews AFB
Washington, DC 20334
ATTN DLCA
ATTN Capt. T. Seale
ATTN XRLA Maj. R. Stead

Air Force Technical Applications Center
Patrick AFB, FL 32925
ATTN TAE

Commander
Air Force Weapons Laboratory, AFSC
Kirtland AFB, NM 87117
ATTN SUL
ATTN ELP J. Ferry
ATTN ELP Capt. M. Knoll
ATTN ELP Lt. Col. A. Loggins
ATTN ELP R. Maier
ATTN ELP J. Mullis

Headquarters
Electronic Systems Division
Air Force Systems Command
Hanscom AFB, MA 01731
ATTN Technical Library

Commander
Foreign Technology Division
Air Force Systems Command
Wright-Patterson AFB, OH 45433
ATTN FTD/PDJV
ATTN ETDP B. Ballard

Air Force Technical Applications Center
Patrick AFB, FL 32925
ATTN TAE

Commander
Ogden ALC
Department of the Air Force
Hill AFB, UT 84406
ATTN MMETH Maj. R. Blackburn
ATTN MMGRW G. Fry
ATTN MMEDD C. Graham
ATTN MMIFM S. Mallory
ATTN MMETH Capt. R. Padfield
ATTN MMIFM D. Stanger
ATTN MMETH Maj. F. Walter

Commander
Rome Air Development Center
RADC/RBRM
Griffiss AFB, NY 13441
ATTN RBRM J. Brauer
ATTN RBRP C. Lane

Commander
Rome Air Development Center
Hanscom AFB, MA 01731
ATTN ESR R. Buchanan
ATTN ETS R. Dolan
ATTN ESE A. Kahan
ATTN ESR W. Shedd
ATTN ESR P. Vail

Commander
Space & Missile Systems Command/SK
Post Office Box 92960
Worldway Postal Center
Los Angeles, CA 90009
ATTN AWSC
ATTN SKJ Capt. Barry
ATTN AWSR Lt. Col. K. Blakney
ATTN DYS Maj. L. Darda
ATTN SZJ Maj. R. Davis
ATTN C. Kelly
ATTN MNNL Lt. Col. S. Kennedy
ATTN AW Col. W. Schlosser
ATTN SKF P. Stadler

Commander
Space and Missile Systems Organization
Norton AFB, CA 92409
ATTN MNNG
ATTN MNNH Capt. J. Tucker

National Aeronautics and Space Agency

NASA Headquarters
Washington, D.C. 20546
ATTN J. Murphy

Director
NASA Ames Research Center
M/S 2445
Moffett Field, CA 90035
ATTN G. DeYoung

Director
NASA Goddard Space Flight Center
Greenbelt, MD 20771
ATTN Code 311 J. Adolphsen
ATTN Code 755.1 V. Danchenko

NASA-Lewis Research Center
210100 Brook Park Rd
Cleveland, Ohio 44135
ATTN M. Baddour

Director
NASA Marshall Space Flight Center
Huntsville, AL 35812
ATTN EG02
ATTN EC43 L. Hamiter
ATTN M. Nowakowski
ATTN H. Yearwood

Department of Energy

Albuquerque Operations Office
P.O. Box 5400
Albuquerque, NM 87115
ATTN Document Control for WSSB

University of California
Lawrence Livermore Laboratory
P.O. Box 808
Livermore, CA 94550
ATTN Doc Con for Technical Information Dept.

Los Alamos Scientific Laboratory
P.O. Box 1663
Los Alamos, NM 87545
ATTN Doc Con for J. Freed

Office of Military Application
Department of Energy
Washington, DC 20545
ATTN Doc Con for Classified Library

Sandia Laboratories
P.O. Box 5800
Albuquerque, NM 87185
ATTN J. Barnum
ATTN F. Coppage
ATTN W. Dawes
ATTN R. Gregory
ATTN J. Hood

Department of Commerce

Director
National Bureau of Standards
Washington, D.C. 20234

ATTN A505 S. Chappell
ATTN J. French
ATTN A327 K. Galloway
ATTN C216 J. Humphreys
ATTN A347 J. Mayo-Wells
ATTN B244 W. Bullis
ATTN A327 R. Scace

Other Government

Central Intelligence Agency
Hq Bldg, Rm. 5G48
Washington, DC 20505
ATTN RD/SI

Department of Defense Contractors

Advanced Microdevices, Inc.
901 Thompson Place
Sunnyvale, CA 94086
ATTN J. Schlageter

Aerojet Electro-Systems Co.
Division of Aerojet-General Corp.
P.O. Box 296
1100 W. Hollyvale Drive
Azusa, CA 91702
ATTN T. Hanscome

Aeronutronic-Ford Corporation
Division 3939 Fabian Way
Palo Alto, CA 94303
ATTN D. Cadle

Aeronutronic Ford Corporation
Electronic Technology Department
Ford Road
Newport Beach, CA 92663
ATTN J. Davison

Aerospace Corporation
P.O. Box 92957
Los Angeles, CA 90009
ATTN S. Bower
ATTN D. Fresh
ATTN W. Willis

ARACOR
1223 E. Arques Avenue
Sunnyvale, CA 94086
ATTN R. Armistead

Battelle Memorial Institute
505 King avenue
Columbus, OH 43201
ATTN R. Thatcher

BDM Corporation
2600 Yale Boulevard, S.E.
Albuquerque, NM 87106
ATTN D. Alexander
ATTN R. Peace
ATTN D. Wunch

Bendix Corporation
Flight Systems Division
Dept. 7831
Teterboro, NJ 07608
ATTN E. Meeder

Boeing Aerospace Company
MS-2R-00
P.O. Box 3999
Seattle, WA 98124
ATTN I. Arimura
ATTN D. Egelkrout
ATTN A. Johnston
ATTN C. Rosenberg
ATTN W. Rumpza

Burr-Brown Research Corporation
International Airport Ind. Park
P.O. Box 11400
Tucson, AZ 85734
ATTN H.C. Smith

California Institute of Technology
Jet Propulsion Laboratory
4800 Oak Grove Drive
Pasadena, CA 91103
ATTN W. Price
ATTN A. Shumka
ATTN A. Stanley

Charles Stark Draper Laboratories
555 Technology Square
Mail Station 62
Cambridge, MA 02139
ATTN R. Bedingfield
ATTN P. Greiff
ATTN C. Lai
ATTN R. Ledger
ATTN A. Schutz

Cincinnati Electronics Corp.
2630 Glendale-Milford Road
Cincinnati, OH 45241
ATTN L. Hammond
ATTN C. Stump

Control Data Corporation
P.O. Box 0
Minneapolis, MN 55440
ATTN J. Meehan

Denver Research Institute
University of Colorado
P.O. Box 10127
Denver, CO 80210
ATTN F. Venditti

E-Systems, Inc,,
P.O. Box 6118
Dallas, TX 75222
ATTN K. Reis

EMM Corporation
3883 No. 28th Avenue
Phoenix, AZ 85017
ATTN F. Krch

Exp. & Math. Physics Consultants
P.O. Box 66331
Los Angeles, CA 90066
ATTN T. Jordan

Fairchild Camera and Instrument Corp.
464 Ellis Street
Mountain View, CA 94040
ATTN D. Myers
ATTN R. Marshall

Ford Aerospace & Communications Corp.
Ford & Jamboree Roads
Newport Beach, CA 92663
ATTN Tech Info Services

Franklin Institute
20th Street and Parkway
Philadelphia, PA 19103
ATTN R. Thompson

Garrett Corporation
P.O. Box 92248
9851 Sepulveda Blvd
Los Angeles, CA 90009
ATTN R. Weir

General Dynamics Corporation
Convair Aerospace Division
P.O. Box 1128
San Diego, CA 92112
ATTN W. Hansen

General Dynamics Corporation
Aerosystems Division
P.O. Box 748
Ft. Worth, TX 76101
ATTN O. Wood
ATTN R. Fields

General Electric Company
P.O. Box 5000
Binghamton, NY 13902
ATTN D. Pepin

General Electric Company
Aerospace Elec Sys Dept
French Road Plant
Utica , NY 13503
ATTN D. Cole
ATTN W. Patterson
ATTN J. Gibson

General Electric Company
Aircraft Engine Business Group
Evendale Plant, Int Hwy 75S
Cincinnati, OH 45215
ATTN R. Hellen

General Electric Company
Ordnance Systems
100 Plastics Avenue
Pittsfield, MA 01201
ATTN J. Reidl

General Electric Company
Re-entry & Environmental Systems Div.
P.O. Box 7722
3198 Chestnut Street
Philadelphia, PA 19101
ATTN R. Benedict
ATTN W. Palchefsky, Jr.
ATTN W. Patterson
ATTN Tech. Lib.

General Electric Company
Valley Forge Space Center
P.O. Box 8555
Philadelphia, PA 19101
ATTN R. Casey
ATTN D. Long
ATTN J. Peden
ATTN L. Sivo

General Electric Company--Tempo
2560 Huntington Avenue
Suite 300
Alexandria, VA 22303
ATTN W. Alfonte

General Electric Company--Tempo
Center for Advanced Studies
816 State Street (P.O. Drawer QQ)
Santa Barbara, CA 93102
ATTn DASIAC E. Espig

General Research Corporation
Santa Barbara Division
P.O. Box 6770
Santa Barbara, CA 93111
ATTN R. Hill
ATTN Tech. Inf. Off.

Georgia Institute of Technology
Georgia Tech Research Institute
Atlanta, GA 30332
ATTN R. Curry

Goodyear Aerospace Corporation
Arizona Division
Litchfield Park, AZ 85340
ATTN Security Control Station

Grumman Aerospace Corporation
South Oyster Bay Road
Bethpage, NY 11714
ATTN J. Rogers

GTE Sylvania, Inc.
Electronics Systems GRP-Eastern Div
77 A Street
Needham, MA 02194
ATTN C. Thornhill
ATTN L. Pauplis

GTE Sylvania Inc.
189 B Street
Needham Heights, MA 02194
ATTN P. Fredrickson
ATTN H & V Group
ATTN C. Ramsbottom
ATTN J. Waldron
ATTN H. Ullman

Harris Corporation
Harris Semiconductor Division
P.O. Box 883
Melbourne, FLA 32901
ATTN J. Cornell
ATTN C. Anderson

Honeywell Inc.
Aerospace & Defense Group
13350 U.S. Highway 19 North
St. Petersburg, FL 33733
ATTN C. Cerulli

Honeywell, Inc.
Government & Aeronautical Prod. Div.
600 2nd Street, North
Hopkins, MN 55343
ATTN K. Gaspard

Honeywell, Inc.
Government & Aeronautical Pro.
2600 Ridgway Road
Minneapolis, MN 55440
ATTN R. Gumm

Honeywell, Inc.
Radiation Center
2 Forbes Road
Lexington, MA 02173
ATTN Technical Library

Hughes Aircraft Company
Centinela and Teale
Culver City, CA 90230
ATTN R. McGowan
ATTN J. Singletary

Hughes Aircraft Company
El Segundo Site
P.O. Box 92919
Los Angeles, CA 90009
ATTN E. Smith
ATTN W. Scott

IBM
Department L99, Bldg. 002A
Route 17C
Owego, NY 13827
ATTN F. Tietse
ATTN H. Mathers
ATTN T. Martin

IBM Research Laboratories
Box 218
Yorktown Heights, NY 10598
ATTN J. Ziegler

IIT Research Institute
10 West 35th Street
Chicago, IL 60616
ATTN I. Mindel

Institute for Defense Analyses
400 Army-Navy Drive
Arlington, VA 22202
ATTN Tech. Info. Services

Intel Corporation
3065 Bowers Avenue
Mail Stop 1-156
Santa Clara, CA 95051
ATTN M. Jordan

International Tel. & Telegraph Corp.
500 Washington Avenue
Nutley, NJ 07110
ATTN A. Richardson
ATTN Dept 608

Intersil Inc.
3250 Scott Boulevard
Santa Clara, CA 95051
ATTN D. MacDonald

IRT Corporation
P.O. Box 81087
San Diego, CA 92138
ATTN J. Harrity

JAYCOR
1401 Camino del Mar
Del Mar, CA 92014
ATTN L. Scott

Johns Hopkins University
Applied Physics Laboratory
Johns Hopkins Road
Laurel, MD 20810
ATTN P. Partridge

Kaman Sciencs Corporation
P.O. Box 7463
Colorado Springs, CO 80933
ATTN J. Lubell

Litton Systems, Inc.
Guidance and Control Systems Division
5500 Canoga Avenue
Woodland Hills, CA 91364
ATTN G. Maddox

Lockheed Missiles and Space Co., Inc.
P.O. Box 504
Sunnyvale, CA 94088
ATTN P. Bene
ATTN H. Phillips
ATTN E. Smith
ATTN C. Thompson

Lockheed Missiles and Space Co., Inc.
Research Division
3251 Hanover Street
Palo Alto, CA 94304
ATTN J. Crowley
ATTN J. Smith

Martin Marietta Corporation
Denver Division
P.O. Box 179
Denver, CO 80201
ATTN E. Carter

Martin Marietta Corporation
MP 148 Orlando Division
P.O. Box 5837
Orlando, FL 32805
ATTN W. Brochett
ATTN H. Cates
ATTN R. Gaynor
ATTN W. Janocko

McDonnell Douglas Corporation
5301 Bolsa Avenue
Huntington Beach, CA 92647
ATTN D. Fitzgerald
ATTN J. Holmgrem

McDonnell Douglas Corporation
Standards Engineering
P.O. Box 516
St. Louis, MO 63166
ATTN M. Stitch
ATTN D. Dohm
ATTN Library

McDonnell Douglas Corp.
3855 Lakewood Boulevard
Long Beach, CA 90846
ATTN Tech. Lib.

Mission Research Corporation
1150 Silverado Street
P.O. Box 1209
La Jolla, CA 92038
ATTN J. Azarewicz
ATTN R. Berger
ATTN J. Raymond
ATTN V. Van Lint

Mission Research Corp.
735 State Street
Santa Barbara, CA 93202
ATTN C. Longmire

Massachusetts Institute of Technology
Lincoln Laboratory
P.O. Box 73
Lexington, MA 02173
ATTN P. McKenzie
ATTN Library A-082

Mitre Corporation
P.O. Box 208
Bedford, MA 01730
ATTN M. Fitzgerald

Motorola Government Electronics Division
8201 E. McDowell Road
Scottsdale, AZ 85252
ATTN A. Christensen

Motorola Semiconductor Products, Inc.
P.O. Box 20912
Phoenix, AZ 85036
ATTN L. Clark

National Semiconductor Corp.
2900 Semiconductor Drive
Santa Clara, CA 95051
ATTN R. Wang
ATTN A. London

New Mexico University
Elec. Eng. & Computer Science Dept
Albuquerque, NM 87131
ATTN H. Southward

Northrop Corporation
Northrop Research & Technology Center
1 Research Park
Palos Verdes Peninsula, CA 90274
ATTN J. Srour

Northrop Corporation
Electronic Division Headquarters
1 Research Park
Palos Verdes Peninsula, CA 90274
ATTN T. Jackson
ATTN P. Eisenberg

Northrop Corporation
Electronic Division
2301 West 120th Street
Hawthorne, CA 90250
ATTN L. Apodaca
ATTN P. Gardner
ATTN D. Strobel

Physics International Company
2700 Merced Street
San Leandro, CA 94577
ATTN Div 6000
ATTN J. Huntington
ATTN J. Shea

R&D Associates
P.O. Box 9695
4640 Admiralty Way
Marina del Rey, CA 90291
ATTN C. Rogers
ATTN R. Poll

Rand Corporation
1700 Main Street
Santa Monica, CA 90406
ATTN C. Crain

Raytheon Company
Advanced Design Dept.
Hartwell Road
Bedford, MA 01730
ATTN J. Ciccio

Raytheon Company
528 Boston Post Road
Sudbury, MA 01776
ATTN H. Flescher
ATTN A. Van Doren

RCA Corporation
Camden Complex
Front & Cooper Streets
Camden, NJ 08012
ATTN E. Van Keuren

RCA Corporation
David Sarnoff Research Center
P.O. Box 432
Princeton, NJ 08540
ATTN D. OConnor
ATTN Office N103

RCA Corporation
Missile & Surface Radar
Bldg. 108-239, Marne Highway
Moorestown, NJ 08057
ATTN R. Killion

RCA Corporation
Government Systems Division
ASTRO Electronics Division
P.O. Box 800, Locust Corner
Princeton, NJ 08540
ATTN G. Bruckar
ATTN V. Mancino

RCA Corporation
Solid State Division
Box 3200
Somerville, NJ 08876
ATTN W. Allen

Rensselaer Polytechnic Institute
P.O. Box 965
Troy, NY 12181
ATTN R. Gutmann

Research Triangle Institute
P.O. Box 23194
Research Triangle Park, NC 27709
ATTN Eng Div M. Simons Jr.

Rockwell International Corp.
5701 West Imperial Highway
Los Angeles, CA 90009
ATTN TIC BA08
ATTN T. Yates

Rockwell International Corp.
Autonetics Group
3370 Miraloma Avenue
P.O. Box 3105
Anaheim, CA 92803
ATTN J. Bell
ATTN V. DeMartino
ATTN G. Messenger
ATTN T. Oki
ATTN V. Strahan

Rockwell International Corp.
Space Division
12214 South Lakewood Boulevard
Downey, CA 90241
ATTN D. Stevens

Sanders Associates, Inc.
95 Canal Street
Nashua, NH 03060
ATTN M. Aitel
ATTN L. Brodeur

Science Applications, Inc.
2860 S. Circle Drive
Suite 2224
Colorado Springs, CO 80906
ATTN D. Stribling

Science Applications, Inc.
1200 Prospect Street
P.O. Box 2351
La Jolla, CA 92038
ATTN J. Naber
ATTN V. Orphan
ATTN V. Verbinski

Science Applications, Inc.
8400 Westpark Drive
McLean, VA 22101
ATTN W. Chadsey

Singer Company-Kearfott Div.
Dept. 5830
150 Totowa Road
Wayne, NJ 07470
ATTN R. Spiegel

Singer Company
Kearfott Division
1150 McBride Avenue
Little Falls, NJ 07424
ATTN J. Brinkman

Sperry Rand Corporation
Sperry Microwave Electronics
P.O. Box 4648
Clearwater, FL 33518
ATTN Engineering Laboratory

Sperry Rand Corporation
Sperry Division
Marcus Avenue
Great Neck, NY 11020
ATTN C. Craig
ATTN P. Maraffino
ATTN F. Scaravaglione
ATTN R. Viola

Sperry Rand Corporation
Sperry Flight Systems
P.O. Box 21111
Phoenix, AZ 85036
ATTN D. Schow

Sperry Univac
Univac Park
P.O. Box 3525
St. Paul, MN 55165
ATTN J. Inda

Spire Corporation
P.O. Box D
Bedford, MA 01730
ATTN R. Little

SRI International
333 Ravenswood Avenue
Menlo Park, CA 94025
ATTN A. Whitson
ATTN P. Dolan

Teledyne Ryan Aeronautical
Box 311
San Diego, CA 92112
ATTN J. Rawlings

Texas Instruments, Inc.
13500 N. Central Expressway
P.O. Box 5474, M.S. 262
Dallas, TX 75222
ATTN A. Peletier
ATTN R. Stehlin

TRW Incorporated
Defense and Space Systems Group
One Space Park
Redondo Beach, CA 90278
ATTN O. Adams
ATTN P. Guilfoyle
ATTN H. Haid
ATTN H. Holloway
ATTN R. Kingsland
ATTN A. Pavelko
ATTN R. Schnieder
ATTN A. Witteles

TRW Defense & Space Sys Group
San Bernardino Operations
P.O. Box 1310
San Bernardino, CA 92402
ATTN M. Gorman
ATTN R. Kitter
ATTN F. Fay

TRW Systems and Energy
P.O. Box 368
Clearfield, Utah 84015
ATTN J. Spehar
ATTN D. Millward

Vought Corporation
P.O. Box 5907
Dallas, TX 75222
ATTN Library
ATTN Tech Data Ctr
ATTN R. Tomme

Westinghouse Electric Corporation
Radiation Effects Technology
P.O. Box 1521 M/S 3330
Baltimore, MD 21203
ATTN D. Crichi
ATTN H. Kalapaca

Westinghouse Electric Corporation
Aerospace Division
P.O. Box 746, M/S 292
Baltimore, MD 21203
ATTN L. McPherson

Other Organizations

Aerospace Industries Association
of America Inc.
1725 E. Sales Street, N.W.
Washington, DC 20036
ATTN S. Siegel

Electronic Industries Association
2001 Eye Street, N.W.
Washington, DC 20006
ATTN J. Hessman

*U.S. GOVERNMENT PRINTING OFFICE: 1979 281-484/241 1-3